Faculty of Engineering of the University of Porto

Microgrid Reliability Assessment

José Miguel Gomes Campos Costa

Dissertation conducted under the Integrated Master in Electrical and Computers Engineering
Major in Energy

Supervisor: Prof. Vladimiro Miranda, Ph.D.
Co-Supervisor: Prof. Leonel Carvalho, Ph.D.

29th July 2016

Resumo

A crescente necessidade de descarbonização do setor elétrico e aumento de penetração de energia renovável, os avanços tecnológicos no campo da microgeração e o desejo de mudança no paradigma do sistema elétrico, tendo em vista a implementação do conceito de *smart grids,* conduziram a uma forte investigação acerca do potencial e possíveis vantagens - não só ambientais, como também económicas - derivadas da utilização de micro-redes no sistema de distribuição. Entre elas destacam-se o aumento da eficiência energética das instalações e do uso de energias renováveis, redução da emissão de gases poluentes e do custo da energia, minimização das perdas na rede e um melhoramento na qualidade de serviço.

Embora as vantagens inerentes à implementação de micro-redes no sistema de distribuição sejam bastante apelativas, existem ainda vários obstáculos técnicos e legais que impedem que esta transição paradigmática do modo como um sistema elétrico de energia é concebido e operado seja trivial. No domínio técnico as principais dificuldades advêm da monitorização, controlo e sistema de proteção a implementar. Relativamente às questões legais, existe a necessidade premente de desenvolver políticas regulatórias que englobem tanto assuntos ambientais, como níveis de tensão estipulados, e que assegurem o funcionamento das micro-redes como entidades legais.

Uma micro-rede pode ser definida como uma rede de BT, sendo constituída por um conjunto de unidades de produção distribuída e sistemas de armazenamento de energia que operam de forma coordenada de modo a fornecer energia elétrica ao seu aglomerado de cargas (consumidores). A micro-rede pode operar interligada à rede situada a montante ou em modo isolado.

Nesta dissertação é apresentado um estudo de fiabilidade de uma micro-rede teste composta apenas por produção renovável, mais concretamente geração fotovoltaica, e as consequências da sua implementação para a rede de MT a montante. De modo a assegurar o funcionamento da micro-rede em modo isolado, uma bateria é adicionada ao sistema. O estudo desenvolvido foca-se no funcionamento em modo isolado, ou de emergência, da micro-rede, devido a uma falha de alimentação a partir do sistema de nível superior; não sendo, portanto, considerado um isolamento planeado, por razões de manutenção, por exemplo.

O algoritmo desenvolvido no decorrer deste trabalho baseia-se no método de Monte Carlo sequencial. Esta ferramenta de simulação permite a obtenção do valor esperado dos índices de fiabilidade desejados através do sorteio aleatório do período do ano em que a falha de alimentação ocorre e da duração dessa interrupção, construindo, assim, uma amostra significativa do comportamento da micro-rede.

Abstract

The growing need of decarbonizing the electrical sector and increase the penetration of renewable energy, the technological advances in the field of MicroGrids and the desire to change the paradigm of the electrical system, having in mind the implementation of the Smart Grid concept, led to an important investigation about the potential and possible advantages – both environmental and economic – deriving from the use of Microgrids in the distribution system. Among these advantages, it should be highlighted the increase in the energetic efficiency of the buildings and the use of renewable energies, the decrease in the emission of pollutant gases and the cost of energy, the minimization of grid losses and an improvement in the quality of the service.

Although the benefits achieved with the implementation of the Microgrids in the distribution system are very appealing, there are still many technical and legal obstacles that prevent this paradigmatic transition of the way how an electric power system is conceived and operated to be trivial. As far as the technical field is concerned, the main difficulties come from the monitoring, controlling and the protection system to implement. In which concerns the legal matters, there is the urgent need to develop regulatory policies that include not only environmental issues but also specified levels of voltage and that assure the operation of a Microgrids as a legal entity.

A Microgrid can be defined as a LV grid, consisting of a set of units of distributed generation and energy storage systems that work in a coordinate way to supply energy to its agglomerate of loads (consumers). The Microgrid can operate interconnected with the upstream network or in islanded mode.

In this thesis, a study is presented about the reliability of a Microgrid that is composed of renewable generation, more precisely photovoltaic generation, and the consequences of its implementation to the upstream grid. In order to ensure a proper MG operation, when in islanded mode, a battery is added to the system. This study focuses on the operation in stand-alone mode, or on the emergency mode, of the Microgrid due to an upper system failure, therefore, it is not considered a planned islanding for maintenance reasons, for example.

The algorithm developed in the course of this work is based on the Monte Carlo sequential method. This simulation tool allows the attainment of the expected value of the intended reliability indexes through the randomly draw of the period in which the failure happens and its duration, creating, thus, a meaningful of the Microgrid behavior.

Acknowledgments

Firstly, I would like to express my gratitude to my thesis supervisor, Professor Vladimiro Henrique Barrosa Pinto de Miranda, Ph.D., whose passion for science and knowledge inspired me to embrace this dissertation. His guidance and support made this work possible. I would also like to give a special thanks to my co-supervisor, Professor Leonel de Magalhães Carvalho, Ph.D., who, week after week, received me and clarified, with patience, my constant stream of doubts. His readiness in helped me solve the apparently unsolvable problems made me believe that I was able to perform this work.

Next, I would like to thank my dear friend João Sampaio for several reasons: for impregnate our school days with humor and joviality, for his tireless effort in teasing me to be a better student and, even with a full time job, for the time spent skyping in order to help me making this thesis presentable.

I would also like to show my sincere acknowledgement to my family, namely to my "for life" little sister Teresa, whose ambition and intrepidity never ceases to amaze me; to my grandmother Micas, my kindhearted college flatmate for four years, who taught me life can be guided by tenderness and nobleness; and to my grandfather Gomes, my longtime companion of adventures, whose kindness and cheerfulness way of living made me consider age only as a number.

These acknowledgments would never be completed without referring my distinct and never forgotten friends, my family by choice, who, through a magnificent serendipity, I have the pleasure to know: Ana, Barros, Bruno, Carolina, César, David, Duarte, Fred, Isabel, João Guilherme, Luis, Marco, Maria, Paulo, Rui and Teresa. Thank you for the affection, the healthy dose of chaos in which you embed my life and for helping me living the dream.

The wonderful people that I met in my gap year also deserve a prominent special mention here. I would like to address a special thanks, among all of them, to Dave, Granny, Lara and Marianne for making me feel so comfortable outside my comfort zone and for all your genuine love.

Last, but not least, I would like to dedicate the most special thanks to my life supervisor in the last 24 years: my Mother. Thank you for the constant faith and for appeasing my restlessness as nobody in the world. You are an example of strength, bravery and dedication. This work is dedicated to you.

Contents

List of Figures

List of Tables

List of Acronyms and Symbols

List of Acronyms

AC	Alternating Current
CERTS	Consortium for Electric Reliability Technology Solutions
CO_2	Carbon Dioxide
CHP	Combined Heat and Power
DC	Direct Current
DER	Distributed Energy Resources
DG	Distributed Generation
DN	Distribution Network
DR	Demand Response
DSM	Demand Side Management
EA	Evolutionary Algorithm
EENS	Expected Energy Not Supplied
EENU	Expect Energy Not Used
EPNS	Expected Power Not Supplied
ESS	Energy Storage Systems
EV	Electric Vehicles
EU	European Union
FOR	Forced Outage Rate
FTA	Fault Tree Analysis
GA	Genetic Algorithm
GCOT	Generalized Capacity Outage Table
GDP	Gross Domestic Product
GHG	Greenhouse gases
GLR	Generation-to-Load Ratio
HRDS	High Reliability Distribution System
ICT	Information and Communication Technologies
IEA	International Energy Agency
IM	Islanding Mode
LHS	Latin Hypercube Sampling
LOGD	Loss of Generation Duration
LOGE	Loss of Generation Expectation
LOGF	Loss of Generation Frequency

LOGP	Loss of Generation Probability
LOLD	Loss of Load Duration
LOLE	Loss of Load Expectation
LOLF	Loss of Load Frequency
LOLP	Loss of Load Probability
LV	Low Voltage
MC	Monte Carlo
MCMC	Markov Chain Monte Carlo
MG	MicroGrid
MMG	Multi MicroGrid
MTBF	Mean Time Between Failures
MTTF	Mean Time to Failure
MTTR	Mean Time to Repair
MV	Medium Voltage
NIM	Normal Interconnected Mode
NLV	Normal Low Voltage
OPF	Optimal Power Flow
PB	Population-based
PCC	Point of Common Coupling
PDIPM	Primal-Dual Interior Point Method
PNS	Power Not Supplied
PSO	Particle Swarm Optimization
PV	Photovoltaic
RBD	Reliability Block Diagram
RES	Renewable Energy Sources
SAIDI	System Average Interruption Duration Index
SAIFI	System Average Interruption Frequency Index
SOC	State of Charge
SGD	Stochastic Distributed Generation
SDSM	State Duration Sampling Method
SIPS	Small Isolated Power System
SSM	State Sampling Method
SG	Smart Grid
VMG	Value of the MG

List of Symbols

λ	Failure rate

Chapter 1 - **Introduction**

In this chapter it will be firstly explained the framework of this thesis, i.e., the motivation subjacent to this work, where the drivers behind the interest in and the growth of the MicroGrids (MGs) will be presented, as well as their advantages, imposed challenges and some cornerstone concepts related to this field of study and their interrelations. Some information concerning Energy Storage Systems (ESS) will also be displayed, since they play such a crucial role in the performance of a MG.

Secondly, some of the most relevant current study projects concerning MGs will be enumerated. Subsequently, the scope and the underlying objectives of this project will be stated, and finally this chapter will end with a brief outline of the present work.

1.1 Framework

It is undeniable that electrical energy plays a crucial role in today's society, being involved in almost all aspects of one's routine. Thus it takes a central position in the economic, social, technological, cultural and industrial growth of humanity.

The increase in electricity demand has been accentuated in recent decades and follows a growing pattern: it is expected that by 2050 the energy consumption will double when compared with today's values [1]. To supply this crescent demand, which is projected to reach 32 trillion kWh in 2030 [2], new generating unities need to be implemented.

A global environmental concern, regarding the utilization of fossil fuels in energy production, has emerged in recent decades, not only because of the need to reduce greenhouse gases (GHG) emissions, but also because of the potential scarcity of these sources. Following that conscious political trend, the European Union (EU), through "The Union of the Electricity Industry – EURELECTRIC", has set ambitious targets concerning Carbon Dioxide (CO_2) emissions. The goal is that the countries that compose this political and economic union would experience a 75% reduction for CO_2 by 2050 [1], thus achieving carbon neutrality, which can be defined through the following conditions [1]: calculating emissions in a transparent way; reducing emissions to the maximum possible extent and offsetting residual emissions through actions to minimize GHG elsewhere, as for example, via reforestation. This extreme decarbonisation can't be accomplished without the contribution of the electricity sector, since it's responsible for 24% of GHG emissions [2].

Besides the environmental and sustainability issues, concerns have been raised about the efficiency and reliability of the decades-old power grid equipment [3]. Therefore, considering all the above-mentioned facts and the deregulation of the power industry, a fundamental

paradigmatic shift respecting the way electricity is generated, delivered and utilized must take place.

Towards the fulfillment of that needful objective, by means of government incentives and boost in renewable energy related technology, the penetration of Renewable Energy Sources (RES) is increasing at a rapid rate [3]–[6]. The International Energy Agency (IEA) has estimated that the electricity generation from RES will reach 31% of the world's total power generation [3]. It is expected that the implementation of bulk and Distributed Generation (DG) – small sources of energy located at or near the point of use, whose technologies normally include photovoltaic (PV), wind, microturbines and fuel cells [4] -, based on RES, will gradually replace pollutant generation sources. Notwithstanding, the intermittence of the RES, derived from the variability of the atmospheric conditions, requires a proper spinning reserve management, so that the system robustness may be maintained [7].

The high penetration of RES and adoption of Demand Response (DR) – the flexibility of client's consumption of electricity in response to supply conditions [3] -, create a challenge to the operation of the electrical grid, which was conceived for generators whose outputs were controllable and for load demands that were passive [2].

Moreover, higher penetration of DER creates technical and non-technical issues, related to the power quality, surety and management, among others [8]. Thus, a Smart Grid (SG) is needed to adopt these changes.

A SG can be defined as an electricity grid supported by Information and Communication Technologies (ICT), which promotes the active management and control of Distributed Energy Resources (DER), such as RES and storage, Electric Vehicles (EV) and responsive loads [9]–[11]. The main difference between the SG and the current system is the integration of new actors, like DER and EV, whose connection points belong to the Distribution Network (DN), at the Medium (MV) or Low Voltage (LV) levels [11]. The interest, provided by this scenario, in local connection of DER at the DN has gained lots of attention of the industry and is turning conventional distribution systems into multiple small, modern and interconnected distribution systems – the MicroGrid [12]. The development of this concept will contribute to the decentralization of the DN's management and control [13]. So, MGs can be used to mitigate the negative effects of power fluctuation and, concomitantly, respect the environmental and operational requirements of the electrical system [14], while avoiding the necessity of a complex and branched central coordination [15].

Summarizing, a list of the most significant drivers behind the concept of MGs are presented [16]:

- Urge in reducing the GHG emissions;
- High penetration of DER, furthermore increasing at a fast rate;
- Deferment of the renovation of the transmission system;
- Improvement in the fields of reliability and quality, efficiency and security;
- Inherent DER's use economic advantages;
- Deregulation of the electric market.

A MG can be defined as an agglomerate of loads, DER units and possibly Energy Storage Systems (ESSs) and small scale fossil-fired Combined Heat and Power technology (CHP) operated in such a coordinated way that a reliable, secure and environmentally friendly electricity supply is attained. The point of its connection with the upstream network, at the distribution level, is designated as Point of Common Coupling (PCC). Since a MG acts within distinctly defined

electrical boundaries, it can be seen as a single controllable load from the system operator's perspective [15]–[19]. An example of a MG can be seen in figure 1.1.

The MG can operate in two distinct modes [15], [20]:

- Normal Interconnected Mode (NIM) – the MG is interconnected with the main upstream network, either injecting power (power surplus) in the MV grid or absorbing it (power deficit).
- Islanded Mode (IM) – after disconnecting from the main grid, the MG operates in an autonomous manner, likewise a physical island. This mode of operation can be intentional, for schedule maintenance purposes or when degraded power quality from the grid can harm the MG operation, or it can be unintentional, which can succeed after the occurrence of a fault. In stand-alone mode, the operation of the MG is more challenging, since the equilibrium between demand and supply, requires the implementation of special mechanisms to harmonize power imbalances.

When in NIM, the MG frequency is settled by the main grid, so, potential power mismatches will merely impact the power exchange between the MG and the upstream network [21].

The principal concerns are related to the operation of the MG in IM, preceded by sudden islanding, where abrupt changes on the MG demand or generation will cause frequency deviations. Therefore, the stability of the system can be compromised [21]. It is part of the DER functions to maintain adequate frequency levels in IM, through frequency control droops. Other mechanisms can be exploited to maintain the stability of the MG, such as load shedding schemes and proper response of the storage devices [4].

Voltage regulation is also mandatory, since without it the MG will experience voltage and reactive power oscillations. Being a local problem, voltage control implies the same problems for both modes of operation. Therefore, a voltage vs. reactive power droop control is required [4].

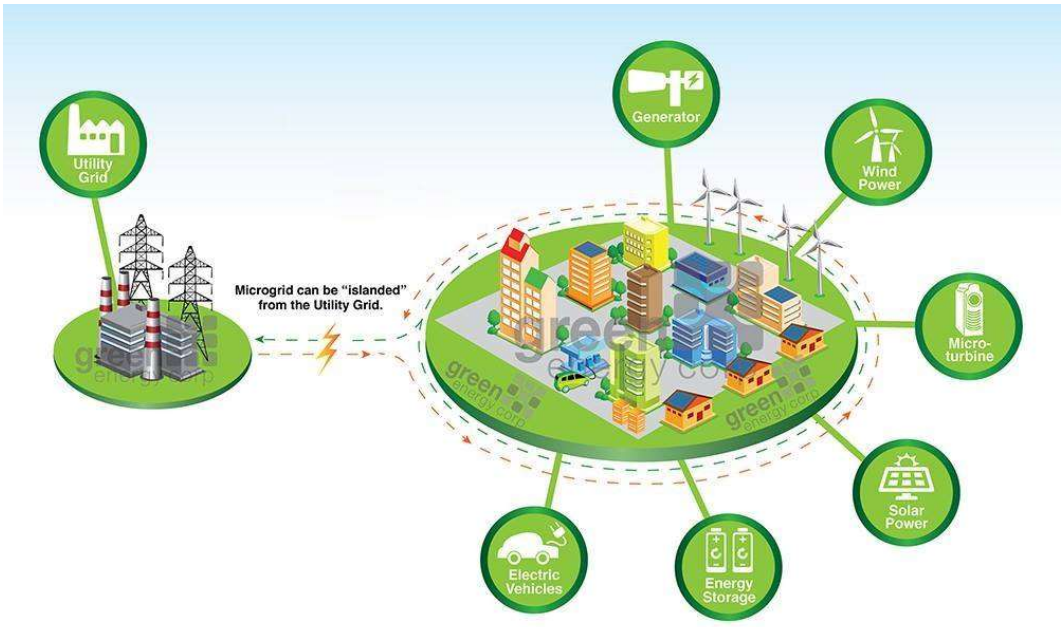

Figure 1.1 - Illustration of a MicroGrid, adapted from [30].

The implementation of the MG concept has diverse prominent advantages, namely [4], [8], [16], [22]–[27]:

- Provision of an efficient solution to deal with high penetration of RES in the LV distribution grid;
- Improvement of the reliability (felt by the consumers inside the MG and, sometimes, by the ones that are outside) and power quality at lower costs than the currently obtained. The proximity of distributed generators with the loads can decrease the duration and frequency of outages, as well as the energy not supplied;
- Postponement of transmission and distribution system upgrades;
- Amelioration of the electrical market operation, by delegating the multiple decision-making responsibilities in the hands of one agent. This leads to an attenuation in price volatility and to a more profitable coordination of stakeholders' interests ;
- Economic benefits triggered by the on-site generation and ESS's action, which can circumvent peak energy costs and create flows, when selling energy to the main grid. DR programs can also be a source of profit, since they reduce the load on the grid;
- Supply critical loads, like hospitals and public transportation, in the occurrence of a fault in the upstream network;
- The engagement with environmental issues. The operation of a MG is orientated to reach the net zero energy communities goal;
- Improvement of network performances, such as network loss reduction, voltage sag control and congestion mitigation;
- Increase system efficiency, through the use of waste heat CHP;
- Provision of ancillary services;
- Lower exposition to catastrophic failures, admitting its isolated operation.

Despite the vast aforementioned panoply of benefits that come with the proliferation of MGs, the deployment of this concept faces a considerable number of barriers that can prevent the thorough harnessing of the DER's advantages, regarding technical and non-technical challenges, such as [15], [16], [20], [23]:

- Their vulnerability to shortage risks, due to their small size and the intermittency of the RES. The only possible defenses are to buy energy from the grid at spot prices or to settle a contract with energy service companies;
- The need for an adequate conception of Demand Side Management (DSM) schemes that enable the users' reaction to the grid's necessities;
- The imperative redesign of the system protection schemes of the DN, in order to account the bidirectional flow;
- The occurrence of local oscillations that may appear due to the interaction of DG units' control systems. Furthermore, a transient stability analysis is required to guarantee a seamless transition between the NIM and IM;
- The low inertia that MGs can present, unlike the high one that characterized the power systems with an elevated number of synchronous generators. The low inertia can provoke harmful frequency oscillations in IM of operation;
- The uncertainty that comes with the variability of load profiles and atmospheric conditions. To cope with that challenge a certain level of coordination among the

DERs, distinguished by its efficient supervisory and monitoring system, is mandatory;
- The absence of standardized communication;
- The prohibition of IM of operation in distribution systems;
- The lack of new regulation regarding ancillary services such as frequency and voltage control, since the provision of such services, in stand-alone mode, are guaranteed by storage devices and microgeneration units, and not by the conventional generators.

Considering the variable nature of the RES and its implications to the performance of the MGs where they are installed, these mainly dependent on RES-systems should have a backup supply in order to ensure that they provide a stable source of energy to its consumers. An ESS can help in the achievement of that goal.

There is a plurality of ESSs that can be incorporated in MGs, such as batteries, supercapacitors and flywheels. Batteries, which store electrical energy in the form of chemical energy, are Direct Current (DC) power systems that require power electronic devices to convert the stored energy to and from Alternating Current (AC) power. The majority of batteries are composed by bidirectional converters in order to enable the energy to be stored and taken from them [4].

Normally, a Thevenin-based circuit is used in microscopic battery models, where the battery internal resistance is a non-linear function of its State of Charge (SOC), which can be defined as the energetic available capacity of the battery. Thereby, the energy losses related to the battery charging and discharging cycles are dependent on the SOC [3]. Regarding the macroscopic battery model, the following properties need to be considered [3]:

- A certain quantity of energy is lost in each charging or discharging event, due to the battery internal resistance and energy conversion loss;
- The lifetime of a battery deteriorates after each charging and discharging cycle, notwithstanding, this decay is practically undetectable in a daily basis;
- A battery can be charging or discharging, but not acting as a generator and load simultaneously. A good practice to improve the lifetime of one battery is to avoid its SOC to drop below a pre-defined threshold;
- Due to battery self-discharge rate, the energy stored diminishes over time.

There are several types of batteries, such as the lead-acid batteries, which are considered the most cost-efficient for power-supported applications, despite their short life cycle. Li-ion batteries provide the more competitive solution for high-power and high-energy applications [16].

The main advantages of using batteries are [3], [4], [15], [16], [24]:

- The capacity to buffer peak surges in electricity demand, antagonizing the impact of power disturbances;
- The induced improvement in reliability, by supplying local loads in the event of an outage at the generation level, and reduction in system losses.
- The enabled large-scale penetration of RES;
- The melioration in the voltage and frequency control of a MG, since they can provide a similar function to the one that comes from the inertia of synchronous

generators by absorbing or injecting active or reactive power in the islanded system, smoothing the mismatches between generation and demand;

- The capability to reduce the use of expensive energy sources in a MG in the course of peak hours;
- The possibility to enhance the power quality of a MG and to reduce its overall cost of operation, due to the fact that it can inject energy in the grid when electricity price is high and absorb it when the price is low.

Despite all the aforementioned benefits that come with the integration of ESSs, especially in MGs, they have not been fully implemented. The principal barriers to its installation are related to its high cost and to the lack of adequate control and management strategies [15]. However, more and more researches are being orientated to this field of study in order to overcome the mentioned challenges.

1.2 MicroGrid Research Projects

The MG concept was introduced to the scientific community by the Consortium for Electric Reliability Technology Solutions (CERTS) in 2001, with the objective of improving the reliability of LV systems, through the integration of small scale generators, ESS and controllable loads [28], [29]. Since then this concept has been suffering expressive developments, yet there are plenty of obstacles to overcome, like the ones mentioned in the previous section. Figure 1.2 chronologically depicts the progresses achieved since 2006 and the settled goals for the near future.

The MICROGRIDS and MORE MICROGRIDS projects, with the goal of enabling MG's stand-alone operation, developed the MG concept in Europe. Their objectives were to improve the reliability of DNs, through the design of active control strategies in order to permit the safe penetration of large quantities of RES [30].

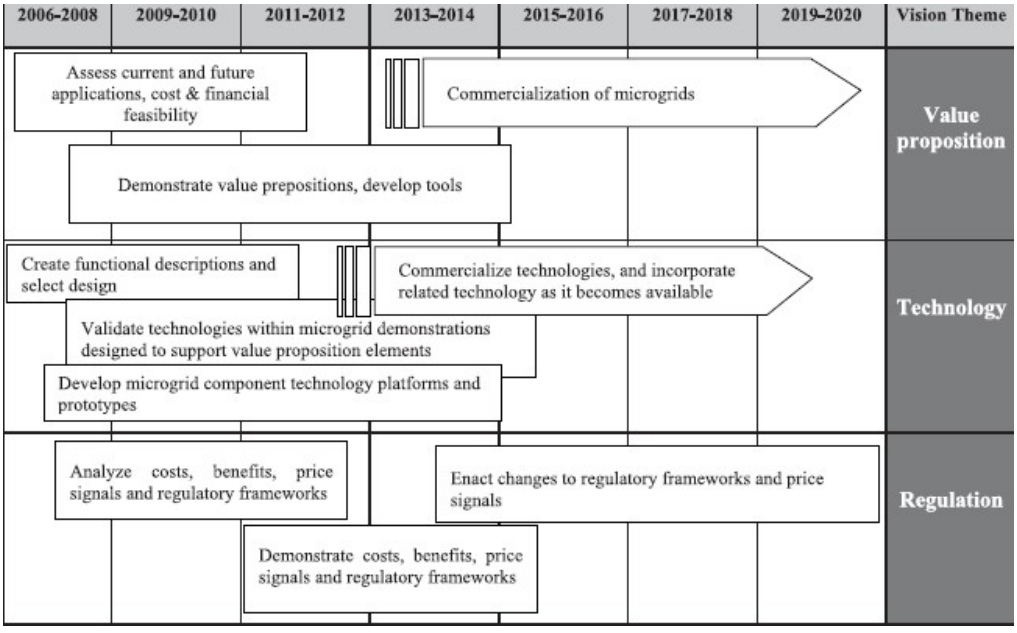

Figure 1.2 - MG evolution roadmap developed by NAVIGANT Consulting [27].

Started in 2008, the InovGrid project was considered a remarkable case study for testing and validation of SG concepts. This project aims to endow the distribution network with information and intelligent equipment capable of integrating EV and DER, stimulate an active consumers' participation, improve service quality and reduce grid operating costs, while fomenting environmental sustainability and energy efficiency. InovGrid is headed by the *EDP Distribuição* – Portuguese DSO -, although it gathers many industry partners and research institutions. Évora was the chosen city to serve as a test for the implementation of the SG concept. It is expected that other Portuguese cities, like Guimarães, will be part of this project as well [31]. InovGrid is part of a broader European project, the InSmart, whose principal objective is to develop sustainable energy action plans to implement in each partner city (Évora, Nottingham, Trikala and Cesena) [32].

Some other relevant experimental MG test systems are taking place around the world, namely [33]:

- Boston Bar – BC Hydro, Canada;
- Boralex Planned Islanding – Hydro Quebec (HQ), Canada;
- UW MG – United States;
- Bronsbergen Holiday Park MG – Netherlands;
- The Residential MG of Am Steinweg in Stutensee – Germany;
- CESI RICERCA DER Test MG – Italy;
- Kythons Island MG – Greece;
- Laboratory-scale MG System at National Technical University of Athens (NTUA) – Greece;
- DeMoTec Test MG System – Germany;
- University of Manchester MG/Flywheel Energy Storage Laboratory Prototype – UK;
- Aichi MG Project – Central Japan Airport City;
- Kyoto Eco-Energy Project (Kyotango Project) – Japan;
- Hachinohe Project – Japan;
- Sendai Project – Japan
- Test Network at Akagi of the Central Research Institute of Electric Power Industry (CRIEPI) – Japan;
- MG Testbed in Hefei University of Technology (HFUT) – China.

1.3 Objectives

The main purpose of this dissertation is to evaluate the reliability of a MG, and its advantages to the distribution system, operating in stand-alone mode, where reliability issues are more relevant and challenging, since while operating in NIM the various studies are more focused on addressing the interaction with the upstream network and its dynamic-related problems.

As mentioned in the previous section, to attain a successful deployment of the MG concept, an adequate regulation in view of a MG fully integration into distribution systems must be settled. As in every regulatory process, the identification of costs and benefits that the new concept may bring about is vital. It's clear that a reliability assessment is a crucial precedent stage of the development of such a regulation framework, since it can enrich the discussion about the way costs can be parted amid the different agents that benefit from MG operation.

The reliability security assessment is beyond the scope of this work, since the MG's dynamics and transient perturbations aren't considered. Thus, when the expression "reliability assessment" is presented, it refers to the reliability adequacy, whose concerns solely comprise the existence, or the lack of it, of enough generation to meet the demand. Due to the computational and simulational burden that the consideration of the system dynamic behavior would add to this problem, only static conditions are contemplated. It was admitted that the frequency and voltage regulation were provided by the ESS. This hypothesis is not unrealistic, since it was already addressed in the current literature [16], [34] and [35].

Being the chosen MG merely composed by solar photovoltaic (PV) microgeneration units, the presence of an ESS is demanded. In order to evaluate the impact of the ESS in MG's reliability assessment, several types of batteries were tested. This diversified evaluation helps to understand how the electric characteristics of the ESS influence the MG behavior in IM of operation.

In all the different simulations it was assumed that the microgeneration units were always available during the operation in IM, i.e., their probability of being unavailable is considered to be zero. It was assumed that the transition to the IM of operation was due to an upper system disconnection, through the action of the protection system. To simulate this transition, a random drawing of the hour, within one year, in which the failure occurred and its duration were executed.

To assess the performance of the MG the frequency and the duration of the outages were analyzed, as well as the Power Not Supplied (PNS) and other reliability indexes.

The software that was used to support the simulation framework based on the sequential Monte Carlo (MC) method was MATPOWER.

1.4 Outline

The work developed in this dissertation is organized into five different chapters. The first one covers the conjuncture that led to the study of this problem by referring its underlying motivation. The drivers behind the development of the MG concept; its social, economic and quality-related advantages; the current challenges imposed by its implementation and a concise information about ESSs are addressed. Also in this chapter, the objectives of this thesis are enumerated and explained, as well as some of the projects related to the concerned topic that are being carried out.

In chapter 2 the state of the art, regarding the most relevant studies that address the topic of reliability in a MG operating in NIM or IM, is presented. This chapter starts with a brief description of the MC method, more specifically the sequential simulation, where the mathematical expressions that characterized the Markov's based model of a two state component are also incorporated. The main reliability indexes related to the loss of load are defined and their purposes identified.

Chapter 3 presents all the aspects that required a proper modeling in order to describe the operation of the MG in stand-alone mode. The first section of the present chapter refers to the drawing process responsible for the sampling of several failures in the connection with the upstream network, being randomly obtained the hour in which the failure occurs and its duration. In this chapter an explanation concerning the technique to represent the load and PV generation within the whole year, divided in fifteen minutes time intervals, is provided. The

employed method to model the load and PV generation curtailment and the battery behavior is also addressed. Due to its relevancy, the formulation of the ESS is presented, regarding all its constraints, expression and other needed assumptions to simulate its behavior. Since it was used the software MATPOWER to run one OPF for each simulated period, its formulation is referred as part of the modelling-related topics. To finalize this chapter, and with the goal of introducing the next chapter, an explanation regarding the calculation of the reliability indexes whose comparison led to conclusions, the adopted stopping criteria and the proposed algorithm are addressed.

In chapter 4 the main results attained with the proposed algorithm are presented. First, a study about the impact of the chosen ESS model is conducted by performing diverse simulations with the five batteries considered. Subsequently, in order to yield an insight about the MG operation in stand-alone mode during an event, an analysis of the behavior of the test MG throughout the last three days of July is provided. Afterwards, an evaluation of the impact of different failure rates and MTTR in the component responsible for the failure is conducted, through the assignment of several values to the aforementioned parameters and observation of the induced changes in the reliability indexes. The comparison of the achieved reliability with and without MG is provided for every simulation. This chapter ends with an introduction of a new concept that allows a simplistic way of evaluating the economic benefits derived from the implementation of the test MG in the system.

Ultimately, the main conclusions of this dissertation are summarized in chapter 5. In view of the employment of future researches, based on the work developed in this thesis, some suggestions are made in this last chapter.

Chapter 2 - State of the Art

In this chapter a summary review of the state of the art of MG's reliability assessment techniques will be made. These studies are of great importance, since they are the basis in which the deployment of MGs can be implemented, with all sort of advantages to the today's and tomorrow's society.

Although much research about MG's reliability has been done in the last years, it's not common in literature to find a pure reliability assessment of a MG operating in stand-alone mode based on the MC simulation. Most of the conducted studies focus on the reliability of the distribution system when considering the implementation of MGs.

Due to the immense and historical importance of MC method on reliability assessment and its relevance to this dissertation, the first section of this chapter presents a brief introductory description of this method; yet, it is not related to the MG concept. Two used techniques to reduce the large number of samples – the Control Variates and the Importance Sampling – are also described in this section, being their mathematical expressions excluded from this description. The mathematical expressions that characterized the Markov's based model of a two state component are also presented.

Subsequently, the most common reliability indexes used to assess a system performance at load level are defined, namely the Loss of Load Probability (LOLP), the Loss of Load Expectation (LOLE), the Loss of Load Duration (LOLD), the Expected Power not Supplied (EPNS) and the Expected Energy Not Supplied (EENS).

The third section, and the state of the art of this thesis' *per se*, is composed of a survey of the current techniques used to assess performance reliability of a MG or a distribution system with various MGs, such as new probabilistic procedures and a new method based of Fault Tree Analysis (FTA).

The last section concerns the chapter's conclusion.

2.1 Monte Carlo Method

Monte Carlo simulation is a powerful tool to assess phenomena characterized by a probabilistic behavior [36]. The estimation of the reliability indexes is attained by simulating the stochastic behavior of the components that compose the system. MC simulation has two main advantages, namely [37]:

- The number of the needed samples to reach a desired level of accuracy is independent of the system size;

- Information about the variability of the reliability indexes is provided, since their probability distributions are known after the simulation.

This method can be divided in two types: the non-chronological and the sequential. As the name implies, the non-chronological MC doesn't consider the time dependence between samples. Therefore, by randomly drawing the state of all system components without taking into account sequential events, time correlations can't be modelled. The system state is attained through the state's drawing of each component. A conventional generator can be in one of the two following states, normally: "1", if the generator is operating, and "0", if it's not providing power at all. However, a multiple state model can be employed in order to consider partially damaged states. To perform a non-chronological simulation it is necessary to know the value of the probability of each component to be unavailable, as known as Forced Outage Rate (FOR), which can be determined through the analysis of the data relative to the occurrence of failures. For new equipment, the FOR has to be estimated by consulting the manufacturers or through analogy with the available information regarding the existing ones.

The sequential or chronological MC samples components up and down cycles, through the information provided by their probability distributions. By combining all the components cycles, the system operating cycle is reached [38]. This method enables the consideration of sequential issues like the time-dependent load curve and the chronological behavior of the system components [37]. Besides the knowledge of the FOR of each component that composes the system, to hold a sequential simulation it is also required to be aware of the probability density function related to the repair and operating times, which are characterized by the repair and failure rate, usually admitting exponential probability distributions.

Considering a component's two state Markov-based model, an illustrative example of its behavior is depicted in figure 2.1, where the up-state is represented by "1" and the down-state by "0".

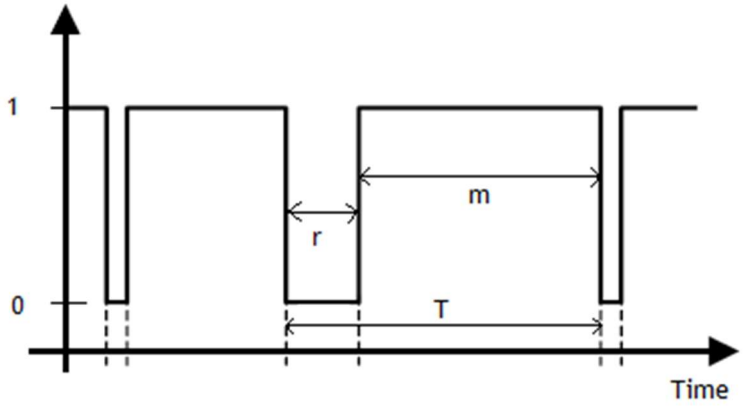

Figure 2.1 - Example of one component's life cycle.

The probability of being in the up-state and the probability of being in the down-state are given, respectively, by:

$$P_1 = \frac{\mu}{\lambda + \mu} = \frac{m}{m + r} \tag{2.1}$$

$$P_0 = \frac{\lambda}{\lambda + \mu} = \frac{r}{m + r} \tag{2.2}$$

where λ and μ represents the failure and repair rate of the component, respectively. Like it is observable in figure 2.1, m and r are time intervals, being the first the mean operating time and the last the mean repair time, usually presented in hours. The cycle time of the component, represented in figure 2.1 by T, corresponds to the sum of the Mean Time to Failure (MTTF) and the Mean Time To Repair (MTTR), and can be defined as the Mean Time Between Failures (MTBF). Expressions including the former concepts can be defined as follows:

$$m = MTTF = \frac{1}{\lambda} \tag{2.3}$$

$$r = MTTR = \frac{1}{\mu} \tag{2.4}$$

$$T = MTBF = m + r = \frac{1}{f} \tag{2.5}$$

where f represents the cycle frequency, i.e., the frequency of encountering a component state.

From equations (2.1), (2.3) and (2.5):

$$P_1 = \frac{m}{m + r} = \frac{m}{T} = \frac{1}{\lambda} \times \frac{1}{T} = \frac{f}{\lambda} \tag{2.6}$$

The same logic can be applied to (2.2):

$$P_0 = \frac{r}{m + r} = \frac{r}{T} = \frac{1}{\mu} \times \frac{1}{T} = \frac{f}{\mu} \tag{2.7}$$

From the equations (2.6) and (2.7) it's valid to conclude that:

$$f = P_1 \lambda = P_0 \mu \tag{2.8}$$

Analyzing the latter equation it can be inferred that the frequency of encountering the operable state can be attained through the product of the probability of being in the operable state and the rate of departure from this state or the product of the probability of not being in the operable state and the rate of entrance into the operable state. This conclusion is merely employed to the long term or average behavior of the system and to time independent frequencies and probabilities [39].

The principal advantage of the chronological MC over the non-chronological is its flexibility in representing precisely these time-dependent correlations, like the one between the load curve and the generator operation cycle, since some of them operate for most of the given time interval and others only start to provide power in periods of need, i.e., peak loads. However, the sequential MC has an obvious drawback: the needed computing time to obtain

the same exigency regarding the convergence criterion is substantially higher than the one attained with the non-chronological MC.

Two different methods for assessing system adequacy are presented in [37]: the State Duration Sampling Method (SDSM), when considering the sequential MC implementation, and the State Sampling Method (SSM), regarding the non-chronological MC simulation.

Since only the sequential MC will be employed further in this thesis, the emphasis will be put in the SDSM.

The first step of the SDSM is to draw the MTTF and the MTTR of each unity, according to the probability distribution of each of those stochastic variables, in order to obtain its lifetime line. After repeating the former step for the settled duration of the event (one year, for example), the chronological evolution of the whole system can be obtained, being the next residence state the one with the lowest transition time, i.e., the time interval until the first failure occurs in a certain component. Subsequently to overlap the load curve, which is normally based on a forecast, with the systems available capacity curve, the reliability indexes can be calculated [37].

The previously described process is repeated until the desired accuracy is achieved, which is specified in terms of a stopping criterion that is settled through the definition of the coefficient of variation of one or more indexes, whose expression (2.9) is presented below:

$$\beta = \sqrt{\frac{\hat{V}(F)}{N \times \hat{E}(F)^2}}, \tag{2.9}$$

where F represents the index to estimate, $\hat{V}(F)$ the non-biased estimation of the index variance, N the number of events and $\hat{E}(F)$ is the estimated expected value of the index. $\hat{V}(F)$ and $\hat{E}(F)$ can be calculated through the following expressions:

$$\hat{E}(F) = \frac{1}{N}\sum_{i=1}^{N} F(x_i) \tag{2.10}$$

$$\hat{V}(F) = \frac{1}{N-1}\sum_{i=1}^{N}\left[F(x_i) - \hat{E}(F)\right]^2 \tag{2.11}$$

The simulation will stop when the coefficient of variation of the chosen indexes is inferior to a threshold value, usually 0.05 %.

The knowledge of $\hat{V}(F)$ allows the estimation of a confidence interval for $\hat{E}(F)$, which means that there will be a certain probability that the confidence interval comprises the exact value of the desired index. The convergence of the MC method is settled through the determination of a sufficiently narrow confidence interval [36]. For a confidence level of 95%, the confidence interval will be:

$$IC(95\%) = \left[\hat{E}(F) - 1.96 \times \hat{E}(F) \times \beta \; ; \; \hat{E}(F) + 1.96 \times \hat{E}(F) \times \beta\right] \tag{2.12}$$

in which 1.96 is the value that corresponds to a probability of 0.95, attained through the integral of the probability density function of N(0,1).

The principal advantages of the SDSM are the simplicity to obtain the reliability indexes related to frequency, the use of non-exponential probability distributions to simulate component state durations and the simple inclusion of the aforementioned generators that only operate when the system load is almost at its peak value.

When compared to the SSM, the SDSM consumes more memory and has a higher computing time.

Figure 2.2 depicts the evolution of the expected value of one reliability index calculated by various different simulations of the MC method. As can be seen, all the simulations converge to similar final values of the reliability index. This difference is due to the fact that MC simulations are statistical based methods, and not analytical ones.

The use of simulation methods requires a vast number of samples in order to obtain acceptable results, which are translated into a heavy computational burden. Observing (2.9), and considering that the coefficient of variation (the method accuracy) is to remain unaltered, it's clear that to achieve a reduction in the number of samples the variance must be decreased. Two techniques have shown their efficiency in the past, namely the Control Variates technique and the Importance Sampling technique [40].

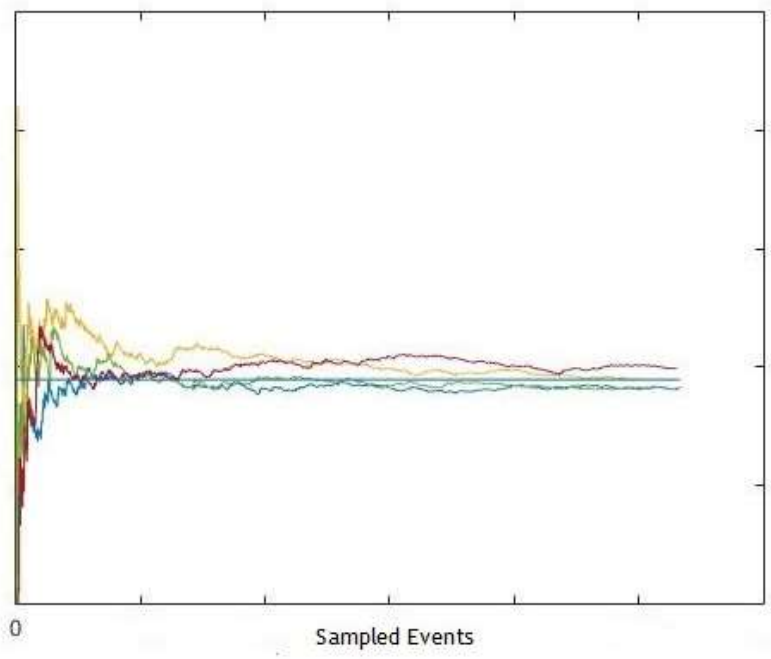

Figure 2.2 - Evolution of the expected value of one reliability index.

An alternative to using the traditional MC method is the employment of Population-based (PB) methods, which consists of enumeration algorithms [41]. The premise behind these methods is that if all the states than contribute to an index could be identified and have their probabilities of occurrence know, the regarded index can be accurately obtained. Thus, PB methods try to find the majority or the totality of the states. These methods can be divided in Evolutionary Algorithms (EAs) and Particle Swarm Optimization algorithms (PSOs).

These methods aren't statistical, so, an interval of confidence for the index is not obtained. The typical stopping criterion relies on the stability of the result, i.e., after a certain number of iterations without significantly progress, it is considered that the method have reached the neighborhood of the real value and, therefore, is stopped. An advantage of using the PB method

is that, if the conducted search is effective, the value will be attained long before any admissible interval of confidence calculated through a MC simulation. A possible drawback is the repeated visits to the same state, in case of a non-satisfactory performance of the method. Also, a memory that enables the tracking of the visited states and the recognition of new ones must be implemented. Searching through this memory will become increasingly time-consuming as the method advances, since a relevant amount of states gave already been visited. However, the search is more important precisely at the end, due to the growing of the rate of visit repetition when the majority of relevant states have been visited. Although, considering that the components have the same characteristics, the obtainment of the permutations or combinations of these elements that produce an equal effect, dispensing the need to visit all states.

The PB can be employed to decrease the computational burden in the sequential MC, as it shown in [42], where a list of generation states with a capacity inferior to the system peak load is created, through the use of a PB method. In a second phase, the generation states sampled with the chronological MC are compared to the ones that compose the list. The goal of this procedure is to decide if the system state evaluation should be performed or not. If the evaluation is employed, the yearly load model and the time-dependency of the generator capacity are considered, in order to create system states which may have loss of load. Otherwise, it is considered that the loss of load is null.

2.1.1 Control Variates Method

The theoretical basis of this convergence acceleration technique is the attainment of one approximate value for the one that is supposed to be determined, through an analytical and Monte Carlo-independent method [36]. The most challenging and important part of this technique regards the choice of the desired index approximation, i.e., the control variable. The more correlated the control variable and the desired index are, the greater the acceleration obtained will be [37].

The MC simulation is, therefore, used to determine the difference between the approximation and the desired index.

2.1.2 Importance Sampling Method

In order to apply this method a distortion of the probability density function of sampling is carried out, with the objective of increasing the occurrence probability of relevant events, to the detriment of the occurrence of the irrelevant ones. In power system reliability analysis, a relevant event is the one that leads to a load curtailment. This technique requires the knowledge of an auxiliary probability density function, from which the events are drawn, obtained through the use of analytical processes. Analogously to the aforementioned control variates method, the variance reduction relies on the similarity between the two probability density functions. The knowledge contained in the analytical probability density function enables the reduction of the estimated variance obtained through the use of the MC method.

Theoretically, it is possible to achieve the estimation of the expected value of the desired index with solely one sample, but this phenomenon depends on the knowledge about the value that is supposed to be estimated, thus it is impossible to apply [36].

In [43], a new algorithm, based on a combination between the cross-entropy concept with the usual analytical assessment, to estimate the optimal importance sampling probability distribution in generating capacity reliability problems is presented. An analysis of the cross-entropy typical equations was employed in order to demonstrate that the optimal sampling distribution can be attained through the quotient between the generating capacity reliability indexes and two different system configurations. The results obtained in this research, which is based on the fast Fourier transform, proved an equivalency between the proposed approach and the standard cross-entropy optimization method, in terms of accuracy and computational burden. Nevertheless, the technique suggested in this work provides a significantly easier implementation.

Empirical data evidence the easiness of applying the control variates method over the previously described, due to the difficulty in setting a probability density function with the desired properties [36].

2.2 Definition of the Main Reliability Indexes

The most used indexes that can be obtained from a sequential MC simulation are:

- Loss of Load Probability (LOLP);
- Loss of Load Expectation (LOLE);
- Loss of Load Frequency (LOLF);
- Loss of Load Duration (LOLD);
- Expected Power Not Supplied (EPNS)

Both LOLP and LOLE represent the probability of the incapacity of the system to supply the demand, i.e., the average number of fifteen minute periods, hours or days – depending on the basis of the load and RES generation models -, where it is expected that the peak load will exceed the available generating capacity in the assessment period (one year, for example). The difference between these two indexes relies on the fact the LOLP is dimensionless and can assume a value between 0 and 1, since it's a probability measure, whereas the LOLE is represented in hours per day, for example. The relation between both is represented by the equation (2.13).

$$LOLE = LOLP \times \Delta T \ , \tag{2.13}$$

where ΔT represents the duration of the assessment period.

The LOLF expresses the expected number of occurrences of a load curtailment during the assessment period, and is normally presented in failures per year.

The LOLD measures the expected duration of a failure and is normally presented in hour/occurrence. Known the LOLE and the LOLF, the LOLD can be calculated as follows:

$$LOLD = \frac{LOLE}{LOLF} \tag{2.14}$$

The last one, the EPNS, measures the real impact of the system unavailability from a power point of view. The EPNS represents the expected power that won't be supplied, due to failures. This index is normally presented in MW.

2.3 MicroGrid's Reliability Assessments – Proposed Approaches

A global view regarding islanded MG's or distributions systems with MG's reliability assessments will be presented in this section. After a conducted research about the topic under study the employed methods can be divided as follows:

- MC simulation;
- Markov Chain Monte Carlo (MCMC);
- Hybrid approach combining Genetic Algorithms and MC simulation;
- Approaches based on MC simulation;
- Other probabilistic approaches;
- New approach based on Fault Tree Analysis (FTA);
- Short-term Outage Model;
- New approach based on Markov processes;
- New analytical technique.

2.3.1 MC Simulation

In [14], a procedure of reliability assessment for MGs including RES, more specifically wind power and PV cells was proposed. An index to reflect the impact of power outages using MC simulation and another one for evaluate MG's reliability based on the generation-demand equilibrium was introduced, from the customers' perspective. The consequences of ESS were also examined.

The first step of this analysis is the initialization of the system state, succeeded by the sample of fault conditions reflecting the failure rates of all components. A load flow analysis was employed to verify the occurrence of a system contingency, due to the happening of an equipment failure. In the event of a contingency this work proposes a solution based on emergency operation of the concerned area. If this option is unavailable, the area where a supply interruption occurred is identified and the unsupplied load is quantified. These steps are repeated until the desired accuracy is obtained. Lastly, the initially proposed reliability indexes are calculated, namely the interruption cost and the demand and supply balance cost.

A reliability comparison between two different networks – radial and looped - is also made. As expected, the interruption duration and the Expected Energy Not Supplied (EENS) are higher in the radial configuration, owing to the fact that in the event of a failure the looped network is still capable of supplying the demand because its inherent redundancy.

The addition of one battery led to a reduction on the interruption cost and demand and supply balance cost.

2.3.2 Markov Chain MC Simulation

The economic impact of High Reliability Distribution System (HRDS) in a MG composed of DER, controllable loads and storage, is studied in [24]. The implementation of MG loops is achieved through the use of automatic switches in HRDS.

The MG is operating in NIM, using both local DER and the main grid for the economically supply of its hourly load, being this operation subject to reliability requirements. The availability of feeders, upstream grid supply and MG generation is considered using the MCMC simulation. The frequency and duration of outages are evaluated at the MG and load point level. The random outages are represented by the MC method, while the Latin Hypercube Sampling (LHS) technique is utilized in order to generate a vast number of scenarios with equal occurrence probabilities. A two-state Markov Chain process is employed to represent MG's outages, in accordance with its component's failure and repair rates. With the aim of eliminating the low probability events, a scenario reduction technique is applied. MG's reliability indexes are obtained and then compared with and without HRDS switches.

This paper has concluded that ESS can reduce the operating cost of a MG, since it can supply the demand in the occurrence of failures, avoiding load curtailments. The same can be said for the implementation of HRDS switches, which reduced the test MG (Illinois Institute of Technology MG) expected loss of load frequency and duration, and its EENS. HRDS also provoked economic benefits regarding the MG operating cost, since they have the ability to reduce load curtailments.

2.3.3 Hybrid approach combining Genetic Algorithms and MC simulation

A reliability evaluation of a Small Isolated Power System (SIPS) with RES and storage capacity is employed in [44]. This work studies the effect of customer worth of interrupted supply on the optimal design of the aforementioned SIPS, which is implemented with a GA combined with local search procedure. Sequential MC simulation is employed to evaluate the effect of the FOR of SIPS components on its optimal design. The goal of this analysis is to evidence the difference between the results achieved with and without the consideration of customer worth of interrupted supply and component's FOR.

The customer worth of interrupted supply can be defined as cost, presented in €/kW, that depends on the interruption duration and the customer sector (agricultural, residential or industrial).

The reliability indexes increased with the consideration of the component FOR, as expected, since the FOR represents the component probability of being in down-state. When considering the customer worth of interrupted supply the variability of the reliability indexes and the cost of energy increased, which can transform a feasible solution of the conventional optimization into an impracticable one, hence the relevance of this analysis for the performance of SIPS.

2.3.4 MC simulation-based Approaches

In [45] a new approach to assess the reliability of a distribution system while considering MGs operating in stand-alone mode is presented. Probabilistic models were used to obtain the adequacy of conventional generators and RES as MG sources of supply. This paper provides a

set of analytical expressions to evaluate the performance of distribution systems in terms of reliability, being the MGs allowed to operate in IM, so that the MMG concept can be implemented.

Another analytical expression is presented in order to calculate the adequacy of MGs while taking into account load curtailment. The sequential MC simulation is used due to variability of distributed generators, whose output heavily depends on the on-site weather conditions, and provides the value of the classic reliability indexes, such as LOLE, LOLP and EENS.

It has been demonstrated, through the application of the proposed procedure on the IEEE RBTS-BUS6 network, with some conventional generators and RES added to it, that when islanded operation was enabled, the local and global reliability indexes suffered a notably improvement.

In this paper the dynamic aspects were neglected, and assumptions have been made about the availability of an advanced automation and protection scheme, in such a way that incompatibilities between the interface of distributed generators and network protections were prevented.

A MC simulation-based technique for reliability assessment of active distribution systems with several MGs is proposed in [46]. In order to represent diverse types of distributed generators, multi-state models based on Generalized Capacity Outage Tables (GCOTs) were developed. Then, a novel concept – the virtual power plant, which can be defined as single unity that aggregates all MG components – to model MG with RES is introduced and its reliability is characterized resorting to a GCOT. Furthermore, the non-chronological MC method is used to evaluate the reliability of the active distribution system, either at MG or at main grid levels. In this assessment distinct operations modes are regarded. The convergence of the non-sequential MC method is accelerated through the adoption of some techniques, such as the two-step sampling and the minimal path search.

Adequate models for distributed generators were adopted in order to account for the inherent intermittency and characteristics of its conversion systems. A GCOT with information concerning distributed generators, distribution lines and the load of a MG was attained, after setting the GCOT for each distributed generator. The multi-state virtual power plant model is established through the GCOT of the MG, which indicates the MG mode of operation and whether it's viewed as a load or a source, from the distribution system perspective.

After the application of this method to the RBTS test feeder and to a distribution system in Northwest China, it was observed that the reliability indexes of the entire system improved in the presence of MGs.

In [47], a reliability evaluation for MGs operating in stand-alone mode that represents DER and its stochastic behavior is introduced. This assessment is based on MC simulation, which allows the representation of a component failure and repair cycle, being used historical data to model the distribution generators intermittent output. For each component is assumed an independent probability distribution function, which translates in a disregarding of the co-dependent failures of distributed generators. A set of reliability indexes is obtained after the application of the MC, namely the EENS, the unavailability, the repair time and the interruption frequency. An interruption occurs whenever the available capacity is inferior to the load level, after subtracting the voluntary load curtailment.

This method also analyses the impact of the correlation between the distributed generators and the load in the MG reliability, being obtained a correlation coefficient. DG is allocated based on a prioritized load order that considers the dynamic reconfiguration of the MG in the

occurrence of a fault. Dispatchable DERs aren't considered in this work, since the MG is composed only by PV generation.

Other aspect that is studied in this paper is the consequences for the reliability that a voluntary load curtailment can bring. Thus a load curtailment coefficient is calculated, being the reliability indexes evaluated as a function of it.

After the simulations, it was concluded that as the value of the load curtailment coefficient increases, EENS experiences an expressive reduction, due to the fact that the load that may be involuntary curtailed suffers a reduction as well. This coefficient doesn't inflict major changes in the value of the frequency and duration of interruptions. It was also inferred that the rise of the correlation coefficient can deteriorate the reliability of the MG.

A two-step MC simulation is developed in [48] in order to accomplish an assessment not only of the reliability of a MG with distributed generators, but also of the DN considering the implementation of MGs. The goal of the first step is to evaluate the reliability of the distribution system while considering MGs as loads connected at their PCC. In the second step of this proposed method, the distribution system is replaced by an equivalent conventional generator and the reliability of the MG is assessed. New indexes to evaluate the effects of interruptions in the distribution system and the transition between the MG two modes of operation are presented. A two-step MC method was chosen due to the inefficiency inflicted by the distinct time units that characterized the MTTF and the MTTR, on one hand, and the variability of atmospheric conditions, on the other one. The proposed work is then applied in the IEEE-RBTS.

It was deduced that a higher renewable power penetration led to an increasing in the reliability indexes, mainly because of its intermittency, especially when the MG is operating in IM., where the interruptions in the load supply are more recurrent. Improvements in the reliability of the distribution system were observed when considering the presence of MGs.

The dynamic aspects of islanding and the transient behavior of generators and electronic devices was neglected in [48].

2.3.5 Other Probabilistic Approaches

In [49], a probabilistic technique to evaluate the reliability performance of a MG with high PV penetration operating in IM is presented. This method regards the intermittency of ESS and PV generating units. The MG is composed by conventional generators as well. In order to consider the effect of component's fast ramp up/down in the reliability adequacy of the MG, whose impact is reflected in the EENS and Expect Energy Not Used (EENU), a minutely time step is adopted. A representative model of the variation of the storage's SOC is also proposed. To express the reliability of the PV system it was employed a model based on the total cross-tied configuration of PV cells and arrays.

To assess the reliability of the PV system a two-state component reliability model is used to determine the system contingency states, considering component's failures. It was supposed that the PV units' inverters could be controlled in order to achieve the maximum possible output power. Concerning the load characteristics, it was assumed that within each minute the load level is ramping upwards or downwards.

Considering the minutely changes in load levels and RES, conventional generators and ESSs need to ramp up or down to balance the mismatch between generation and demand. Three different cases were tested to evaluate the efficiency of islanded MGs under diverse conditions, namely: a MG with conventional generation; a MG with conventional generation and PV systems;

a MG with conventional generation, PV systems and ESSs. It was shown that the addition of PV systems increases the values of EENS and EENU, due to its variability, when compared to the case with solely conventional generators. The presence of an ESS reduces the EENS and the EENU.

In order to assess the reliability of the distribution system with wind-based distributed generators during the IM of operation, a probabilistic technique is proposed in [50]. A new constrained Grey predictor method for wind speed estimation is employed.

The first stage of this approach is to calculate the probability of establishing an island, which relates to the system configuration. This was achieved through the application of the segmentation concept, i.e., modeling the distribution system based on segments, not components. A segment can be defined as an agglomerate of components whose input component is a protective device.

Subsequently, the probability of the island to succeed, which depends on the intermittent behavior of the distributed generators and the demand profile, will be determined. To consider the island operation a success the power output of its distributed generators must be superior or equal to its demand plus the inherent power losses. Considering that the probabilities obtained in the aforementioned two steps are independent, the probability of the occurrence of an islanding and its adequate operation can be obtained by the product of the two probabilities.

It was observed that the amelioration in the system reliability tends to stabilize with the increase of the wind power penetration, thus, from the reliability perspective, it's superfluous to higher this penetration above certain level. However, other aspects can be analyzed, such as the economic and environmental impacts.

2.3.6 New FTA-based Approach

A new approach based on FTA analysis to assess the reliability of a MG, from the consumers' point of view, operating in IM is discussed in [51]. FTA, which analysis the connection between components and system's failures, is one of the most utilized methods in reliability evaluation.

The assessment process contains five diverse steps, namely: the development of consumers Reliability Block Diagram (RBD); the design of the fault tree, which depicts all the possible sequence of events whose happening provokes the unwanted event (load curtailment, for example); the setting of components failure rates and probabilities; the determination of the probability of interruptions in the power supplying and the calculation of measures of importance.

The method was tested on a LV MG benchmark composed by a small number of diesel-fueled generators and consumers, wind turbines and an ESS.

2.3.7 Short-term Outage Model

In [6] is presented a short-term outage model that analysis the impact of the protection system and operating conditions on the reliability indexes of a MG. To achieve that, failures on the main feeder and on the lateral distributor are modeled. A hybrid approach that relates scenario selection, in order to reduce the computational burden, and enumerative analysis incorporated in a heuristic sequence approach is therefore proposed, with the goal of evaluating the operational reliability of the MG.

The reliability indexes attained with this model are analogous to the ones employed for distribution system reliability assessment, such as the System Average Interruption Frequency Index (SAIFI), the System Average Interruption Duration Index (SAIDI) and the EENS.

The influence of different types of microsources, the site-related meteorological conditions and the load fluctuation in the MG reliability was investigated as well.

This proposed approach yields a feasible solution to evaluate the impact of protection system incorrect actions on the reliability assessment.

2.3.8 New Markov-based Approach

A new method for quantifying the reliability of a MG operating in IM with limited stochastic resources is proposed in [52]. The correlation between PV generation and the load is considered through the creation of a combined Generation-to-Load Ratio (GLR), modeled as a Markov process, which is defined with respect to a load curtailment coefficient. The influence of Stochastic Distribution Generation (SGD) on an islanded MG's reliability is studied in this paper, as well as the advantage to the reliability that comes in enabling load curtailment or increasing local generation.

The attained results showed that the behavior of the SGD and the load have a relevant impact on the reliability indexes. A higher PV penetration or an increasing enabled load curtailment can lead to an increase of the interruption frequency.

2.3.9 New Analytical Technique

An analytical method to assess the reliability of customers in a MG with DG is presented in [53]. The subject system includes PV systems and fuses. In order to gather information on the restoration sequence in case of failure, connection matrices of distribution generators were defined. It's proposed a novel algorithm to recursively compose the connection matrix of DG, by means of using a matrix to express the physical configuration of the distribution system. The RBTS Bus 4-based case study includes diesel and PV generators and fuses.

It was assumed that each MG priority is to supply their own customers, therefore it isn't responsible for the customers of other MGs. The equations to assess system reliability were transformed in order to cover the situations where there are two or more components in a specific section.

Three different numerical studies were conducted: the first used a MC simulation to serve as a comparative basis for the proposed method; the second one tested the introduced analytical technique and the last one differs from this one because it uses peak load instead of the load duration curve. It was observed that the accuracy of the novel proposed technique is similar to the one attained from MC simulation.

2.4 Conclusions

An overview of the state of the art, regarding MG's reliability assessment, was presented in this chapter. Several methods can be employed to evaluate MG reliability, having each one of them their advantages and drawbacks. Depending on the specific purpose of the research, one technique can be more appealing than the others.

As it was discussed, most of the developed studies focused on the reliability evaluation of a MG when it is operating in NIM, but few was done to quantify the adequacy performance of a MG since the moment that it starts to operate in stand-alone mode until it's reconnected to the upstream network. Especially when considering a MG composed merely by RES, without any conventional generator, which makes this study more complicated, since its intermittent behavior. Nevertheless, the reliability assessment of an islanded MG is essential for the envisioned implementation of the SG concept.

This work aims to endow the possibility of a more sustainable future for the electric sector, by providing an insight into the performance of a test MG.

Chapter 3 - **Modeling the Problem**

The modeling of all the MG's components will be presented throughout the current chapter, namely the loads, the PV generators and the battery.

Firstly, the mathematical formulation of the two draws, regarding the period of the year in which the occurrence of a fault in the upper system leads the MG to operate in IM and the duration of that islanding, applied to simulate the disconnection from the upstream network is addressed.

Then, in order to characterize the load and generation profiles, it was utilized the information provided by ERSE (*Entidade Reguladora dos Serviços Energéticos)*, the entity responsible for regulating the electricity and natural gas sectors. Under the directive n.º17/2015, to be applied from January 1 until December 31, respecting the year of 2016, two energetic profiles were downloaded and subsequently adopted in this work, namely the demand profile for Normal Low Voltage (NLV) and the generation profile concerning the solar PV small power technology. These profiles are discretized in 35136 periods of 15 minutes, describing the whole year variation. Thus a time frame of fifteen minutes was chosen to observe the chronological evolution of the MG.

A brief description of the chosen technique to obtain the curtailed load and the curtailed PV power is also included in this chapter.

The fourth section concerns the adopted procedure to model the battery behavior. To model its action two dummy generators were added to the bus where the battery was installed. However, it is important to refer that the battery either works as a generator or as a load. A third dummy generator was introduced in order to model the injection of reactive energy into the MG. A diverse range of Li-ion batteries solutions, provided by SAFT, were modeled, considering all its power and energy ratings. The underlying reason to do that is the possibility to assess the impact of the characteristics of an ESS in a MG.

In the next section, the Optimal Power Flow (OPF) formulation implemented in MATPOWER version 5.1 – the adopted software to analyze power flows in this thesis -, used to simulate the MG behavior while in IM of operation in each period of fifteen minutes, is displayed.

The next two sections of this chapter yield information about the adopted stopping criteria, based on the calculation of several coefficients of variation, and the expressions from which the final reliability indexes were attained, considering the results obtained after each simulation.

Having been modeled all the MG components and their corresponding behaviors, an algorithm of the proposed method to assess the system reliability is presented.

In the final section of the present chapter the conclusions will be presented.

3.1 Transition between NIM and IM of Operation

The first step required to model the transition of the MG's mode of operation from NIM to IM is the drawing of the fifteen minute period in which the systemic blackout, with survival of the MG, occurs. This randomly generated number can vary between 1 and 35136, since 2016 has 366 days: $366 \times 24 \times 4 = 35136$. The islanding caused by the aforementioned failure will be denominated as *event* throughout the present dissertation.

The following step concerns the draw of the time interval in which the MG operates in stand-alone mode, i.e., the duration of the event. It was assumed that the state duration of the component responsible for the islanding of the MG follows an exponential distribution. Thus, the sampling value of the duration of the MG islanded mode of operation can be obtained as follows:

$$d_{IM} = -\mathrm{MTTR} \times lnR_t \ , \tag{3.1}$$

where MTTR is the upper system Mean Time to Repair (MTTR), i.e., the average time needed to repair and return it to ordinary operating conditions, and R_t is a uniformly distributed random number between 0 and 1.

To convert that hourly value in a fifteen minute-based one, d_{IM} was rounded to the nearest integral greater than or equal to its former value. Afterwards, a simple product of this number by four indicates the number of fifteen minutes' periods in which the MG operated in stand-alone mode.

3.2 Load and PV Generation Profiles

In order to characterize the demand for the whole year, the data provided by ERSE (*Entidade Reguladora dos Serviços Energéticos)*, the entity responsible for regulating the electricity and natural gas sectors, was employed [54]. The directive n.º17/2015, to be applied from January 1 until December 31, respecting the year of 2016, yields the percentage values of the consumed energy, regarding the annual consumed energy, for every period of fifteen minutes throughout the year.

The provided energy values are discriminated in three different profile classes: NLV A, NLV B and NLV C. These diverse profiles were approved by ERSE under the directive n.º5/2014. The distinction is based on the contracted power and the average annual energy, as shown in the following table:

Table 3.1 - Standard demand profiles for NLV.

Profile Class	Contracted Power (kVA)	Annual Consumed Energy (kWh)
A	>13.8	any
B	<=13.8	>7140
C	<=13.8	<=7140

A proper load bus differentiation is thus required. The first step is the obtainment of the contracted power. It was assumed that the total contracted power of each load bus corresponds to the sum of the contracted power in each of the three-phases.

Subsequently, in order to distinguish the value of the annual consumed energy in each load bus, the inverse of the normal cumulative distribution for a specified mean and standard deviation was calculated. A randomly generated probability corresponding to the normal distribution was assigned to each load bus. Based on historical data regarding the annual consumed energy for each level of contracted power – 3.45, 6.9, 10.35, 13.8 and 17.25 kVA -, the arithmetic mean of the distribution was attained.

Table 3.2 - Average annual energy differentiated by level of contracted power.

Contracted Power (kVA)	Average Annual Energy (kWh)
3.45	2401.05
6.9	4905.93
10.35	6959.20
13.8	10001.49
17.25	14695.98

It was assumed that the standard deviation was 10% of the aforementioned arithmetic means.

The annual consumed energy for each bus was obtained from Excel function NORM.INV, thus allowing the assignment of a profile class to every consumer. The following example depicts the previously described process.

Table 3.3 - Example of the process to assign a profile class to a consumer.

Contr. Power (kVA)	Arith. Mean (kWh)	Stand. Deviation	Prob.	Annual Consumed Energy (kWh)	Profile Class
6.9	4905.931601	490.5931601	0.28	4621.49	C

Since the contracted power is less than 13.8 kVA and the annual consumed energy is less than 7140 kWh, it is assigned to this client the profile class C.

The next step concerns the attainment of the whole year demand variation for each bus, in terms of its two components: active and reactive, represented by equations (3.2) and (3.3), respectively:

$$P_{load_i} = \frac{W_{ERSE_{load}} \times W_i}{\Delta t \times 1000}\ , \tag{3.2}$$

where P_{load_i} (kW) represents the active load in the *ith* bus, $W_{ERSE_{load}}$ the value given by ERSE, W_i the annual consumed energy in the *ith* bus and Δt the time period, so $\Delta t = 15\,\mathrm{min} = 0.25\,h$, which is multiplied by 1000, since the sum of the values provided by ERSE to each profile class is equal to 1000, therefore, in order to obtain the active load in kW this numerical conversion is required.

Considering that each one of the loads has the same power factor ($\cos\varphi$):

$$Q_{load_i} = P_{load_i} \times \tan\varphi\,, \tag{3.3}$$

where Q_{load_i} (kVar) represents the reactive load in the *ith* bus.

Figure 3.1 and 3.2 presents the load (NLV C) and the PV generation profile provided by ERSE, respectively.

A similar method was followed in order to set the PV generation. According to [54] and under the aforenamed directive, the fifteen minutes-based applicable profile to the solar PV small power technology was obtained. This data is provided in terms of energy percentage, therefore a proper unit conversion is required to present the collected information in terms of kWs.

The initial step regards the attainment of the total electricity production from the given system in one year. To estimate this value, the services provided by PVGIS (Photovoltaic Geographical Information System) [55], were utilized. An example of the output of [55], considering Porto, Portugal, as the location, can be seen in figure 3.3. The aforementioned website also allows the selection of the PV technology, the installed peak PV power, the estimation of the system losses and other characteristics of the PV system.

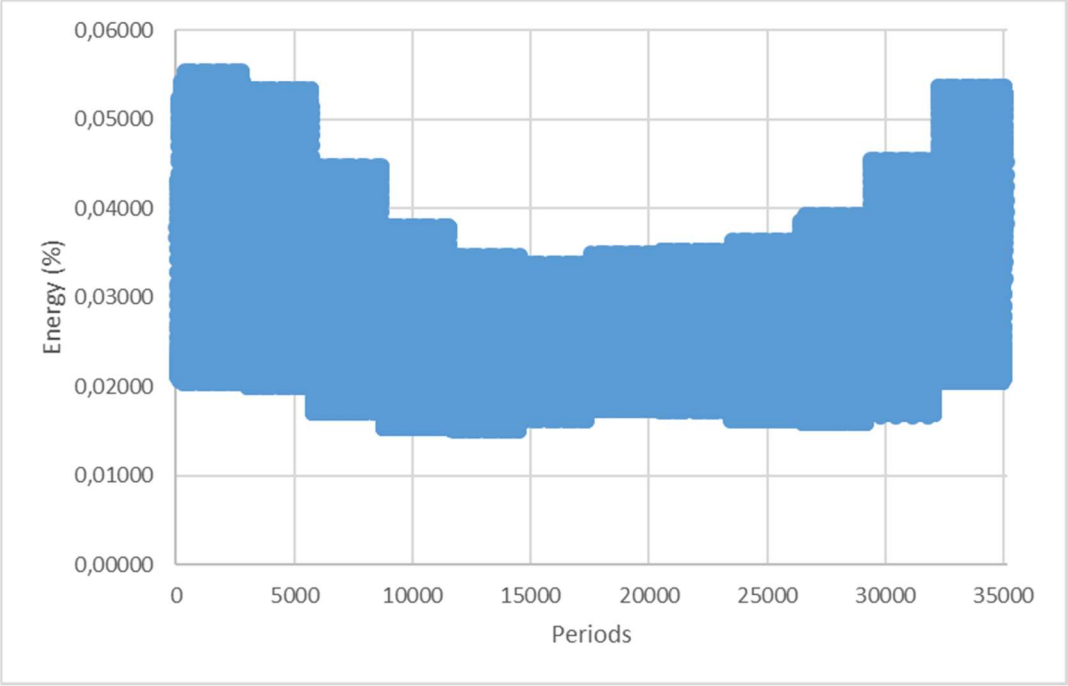

Figure 3.1 - Load profile, of a NLV C client, provided by ERSE.

As it was expected, the consumed energy is higher in the coldest months, due to air conditioning and less sunlight.

Figure 3.2 manifests a well-known outcome as well: in the summer the PV generation is higher, due to longer and more intense sun exposures.

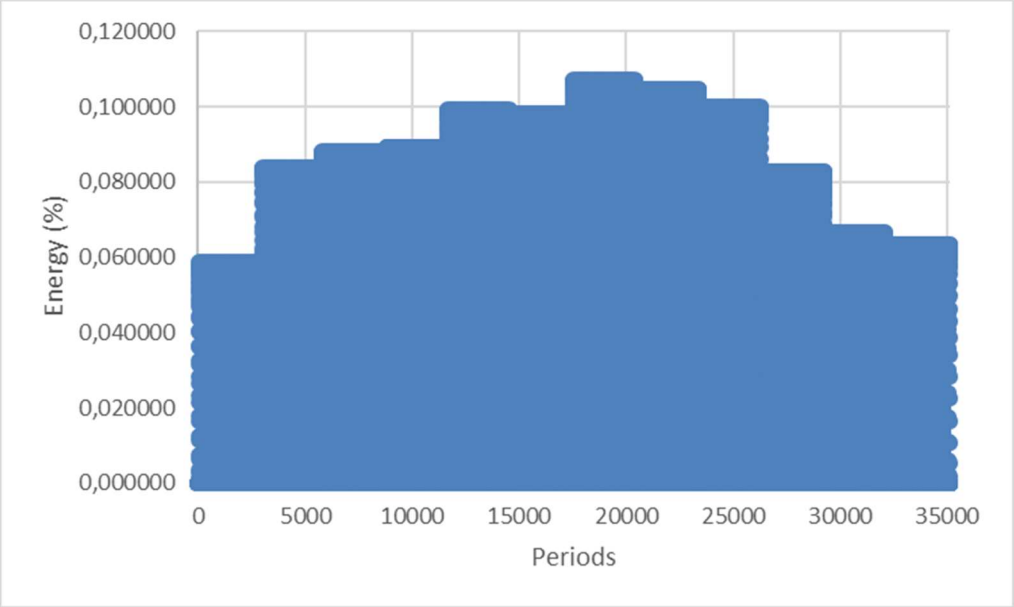

Figure 3.2 – PV generation profile provided by ERSE.

Nominal power of the PV system: 1.0 kW (crystalline silicon)
Estimated losses due to temperature and low irradiance: 11.4% (using local ambient temperature)
Estimated loss due to angular reflectance effects: 2.6%
Other losses (cables, inverter etc.): 14.0%
Combined PV system losses: 25.8%

Fixed system: inclination=34°, orientation=-1° (optimum)				
Month	E_d	E_m	H_d	H_m
Jan	2.84	88.1	3.61	112
Feb	3.72	104	4.80	135
Mar	4.44	138	5.89	183
Apr	4.51	135	6.06	182
May	4.76	148	6.49	201
Jun	5.00	150	6.97	209
Jul	5.27	163	7.40	229
Aug	5.15	160	7.26	225
Sep	4.73	142	6.56	197
Oct	3.89	121	5.22	162
Nov	3.14	94.2	4.09	123
Dec	2.64	81.7	3.36	104
Yearly average	**4.18**	**127**	**5.65**	**172**
Total for year		**1520**		**2060**

E_d: Average daily electricity production from the given system (kWh)
E_m: Average monthly electricity production from the given system (kWh)

Figure 3.3 - Example of the output provided by [51], regarding PV generation.

The following equation enables the obtainment of the PV generation profile for the whole year:

$$P_{PV} = \frac{W_{ERSE_{PV}} \times W_{PV}}{\Delta t \times 1000}, \tag{3.4}$$

where P_{PV} (kW) represents the power generated by the PV system, $W_{ERSE_{PV}}$ the value given by ERSE (1520 kWh, according to the example provided in figure 3.1), W_{PV} the annual generated energy by the PV system, obtained through PVGIS, and Δt as the same aforementioned meaning and value.

A null cost of operation was assigned to all the PV generators.

It is worth mentioning that the values provided by (3.2), (3.3) and (3.4) enable the conceiving of profiles with 35136 different elements. Notwithstanding, from the two draws mentioned and explained in the first section of the present chapter, can result an index mismatch regarding the aforecited profiles. For instance, if the obtained period from the first draw is 35134 and $d_{IM} = 4$, it would result that for the last simulated lapse there wouldn't be available elements of P_{load_i}, Q_{load_i} and P_{PV}. In order to circumvent this setback, it was considered that if the duration of the islanded mode of operation exceeds the last interval, the count will restart from the beginning of the year, i.e., instead of searching for P_{PV} in the 35137th period it will adopt its value in the first one, and so on.

3.3 Load and PV Generation Curtailment

In order to consider load curtailment in the system's simulation, all the MG loads were modeled as dispatchable loads, i.e., as generators with negative power injections [56]. The specified cost assigned to the complete set of loads was 1000 $/MWh. Since the negative cost corresponds to a benefit for consumption, insofar as if all the load is dispatched none of it will be curtailed, minimizing the cost of generation is analogous to maximizing the social welfare. Thus, in the presence of dispatchable loads, a negative objective function means that the profit derived from the demand is superior to the operating costs in the generation. Since the power output of the dispatchable loads is negative and its cost positive, their dispatch will results in operating economic benefits.

The minimum injection of the dispatchable load is equal to the negative of the load in that bus, for a certain period, while the maximum injection is zero. This restrictions can be represented as follows:

$$-P_{load}^{ij} \leq P_{DL}^{ij} \leq 0\,, \tag{3.5}$$

where P_{load}^{ij} (kW) represents the value of the load in the *ith* bus in the *jth* period and P_{DL}^{ij} (kW) represents the load dispatched in the *ith* bus in the *jth* period. Therefore, the curtailed load is attained through the absolute value of the difference between P_{load}^{ij} and P_{DL}^{ij}.

The model adopted in MATPOWER assumes that dispatchable loads have a constant power factor [56], being automatically generated an additional equality constraint to impose a constant power for any dispatchable load when formulating the AC OPF problem.

Dummy generators were added at each bus with a PV generator connected to it in order to model the PV generation curtailment. This strategy is required due to the consideration that PV generators are obliged to produce all the energy available in each lapse, so either the maximum or the minimum value are equal to the data provided by the PV generation profile.

An attempt to model the PV generators output ranging from a minimum of zero to a maximum equal to the value provided by the generation profile described in the previously section was made, however, this technique inducted convergence problems in the OPF.

Actually, these fictional generators operate as dispatchable loads. Thereby, for any interval or bus, their range can be represented by the following expression:

$$-P_{PV}^{max} \leq P_{PV}^{DG} \leq 0\,, \tag{3.6}$$

where P_{PV}^{max} (kW) represents the value given by the PV generators profile and P_{PV}^{DG} represents the curtailed PV generation. Thus, the active injected power by the PV generators in the MG is obtained by the sum of P_{PV}^{max} and P_{PV}^{DG}.

Since the output of these dummy generators is negative, a negative cost was assigned to them in order to reflect the increase in the objective function of the OPF provoked when PV power is curtailed.

Also to avoid the lack of convergence in the diverse simulations, a small constant was added to the maximum and minimum limits of the PV generators output, as shown in (3.7).

$$-InfLim + P_{PV}^{max} \leq P_{PV} \leq P_{PV}^{max} + SupLim\,, \tag{3.7}$$

where $InfLim$ and $SupLim$ represent the additional constant and P_{PV} the output of a PV generator, for a given period and bus. The reason for that procedure is based on the fact that MATPOWER utilizes numerical methods to solve the OPF and errors can emerge from exaggeratedly strict constraints (the ones that involve various decimal places). In other words, those constraints were relaxed.

Another required assumption had to be made due to the numerical approximations in the results obtained in the end of each simulation, since $\left|P_{load}^{ij} - P_{DL}^{ij}\right|$ and $\left|P_{PV}^{DG}\right|$ will never be exactly equal to zero. Therefore, a set of thresholds had to be defined in order to account the occurrences of load or PV generation curtailments, which were considered if the following conditions were verified:

$$\left|P_{load}^{ij} - P_{DL}^{ij}\right| \geq Load\ Curtailment\ Limit \tag{3.8}$$

$$|P_{PV}^{DG}| \geq PV\ Generation\ Curtailment\ Limit \tag{3.9}$$

Each one of the previously mentioned thresholds is presented in table 3.4.

Table 3.4 - Defined values for the thresholds.

	Threshold (MW)
InfLim	1×10^{-6}
SupLim	1×10^{-6}
Load Curtailment Limit	5×10^{-6}
PV Generation Limit	5×10^{-6}

It was assumed that the inverters of the PV units aren't able to inject or absorb reactive power into/from the system, being that function exclusively employed by the ESS.

3.4 Energy Storage System

In order to model the ESS, two dummy generators, with different purposes, were added to the bus where the battery was implemented. Whilst one of them has the objective of simulate the activity of the battery when it's charging (load behavior), the other one is intended to describe the battery operation when it's discharging (generator behavior).

It was admitted that the frequency and voltage regulation were solely provided by the ESS, as it was mentioned before. This hypothesis is not unrealistic, since it was already addressed in the current literature [16], [34] and [35]. Thus, a third dummy generator was specifically added to the bus where the battery was installed to enable a proper performance of the MG in terms of dynamics stability. It was considered that this ESS has the capability of injecting into the MG the required reactive energy in all circumstances with a null associated operating cost, so its maximum reactive power output is high enough to supply the reactive demand in all the simulated periods. Since the unique objective of this dummy generator is the aforementioned one, its ability to inject or absorb active energy is null.

The hour in which the fault occurs and the MG starts to operate in IM is randomly generated, therefore, the first required step to model the behavior of the battery is to draw its initial SOC. The following expression was applied to that purpose:

$$SOC_0 = (SOC_{max} - SOC_{min}) \times R_t + SOC_{min} \ , \tag{3.10}$$

where SOC_{max} (kWh) represents the maximum value of the SOC, SOC_{min} the minimum one and R_t is a uniformly distributed random number between 0 and 1.

Throughout this thesis it was assumed that $SOC_{min} = 0.5 \times SOC_{max}$ in order to enhance the realism of this simulation, since the definition of a threshold for the minimum value of the SOC enables the preservation of the longevity of the battery. Despite the attained duration of the islanding, it was considered that there is no degradation in the capacity of the battery.

Subsequently it is possible to obtain the maximum charging power (kW) and the maximum discharging power (kW) of the battery, respectively represented by (3.11) and (3.12), as functions of its current energy availability.

$$P_{charg}^{max} = \frac{SOC_{max} - SOC_0}{\eta_{bat} \times \Delta t} \tag{3.11}$$

$$P_{disch}^{max} = \frac{(SOC_0 - SOC_{min}) \times \eta_{bat}}{\Delta t}, \tag{3.12}$$

where η_{bat} represents the efficiency of the battery and Δt the time interval, like it was mentioned in the first section of the current chapter.

Other power characteristics of the battery were introduced, namely its continuous discharge power (kW) - P_{disch}^{cont} - and nominal charge power - P_{charg}^{nom}. While the first represents

the maximum power that the battery can inject in the MG in one period, the second represents the maximum power that the battery can absorb from the MG in one period. To model this behavior a new set of constraints were added, with the consequence of potentially decrease the battery performance, since if the maximum discharging power is superior to the continuous discharge power it's the last one that prevails, preventing the battery to thoroughly discharge due to its energetic limitations. The same argument is valid to the maximum charging power.

Table 3.5 resumes the power constraints of both the fictional generators that model the battery operation, considering that FG1 refers to load behavior and FG2 to generator behavior.

Table 3.5 - Power constraints of the fictional generators that model the battery operation.

	Pmin	Pmax	Qmin	Qmax
FG1	0	$min\{P_{disch}^{max}, P_{disch}^{cont}\}$	0	0
FG2	$-min\{P_{charg}^{max}, P_{charg}^{nom}\}$	0	0	0

The next step regards the calculation of the SOC for the next period of simulation. It is, therefore, necessary to evaluate the behavior of the battery, i.e., if it's injecting (generator) or absorbing (load) active power.

After running the OPF, the values of power generated by FG1 and FG2 are added. If the result is positive (the battery is discharging), the SOC of the subsequent iteration will be obtained through the application of (3.13). Otherwise, (3.14) is applied and the battery is charging.

$$SOC_{t+1} = SOC_t - (\frac{P_{bat} \times \Delta t}{\eta_{bat}}) \tag{3.13}$$

$$SOC_{t+1} = SOC_t - (P_{bat} \times \Delta t \times \eta_{bat}) \ , \tag{3.14}$$

where P_{bat} (kW) represents the sum of the two power outputs of the fictional generators.

The described process in this section is repeated throughout all the simulation, for all the periods drew through the method mentioned in the first section of this chapter.

In order to prioritize the charging process of the battery in detriment of the PV generation curtailment, different costs of operation, were attributed to the fictional generators that model the battery behavior and the PV generation curtailment, as presented in table 3.6

Table 3.6 - Operating costs of the fictional generators that model the battery and the PV generation curtailment.

	Operating Cost ($/h)
Battery	0
Fictional PV Generators	$-P_{PV}^{DG}$

Since P_{PV}^{DG} is less than or equal to zero, the operating cost regarding the PV generation curtailment will be greater than or equal to zero, thus this curtailment will prejudice the value of the objective function of the OPF. This inculcated scalability in prices leads to that in the

event of a surplus of generation, this excess will be used to charge the battery, if this one is not at the maximum of its energetic capacity already, instead of being wasted in dump loads.

3.5 OPF Formulation

The software used to realize the Optimal Power Flow (OPF), was the MATPOWER, which is an open-source Matlab-based power system simulation package [57]. MATPOWER is composed by an aggregation of Matlab M-files conceived to provide the best possible performance.

The structure of the OPF enables the easy addition of user-defined variables, costs and linear constraints. The default OPF solver, and the one that was employed in this work, is the Primal-Dual Interior Point Method (PDIPM), implemented in pure Matlab.

The following OPF formulation refers to version 5.1 of MATPOWER, which assumes the subsequent standard form:

$$\min_x f(x) \ , \tag{3.15}$$

subject to:

$$g(x) = 0 \tag{3.16}$$

$$h(x) \leq 0 \tag{3.17}$$

$$x_{min} \leq x \leq x_{max} \ , \tag{3.18}$$

where $f(x)$ represents the objective function, $g(x)$ the set of equality constraints derived from the power balance equations, $h(x)$ the set of inequality constraints that reflects the branch flow limits and x represents the optimization vector.

For the standard AC OPF problem x is composed by $n_b \times 1$ vectors of voltage angles (θ) and voltage magnitudes (V_m) and by $n_g \times 1$ vectors regarding generators real and reactive power injections (P_g and Q_g, respectively), where n_b stands for the number of buses and n_g represents the number of generators, including all the dummy generators as well.

$$x = \begin{bmatrix} \theta \\ V_m \\ P_g \\ Q_g \end{bmatrix} \tag{3.19}$$

The variables included in x have defined upper and lower limits on all bus voltage magnitudes and active and reactive generator injections, as well as an equality restriction on any reference bus angle.

$$\theta_j = \theta_j^{ref} \tag{3.20}$$

$$v_m^{i,min} \leq v_m^i \leq v_m^{i,max}, \qquad i = 1, \dots, n_b \tag{3.21}$$

$$p_g^{k,min} \leq p_g^k \leq p_g^{k,max}, \qquad k = 1, \dots, n_g \tag{3.22}$$

$$q_g^{k,min} \leq q_g^k \leq q_g^{k,max},\ k = 1, \dots, n_g\ , \tag{3.23}$$

where *j* corresponds to the number of the slack bus.

The objective function represented by (3.15) is obtained through the sum of all polynomial cost functions of active power injections (f_P^i) for each generator *i*, either real or fictional. It is also possible to include the polynomial cost functions of reactive power injections in the following expression:

$$\min_x f(x) = \min_{\theta, V_m, P_g, Q_g} \sum_{i=1}^{n_g} f_P^i(P_g^i) \tag{3.24}$$

The $2n_b$ nonlinear power balance equations that compose the set of equality constraints can be divided into its real and reactive components. Assuming the load injections as constants, the equality constraints can be represented as functions of the voltage angles and magnitudes and active and reactive generators power injections:

$$g_P(\theta, V_m, P_g) = P_{bus}(\theta, V_m) + P_d - C_g P_g = 0 \tag{3.25}$$

$$g_Q(\theta, V_m, Q_g) = Q_{bus}(\theta, V_m) + Q_d - C_g Q_g = 0\ , \tag{3.26}$$

where $P_{bus}(\theta, V_m)$ and $Q_{bus}(\theta, V_m)$ represents the nodal active and reactive power injections, respectively; P_d and Q_d represents the active and reactive components of the load and C_g is a sparse $n_b \times n_g$ connection matrix where its (*i,j*)th element is equal to one, if the generator *j* is connected to the *ith* bus, and zero, otherwise.

The inequality constraints are composed by two groups of n_{bra} (number of branches) nonlinear functions that express the branch flow limits, one for the *from* end and other one for the *to* end of each line:

$$h_f(\theta, V_m) = |F_f(\theta, V_m)| \leq F_{max} \tag{3.27}$$

$$h_t(\theta, V_m) = |F_t(\theta, V_m)| \leq F_{max} \tag{3.28}$$

Usually the flows are expressed in terms of apparent power (MVA), notwithstanding MATPOWER allows the representation of flow constraints in other two forms: real power ($P_t(\theta, V_m)$) and current ($I_t(\theta, V_m)$), having the vector of flow limits - F_{max} - and $F_f(\theta, V_m)$ the adequate units, regarding the chosen type of constraint.

$$F_t(\theta, V_m) = \begin{cases} S_t(\theta, V_m) \\ P_t(\theta, V_m) \\ I_t(\theta, V_m) \end{cases} \tag{3.29}$$

3.6 Stopping Criterion

The adopted stopping criterion is based on the calculation of the coefficient of variation, according to (2.9), of the following load curtailment-related reliability indexes: LOLE, LOLF

and EENS. These coefficients of variation are updated in the end of each simulated event and the simulations will only stop when the desired accuracy is achieved for all the above-mentioned reliability indexes.

In the present work the adopted pre-specified threshold for the coefficient of variation is equal to 5%. Therefore, the simulation will stop when:

$$\beta_{LOLE} \leq 0.05 \tag{3.30}$$

$$\beta_{LOLF} \leq 0.05 \tag{3.31}$$

$$\beta_{EENS} \leq 0.05 \tag{3.32}$$

It was observed that the EENS is the last one to converge, i.e., the one that has the lowest convergence speed.

3.7 Reliability Indexes Calculation

In order to compute the desired reliability indexes and other relevant values, the following results are stored in the end of each event:

- Event duration, i.e., the number of periods in which the MG operates in stand-alone mode;
- Number of load curtailments;
- Number of periods in which a load curtailment had occurred;
- Power not supplied (kW);
- Power not supplied per load curtailment (kW/load curtailment);
- Energy not supplied (kWh);
- Battery SOC (kWh);
- Value of the active power absorbed by the battery (kW);
- Value of the active power injected by the battery (kW);
- Number of periods in which the battery has charged;
- Number of periods in which the battery has discharged;
- Number of charges;
- Number of discharges;
- Used PV power (kW);
- Used PV energy (kWh);
- Wasted PV power (kW);
- Wasted PV energy (kWh);

A distinction between the number of curtailments and the number of periods in which a curtailment had occurred was made, since a sequence of ten periods, for instance, with power not being supplied is considered as one single curtailment, and not ten. To increase the number of curtailments, the successive periods with outages needed to be intercalated by a period in which all the load is supplied. This procedure is required to the attainment of the LOLF.

The expected value and the variance of each aforementioned result, as well as the coefficient of convergence of LOLE, LOLF and EENS are calculated in the end of simulation of

a new event, according to (2.10), (2.11) and (2.12), respectively. The simulation will stop when (3.30), (3.31) and (3.32) are verified.

Some reliability indexes can be directly obtained in the end of the simulation, since their value is equal to the expected value of the matching result, namely the LOLF, which is equal to the expected value of the number of load curtailments; the LOLE, whose value corresponds to the expected value of the number of periods in which a load curtailment had occurred; the EPNS, identical to the expected value of the power not supplied in each event (the value of the EPNS per load curtailment corresponds to the mean value of the power not supplied per load curtailment) and the EENS, equal to the mean value of the energy not supplied. Nevertheless, these indexes can also be obtained through the following expressions:

$$LOLF = \frac{Total\ number\ of\ load\ curtailments}{Total\ number\ of\ events} \tag{3.33}$$

$$LOLE = \frac{Total\ number\ of\ periods\ with\ a\ load\ curtailment}{Total\ number\ of\ events} \tag{3.34}$$

$$EPNS = \frac{Total\ curtailed\ load}{Total\ number\ of\ events} \tag{3.35}$$

$$EENS = EPNS \times \Delta t \tag{3.36}$$

Other indexes are obtained *a posteriori*, namely the LOLP and the LOLD. Equation (3.37) and (3.38) present the way to do it.

$$LOLP = \frac{mean\ value\ of\ the\ periods\ with\ load\ curtailment}{mean\ duration\ of\ the\ events} \tag{3.37}$$

$$LOLD = \frac{LOLE}{LOLF} \tag{3.38}$$

From the equations that enable the computing of the classic reliability indexes, it can be inferred that the LOLF will be presented in *load curtailments/event*, the LOLE in *periods with load curtailments/event*, the LOLD in *periods with load curtailment/load curtailment*, the EPNS in *kW/event* and the EENS in *kWh/event*. As the LOLP is a dimensionless value, since it's a probability, it is presented in an event basis.

In order to present these indexes in the typical annual basis - the LOLF in *load curtailments/year*, the LOLE in *hours/year*, the LOLD in *hours/load curtailment*, the EPNS in *kW/year*, the EENS in *kWh/year* and the LOLP in an annual basis -, a proper conversion of units is required.

Considering that the values of the upper system MTTR and MTTF, presented in *hours*, are known, its unavailability (P_0) can be attained through equation (2.2). Other needed value in order to convert the units of the reliability indexes is the upper system frequency cycle, which can be obtained by applying the following equation:

$$f = \frac{8760}{MTTR + MTTF} \quad (events/year)$$

(3.39)

The previous expression differs from (2.5) due to the fact that the MTTR and the MTTF are presented in *hours* and the respective rates (μ and λ) in *events*/*year*, thus it is necessary to multiply by the number of hours in one year.

Subsequently, the ensuing procedure to achieve a representation of the reliability indexes in an annual basis is employed:

$$LOLP_{annual\ basis} = LOLP_{event\ basis} \times P_0 \tag{3.40}$$

$$LOLF_{annual\ basis} = LOLF_{event\ basis} \times f \tag{3.41}$$

$$EPNS_{annual\ basis} = EPNS_{event\ basis} \times f \tag{3.42}$$

$$LOLE_{annual\ basis} = LOLP_{annual\ basis} \times 8760 \tag{3.43}$$

$$LOLD_{annual\ basis} = \frac{LOLE_{annual\ basis}}{LOLF_{annual\ basis}} \tag{3.44}$$

$$EENS_{annual\ basis} = EPNS_{annual\ basis} \times 8760 \tag{3.45}$$

3.7.1 Reliability Indexes without the MG

In order to evaluate the impact of the MG on the reliability of a distribution system, it is necessary to compute the reliability indexes without taking into account its presence, i.e., by considering that entire MG load is "seen" by the upstream network as a single load point, without any RES supplying it.

It was assumed that, in the absence of an upper system disconnection, there wasn't any load curtailments, i.e., that the entire load is supplied.

Non-considering the presence of the MG with its DG and in the event of a fault in the upper system, none of the demand is supplied, therefore:

- The total number of load curtailment corresponds to the total number of events;
- The number of periods with load curtailments is equal to the duration of the diverse outages;
- All load is curtailed during an outage.

The abovementioned facts allow the attainment of the reliability indexes (in an event basis), as follows:

$$LOLP = \frac{Total\ number\ of\ periods\ with\ load\ curtailment}{Total\ number\ of\ periods\ of\ the\ simulation} = 1 \tag{3.46}$$

$$LOLF = \frac{Total\ number\ of\ load\ curtailments}{Total\ number\ of\ events} = 1 \tag{3.47}$$

$$LOLD = \frac{Total\ number\ of\ periods}{Total\ number\ of\ events} \tag{3.48}$$

$$LOLE = LOLF \times LOLD = LOLD \tag{3.49}$$

$$EPNS = \frac{Total\ curtailed\ load\ in\ the\ simulation}{Total\ number\ of\ events} \tag{3.50}$$

$$EENS = EPNS \times \Delta t \tag{3.51}$$

From the abovementioned equations it can be concluded that the employment of the proposed method to assess the reliability of a MG provides upper bounds that allow the evaluation of the reliability improvement induced in the system with the implementation of the MG, since with the previously explained assumptions the worst case scenario is considered – the one in which all the load is curtailed throughout the occurrence of an event. Therefore, the method to attain the reliability indexes without MG don't consider that a client could suffer a partial load curtailment.

The proposed technique to convert the units of the reliability indexes from an event basis to an annual basis presented in the last section can also be employed in this case.

3.8 Proposed Algorithm

After the modeling of all the system components and their chronologic behavior, a succinct algorithm with the previously explained ideas is presented in this section.

Step 1) Initialization of β_{LOLE}, β_{LOLF} and β_{EENS} as unitary coefficients;

Step 2) Drawing of the fifteen-minute period in which the fault occurs, as well as the duration of the event, according to (3.1);

Step 3) Initialization of the required counters to the obtainment of the reliability indexes;

Step 4) Simulation of the MG operation while in IM:

- 4.1) Update of the load and PV generation profiles for the concerned fifteen minutes period;
- 4.2) If the concerned period is the first one: drawing of the initial value of the battery SOC, according to (3.10); or else – move to 4.3);
- 4.3) Update the maximum real power output (discharging) and the minimum real power output (charging) of the fictional generators that model the battery behavior, according to (3.11) and (3.12), respectively;
- 4.4) Run the OPF described in the section 3.5 of the current chapter;
- 4.5) Update the SOC of the battery according to (3.13), if the battery is discharging, or according to (3.14), if the battery is charging;
- 4.6) Update the value of the counters initialized in 2);

- 4.7) If the MG is still operating in stand-alone mode return to 4.1), otherwise move to step 5.

Step 5) Compute the required results, described in the last section, for the obtainment of the reliability indexes;

Step 6) Update the values of β_{LOLE}, β_{LOLF} and β_{EENS} according to (2.9);

Step 7) If the conditions represented by (3.30), (3.31) and (3.32) are verified, the desired accuracy is achieved and the simulation ends; otherwise, return to step 2.

3.9 Conclusions

In this chapter the modeling of all the system components and the required assumptions, in order to simulate the MG operation and conclude about its reliability performance and impact on the distribution system, are presented. A summary algorithm, which ignores all the specifications of the intermediate calculations, of the proposed technique to assess system reliability is settled.

One can see that even with some simplification, such as the assignment of a null probability of unavailability to all the MG components and the non-consideration of the MG dynamic behavior, the implementation of the subject method is not prosaic, being essential the adoption of theoretical concepts, such as fictional generators and dispatchable loads.

Barriers related to the lack of convergence of the OPF for some periods had to be surpassed. The strategy found to overcome those adversities was the relaxation of the constraints related to the maximum and minimum real power output of the PV generators.

Since the MG has several different elements, a proper prioritization of its symbiotic operation is required, in order to maximize the economic and social prerogatives in implementing MGs. This prioritization was achieved due to the assignment of different costs to the dummy generators that model the load and PV generation curtailment and the battery behavior. The goal was never to waste PV energy when the battery still has the capacity to charge, so the price of the fictional generators was superior, in absolute terms, to the one associated with the charging process of the battery, which was assumed to be null.

A methodology was developed in order to present the reliability indexes in the classic units used in literature. The aim of applying such a conversion is to facilitate the comprehension of the attained results and to enable empirical comparisons with other studies.

The subsequent chapter concerns the application of the proposed method to the reliability assessment of a specific MG operating in stand-alone mode and its impact on the performance of the respective distribution system and the demonstration of the obtained results.

Chapter 4 - **Results and Discussion**

In this chapter, it will be presented the most relevant results obtained through the employment of the proposed methodology in chapter 3. The main goal is to assess the impact on the reliability of a system derived from the implementation of a MG capable of operating in IM. In order to achieve that, the following reliability indexes were computed for both scenarios (with and without considering the MG): LOLE, LOLF, LOLD, LOLP, EPNS and EENS.

The first section of the current chapter will introduce the test MG used to employ the developed method, such as other assumptions that were made.

Furthermore, five batteries with diverse electric characteristics will be tested in order to evaluate the impact of different ESSs on the reliability of the test system. The results obtained with the various batteries will be further analyzed and compared, and the one that enables the most compelling reliability indexes will be chosen. In order to provide an insight of the MG operation throughout an event, an analysis of the MG operation in IM is presented for a specified period of time. This analysis will compare the MG operation with the ESS model that led to the best reliability indexes with the one whose presence has resulted in the worst reliability performance.

The third and the fourth section are about the evaluation of the impact of different failure rates and MTTR on the system reliability indexes, respectively. In these sections, the benefits derived from the implementation of the MG are measured.

Afterwards, a simple technique to quantify the economic advantages of implementing the MG is presented. This calculation is based on the difference between the EENS attained without considering the MG and the one obtained when the employment of this concept is contemplated.

As usual, the last section is dedicated to a brief exhibition of the conclusions drawn throughout the present chapter.

All the results presented in this chapter were obtained through a MATLAB script conceived for this purpose.

4.1 Case Study

The adopted MG for the application of the proposed method is presented in figure 4.1. This 0.4 kV LV network is fed by an upstream 15 kV MV network, through a substation with a 250 kVA transformer. The test MG is composed by 28 loads, 15 PV microgenerators and 32 branches.

A MATPOWER file with the MG characteristics was built from the scratch. Since the aforementioned software reads the branch resistance and reactance in per-unit (pu) a proper

conversion of these values was made and can be found in Annex A. To achieve that is required to define the system bases, regarding the apparent power, voltage and impedance, which are presented in table 4.1.

Table 4.1 - System bases.

System bases	
Sb (kVA)	250
Vb (kV)	0.4
Zb (Ω)	0.64

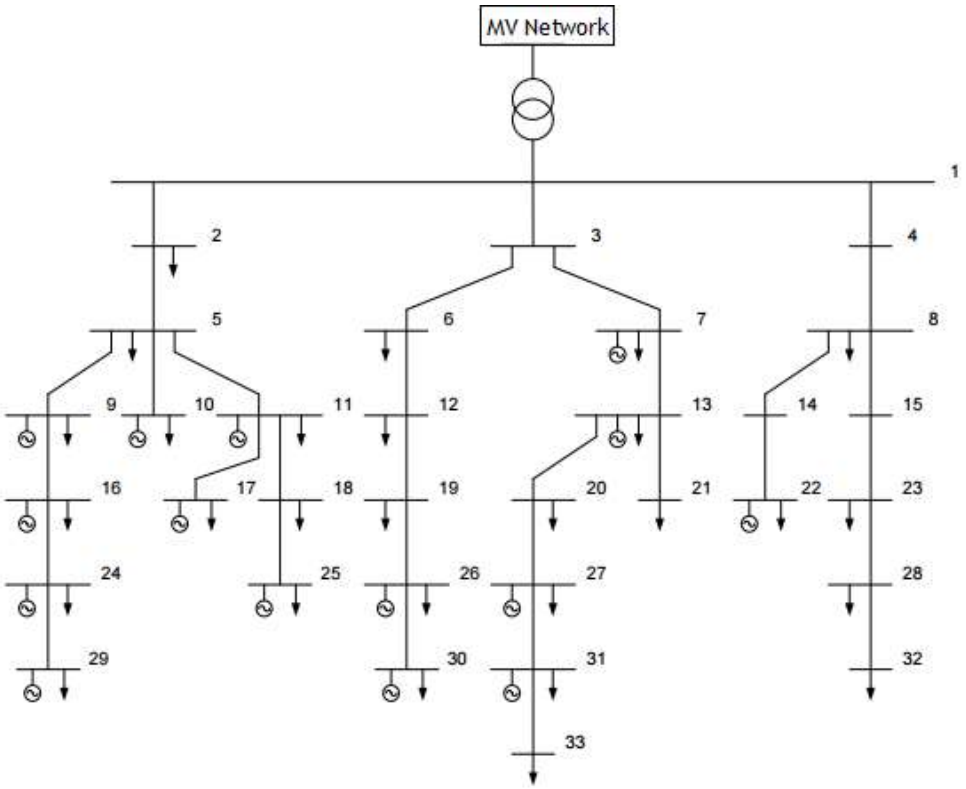

Figure 4.1 - Topology of the test MG.

The impedance base was computed through the following expression:

$$Z_b = \frac{V_b^2}{S_b} \tag{4.1}$$

Afterwards it's possible to attain the branch's resistance and reactance in per-unit, as it is show in (4.2) and (4.3).

$$R_{pu} = \frac{R_\Omega}{Z_b} \tag{4.2}$$

$$Z_{pu} = \frac{Z_{\Omega}}{Z_b} \tag{4.3}$$

It was assumed that each load has a $\tan \varphi = 0.4$ and that the voltage limits in each bus are the ones presented in table 4.2.

Table 4.2 – Bus voltage limits.

Voltage Limits (pu)	
Vmax	1.1
Vmin	0.9

A maximum admissible current of 220 A was adopted.

The fifteen PV microgeneration units that are part of the MG have five different values of installed power, namely 1.7, 3.45, 3.68, 5.15 and 5.38 kW. Through [55], the annual generated energy for each level of capacity was attained and presented in table 4.3.

Table 4.3 – Annual generated energy (kWh) for each level of installed power.

Installed Power (kW)	Annual Generated Energy (kWh)
1.7	2530
3.45	5130
3.68	5470
5.15	7660
5.38	8000

The ESS is installed in bus number 1, being this one the slack bus. All the others are PQ buses, since it was considered that the PV panels don't have the ability to inject or absorb reactive power. Therefore, they are incapable of regulating the voltage levels. That function was delegated to the ESS.

It was assumed that the MG operation in IM mode has its origin in a failure in the MV network.

4.2 Evaluation of the Impact of Different Batteries on the MG Reliability Indexes

The main goal of implementing an ESS in a MG composed by RES is its capability of avoiding load or generation curtailments and smoothing intermittent generation, since it can absorb power in moments of surplus and inject power when the demand exceeds the generation.

The impact of each energy storage solution, provided by Saft, with diverse energetic and power features in the MG reliability will be evaluated. The Li-ion battery systems properties are presented in table 4.4. An efficiency of 90% was assigned to all the different batteries.

Table 4.4 - Batteries characteristics.

	IM 20E	IM+ 20E	IM 20M	IM+20M	IM 20P
Energy (kWh)	620	1020	580	950	420
Continuous Discharge Power (kW)	900	500	1100	2100	1600
Nominal Charge Power (kW)	300	500	600	1000	900

The first considerations of all the simulations employed in the present section considered a MTTR equal to 1 *hour* and a MTTF of 4380 *hours* (corresponding to a failure rate of 2 *events/year)*, respectively. Afterwards, according to (3.44), (2.2) and (2.5), the parameters presented in table 4.5 were computed.

Table 4.5 – Upper system parameters.

MTTR (h)	MTTF (h)	MTBF (h)	f (events/year)	P_0
1	4380	4381	1.9995	0.00023

Through the parameters that compose table 4.5, all the results obtained from the simulation were converted to an annual basis. So, in the absence of a contrary statement, it is assumed that all the values are referred to mentioned basis.

The reliability indexes obtained from the five diverse simulations, for a threshold of 5% referred to the coefficient of variation, are presented in table 4.6.

Table 4.6 – MG reliability indexes for the tested batteries.

	LOLP	LOLF (load curt./year)	LOLE (hours/year)	LOLD (hours/load curt.)	EPNS (kW)	EENS (kWh)
IM 20E	1.46792E-05	0.18771	0.12859	0.68505	17.0792	149613.5
IM+ 20E	0.83083E-05	0.10347	0.07278	0.70343	9.60408	84131.7
IM 20M	1.53565E-05	0.19035	0.13452	0.70671	17.7438	155435.5
IM+ 20M	0.87195E-05	0.11103	0.07638	0.68794	10.0611	88135.6
IM 20P	2.18053E-05	0.27449	0.19101	0.69588	25.4285	222753.9

The battery that most enhances the reliability of the MG operating in stand-alone mode is the IM+ 20E, although the results are similar to the ones obtained with the implementation of IM+ 20M. It can be seen that all reliability indexes are lower with these ESS models, except for the LOLD.

Comparing the data presented in table 4.5 with table 4.6 it becomes evident that the reliability of the MG increases when the value of the battery SOC is higher, being that characteristic more preponderant than the limits imposed by the Continuous Discharge Power and the Nominal Charge Power. Figures 4.2 demonstrate the inverse proportionality between the LOLP and the battery SOC. In the x axis, the number “1” corresponds to IM 20E, the “2” to IM+ 20E, and so on.

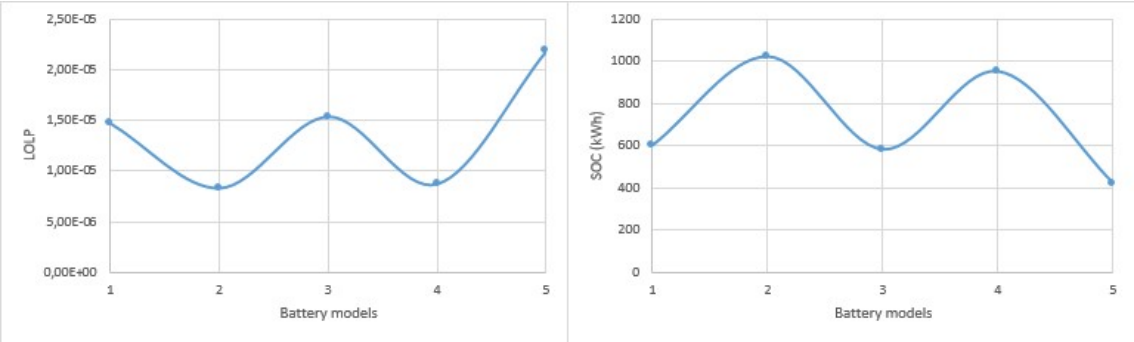

Figure 4.2 - LOLP and SOC (kWh) for each simulation.

That behavior is a bit counter intuitive, since it was expected that the reliability indexes would result of a trade-off between both the Continuous Discharge Power and the Nominal Charge Power and the SOC. For instance, since the SOC of IM 20E and IM 20M are similar, an intuitional *a priori* conclusion would be to affirm that the reliability performance of the MG would be superior with IM 20M, due to the fact that this model enables the injection and absorption of larger quantities of power by the battery, which would be useful to provide power in periods with a deficit of generation.

This outcome can be explained through the mean values of the active power absorbed and injected by the battery in the various simulations, represented in figure 4.3. These values are significantly lower than the Continuous Discharge Power and the Nominal Charge Power of each ESS, therefore, the power output of the battery never reaches the imposed limits. Thus, for the present level of PV generation, these limits don't have a real impact on the performance of the MG. It is expected that, in case of a higher PV generation penetration, the values of the Continuous Discharge Power and the Nominal Charge Power would be more relevant for the reliability of the MG, due to the fact that the ESS would have more energy to inject and absorb. Possibly, the implementation of the IM +20M would result in more reliable performance than the one attained with IM+ 20E, since the power constraints of the first one allow higher levels of power to be inject or absorbed in one period.

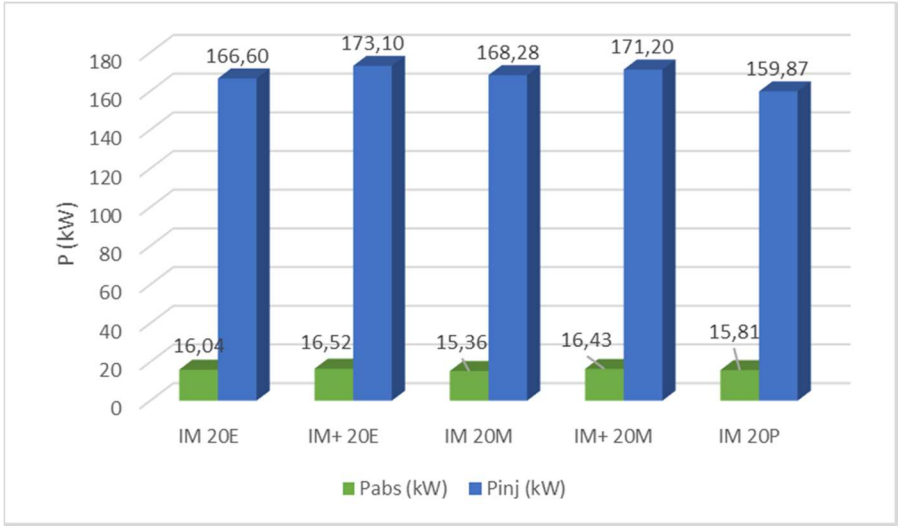

Figure 4.3 - Mean values of the active power absorbed (Pabs) and injected (Pinj) by the battery.

Figures 4.4 and 4.5 depict the adequacy of the performance of the MG for the diverse battery models.

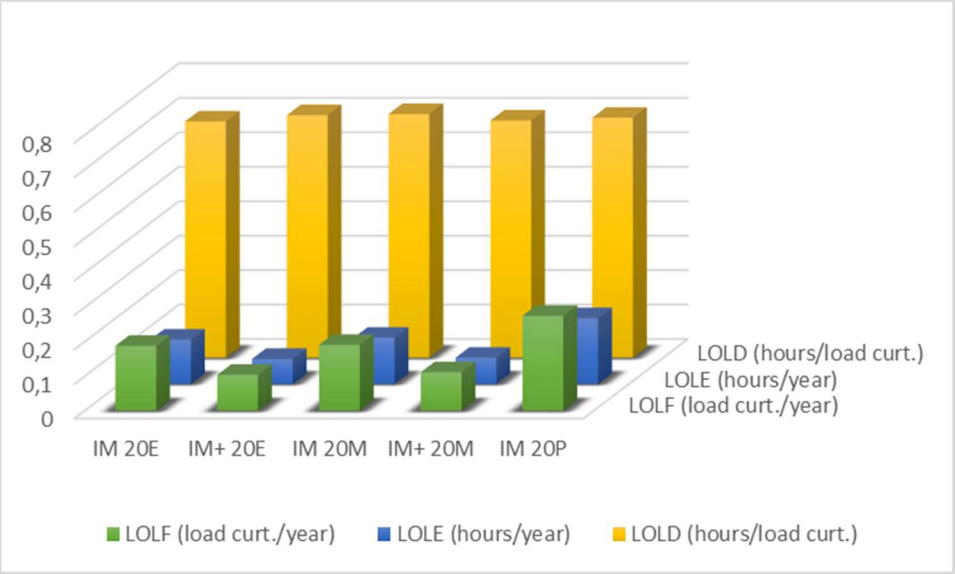

Figure 4.4 - LOLF, LOLE and LOLD obtained in each simulation.

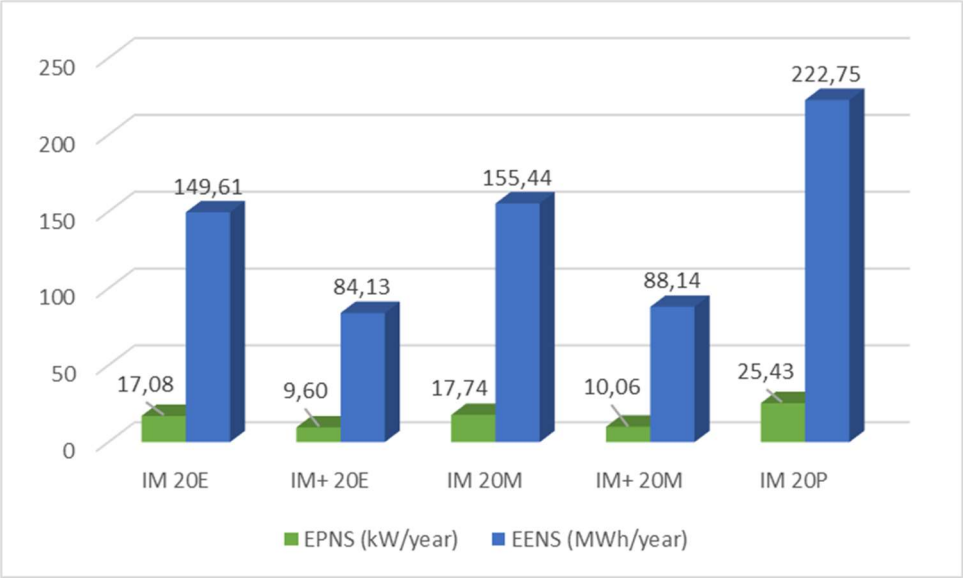

Figure 4.5 - EPNS (kW) and EENS (MWh) attained in each simulation.

Although the deterioration of the ESS is not considered in the proposed method, an important factor that could help to decide the battery model to implement is the mean value of the number of charges and discharges performed, since the aging of a battery is related to its charging/discharging cycles. Figure 4.6 presents the aforementioned mean values for each simulation.

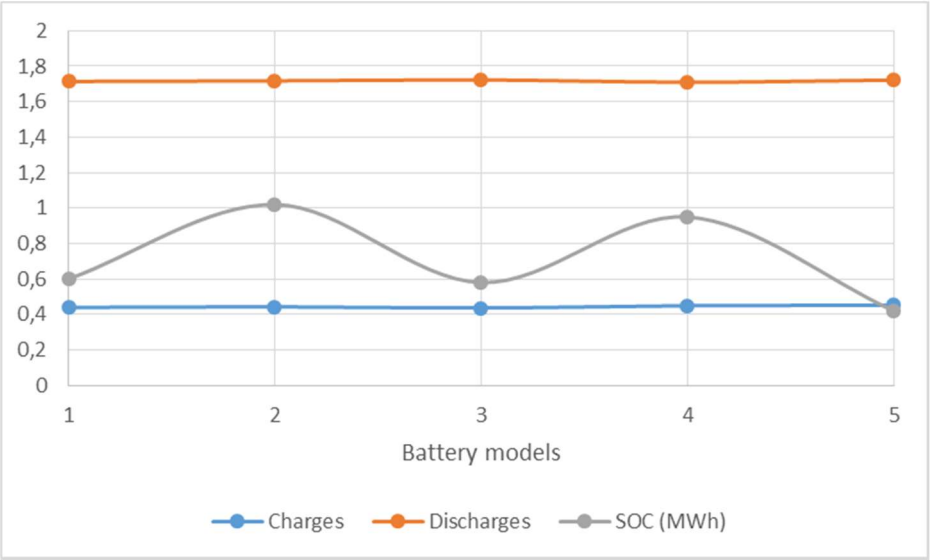

Figure 4.6 - Mean value of the number of charges and discharges of each simulation, and the corresponding SOC (MWh) of the battery model.

As it can be observed, the variability of the expected value of the battery number of charges and discharges is negligible, thus the choice of the IM+ 20E model continues to be unquestionable.

In figure 4.7 the levels of used PV energy are depicted.

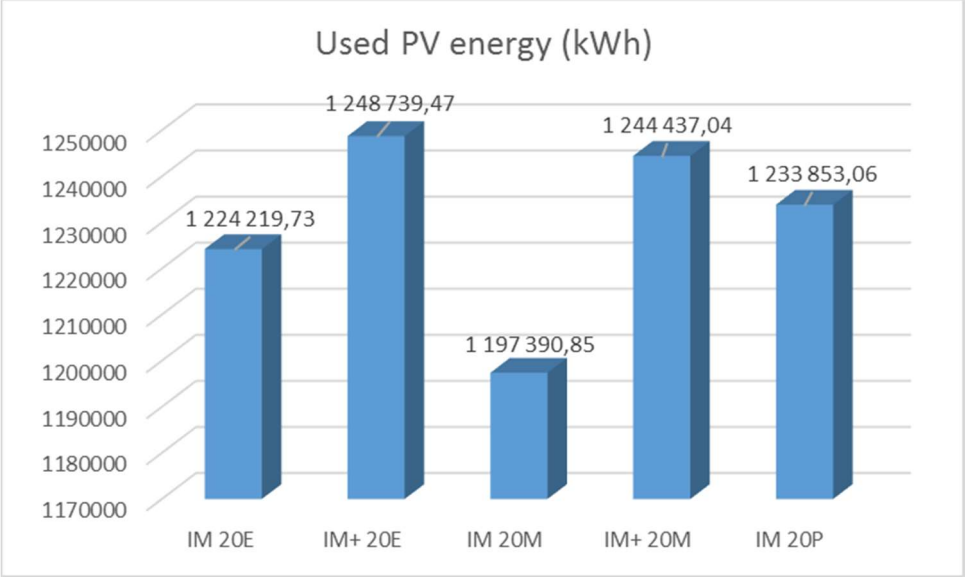

Figure 4.7 - Used PV energy (kWh) in each simulation.

The utilized PV energy rises with the increasing of the battery SOC, i.e., with the increasing of the MG reliability. This is due to the fact that with a higher SOC, the battery achieves higher levels of power absorption from the MG, diminishing the wasted PV energy.

The evolution of the mean value of the LOLE during the second simulation (for the IM+ 20E) is depicted in figure 4.8. As in any MC based-method, the expected value oscillates towards the real one, starting to converge to a value within a confidence interval. This process ceases when the stopping criterion was achieved.

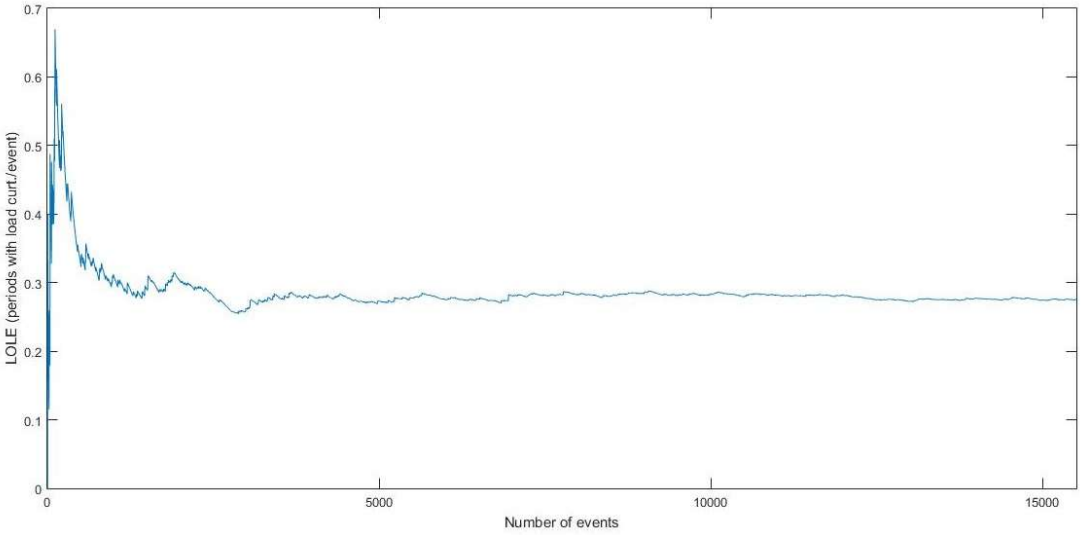

Figure 4.8 – Expected value of the LOLE (periods with load curt./events) during the second simulation.

The LOLE is presented in *periods with load curt./events*, since the conversion is only employed in the end of the simulation.

Since this technique is based on the sequential MC, a confidence level can be settled, in order to determine the confidence interval. Table 4.7 presents the expected values of the reliability indexes that compose the stopping criterion, in an event basis, as well as its coefficient of variation and confidence interval, regarding a confidence level of 95%, which means that there's the probability of 0.95 that the presented confidence interval comprises the exact value of the reliability index.

The considered ESS is the one that yields the best reliability indexes, i.e., the IM+ 20E.

Table 4.7 – Expected value, coefficient of convergence and confidence interval of the reliability indexes considered in the stopping criteria.

	LOLE (per. with load curt./event)	LOLF (load curt./event)	EENS (kWh/event)
Expected Value	0.2678	0.0517	1.2008
β (%)	4.2784	3.3991	4.9969
Confidence Interval	[0.2521 ; 0.2834]	[0.0479 ; 0.0556]	[1.0832 ; 1.3184]

The attained value of the reliability indexes doesn't provide information about the dispersion of the results throughout the simulation, since they represent the mean value of their probability distributions. Thus, a useful source of information are the histograms of the corresponding reliability indexes, which yield the frequency of occurrence of the diverse values they assume in the course of the simulation.

Figure 4.9 presents the histogram of the islanding duration in each simulated event, for a total of 9 bins with a width of 5 periods.

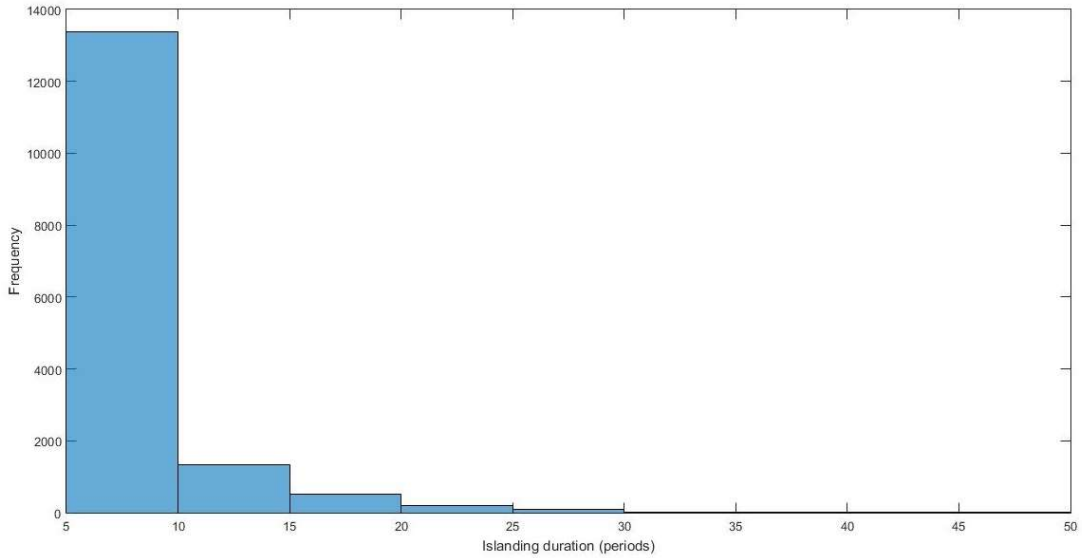

Figure 4.9 – Histogram of the islanding duration in each event.

As it can be seen, the MG operates in stand-alone mode for a length of time between 5 and 10 periods for the vast majority of simulated events. Therefore, a MTTR of 1 hour leads to an islanding that lasts for 2 hours, approximately, in most cases. An approximated probability density function can be settled through the data provided by histograms. A relative frequency is attained by dividing the frequency of one bin by the total number of samples. Table 4.8 presents the approximated probability distribution of the islanding duration.

Table 4.8 – Approximated probability density function of the islanding duration in each event.

Edges	Relative Frequency
5 10	0.863481009
10 15	0.085187335
15 20	0.032694912
20 25	0.012381505
25 30	0.00561037
30 35	0.000386922
35 40	0.000128974
40 45	6.4487E-05
45 50	6.4487E-05

It can be concluded that the probability of having an islanding with a duration superior to 10 periods is around 14%.

Figure 4.10 shows that the bulk of events only have one load curtailment, while table 4.9 reveals that the probability of having two load curtailments is 5 %, approximately.

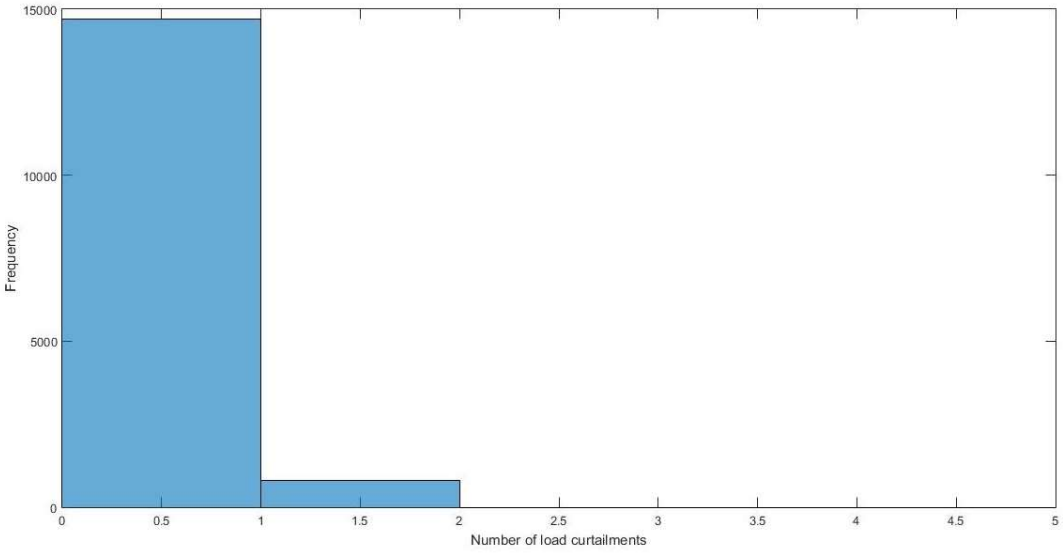

Figure 4.10 – Histogram of the number of load curtailments in each event.

Table 4.9 - Approximated probability density function of the number of load curtailments in each event.

Edges	Relative Frequency
0 1	0,948026825
1 2	0,051973175
2 3	0
3 4	0
4 5	0

In order to provide an insight of the MG operation throughout an event, an analysis of the behavior of the test system in the last three days of July, according to ERSE load and PV generation profiles, will be provided in the following sub section. Thus, 288 periods will be scrutinized. Since the aim of this section is the comparison among different ESS models, a parallelism between the operation of the MG, considering the battery that enables the obtainment of the best (IM+ 20E) and the worst (IM 20P) reliability indexes will be presented.

It was assumed that the initial value of the battery SOC corresponds to its maximum value, presented in table 4.4, in order to standardize the simulations.

4.2.1 MG Performance with the IM+ 20E ESS Model

In figure 4.11 the battery SOC and power output is presented.

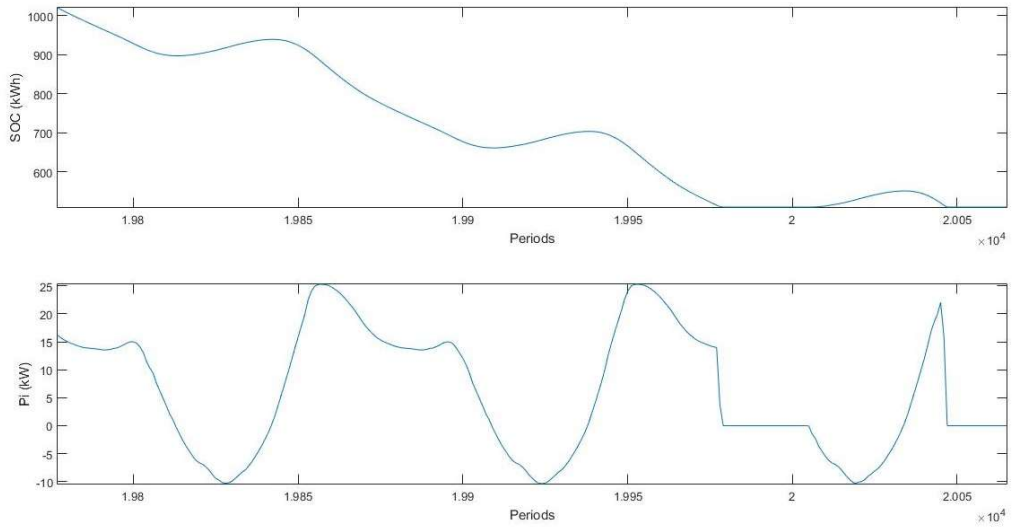

Figure 4.11 - Battery SOC (kWh) and power output (kW) - IM+ 20E.

It is observable that the behavior of the battery follows a pattern in each of the three days: it discharges in the first hours of the day and in the night (when there's not PV generation) and charges in the afternoon (when the PV generation is higher). When the battery is charging, its power output is negative – it works as a load –, and when the battery is discharging, its power output is positive – it works as a generator, as it was expected. Since the PV generation is successively insufficient to return the SOC to its previous value, the battery gradually loses its energy, reaching the minimum value of the SOC in the end of the second day.

The evolution of the PV generation (Pg) the battery power output (Pi), as well as the supplied and curtailed load and the curtailed PV generation, is depicted in figure 4.12. The representation of the active power net losses is also presented in the mentioned figure.

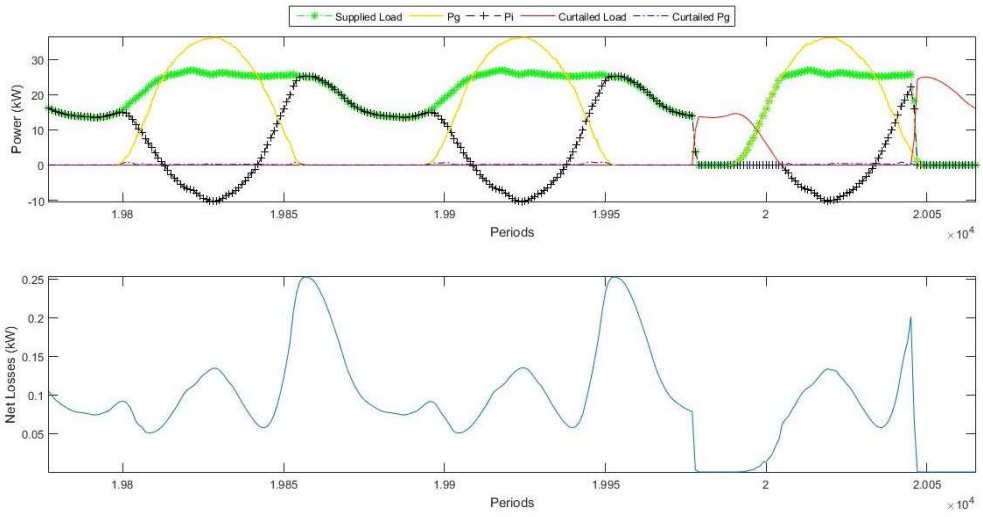

Figure 4.12 - Evolution of the PV generation (Pg), the battery power output (Pi), the supplied and curtailed load and the active net losses (kW) – IM+ 20E.

When there is a surplus in generation, that energy is channeled to charge the ESS, instead of being wasted in a dump load, as it was defined through the scalability of the fictional generators associated costs of operation.

In the beginning of the third day, load starts to be curtailed, due to the fact that there isn't any PV generation available and the battery is completely discharged.

Comparing the two graphs presented in figure 4.12, the correlation between the battery power output and the net losses is noticeable. Although the value of the losses is significantly inferior, its evolution follows the one presented by the power injected or absorbed by the ESS. This behavior was expected, since the battery is implemented in the MG slack bus, the one responsible to provide for system losses.

Figure 4.13 shows the amount of the curtailed load, when compared to the total load of the MG in each period, while figure 4.14 yields the values of the real and reactive curtailed load, depicted in a graph bar.

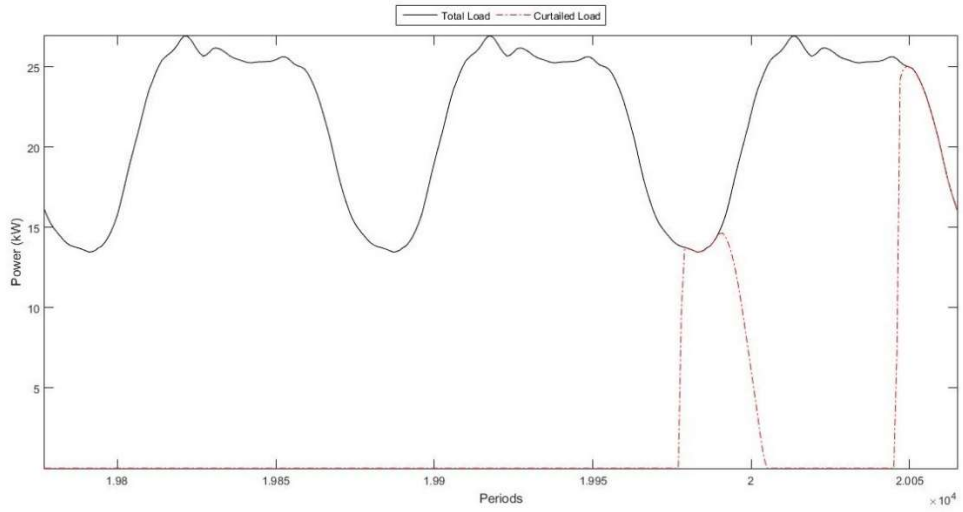

Figure 4.13 - Curtailed and total load (kW) in each period of the simulation - IM+ 20E.

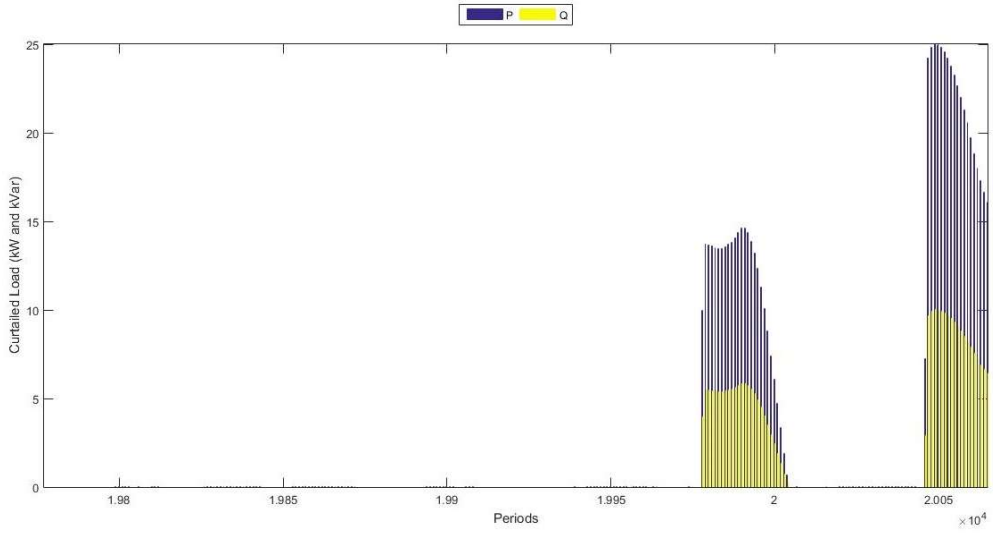

Figure 4.14 - Real (kW) and reactive (kVar) curtailed load in each period of the simulation - IM+ 20E.

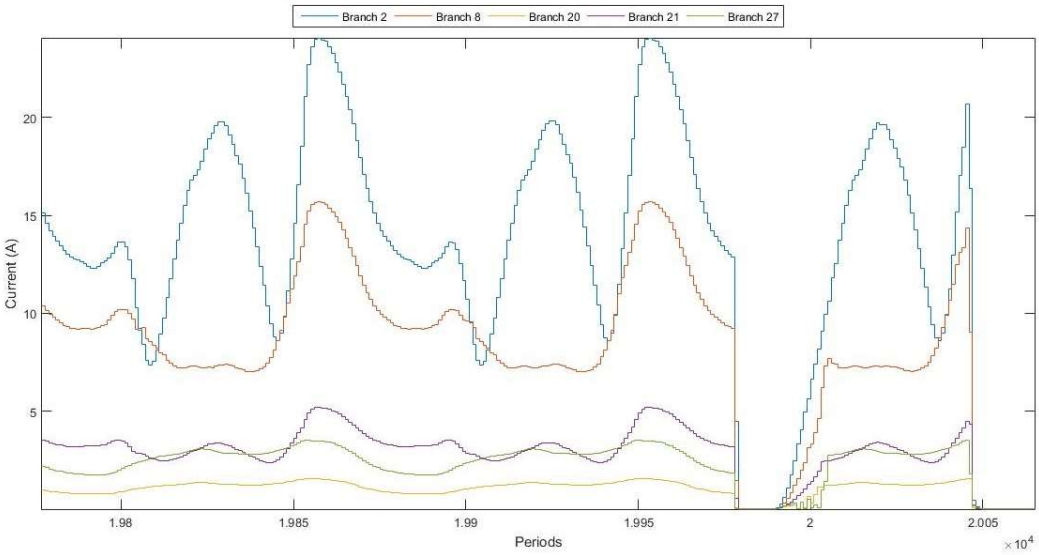

Figure 4.15 – Current (A) in branches 2, 6, 20, 21 and 27 - IM+ 20E.

In order to evaluate the current flow in the MG, two branches for each main conduit were chosen to have its current evolution depicted in figure 4.15, namely branch 2, 6, 20, 21 and 27. On the basis of the above, it can be concluded that the current in the MG branches is considerably below the stipulated maximum value of 220 A, having the higher observed current a magnitude of around 25 A.

In figure 4.16 the evolution of the voltage magnitude in bus 14 and 22, the current in two branches of the correspondent main conduit and the supplied and curtailed load of the MG is presented. The voltage magnitude reaches its maximum limit of 1.1 pu when the load starts to be curtailed, due to the fact that the energy that is flowing in the MG is null, i.e., the loads in bus 14 and 22 are not being supplied. When the load starts to be supplied it is observable that the voltage reaches its limit again, due to the fact that there are still branches in the main conduit without energy flowing.

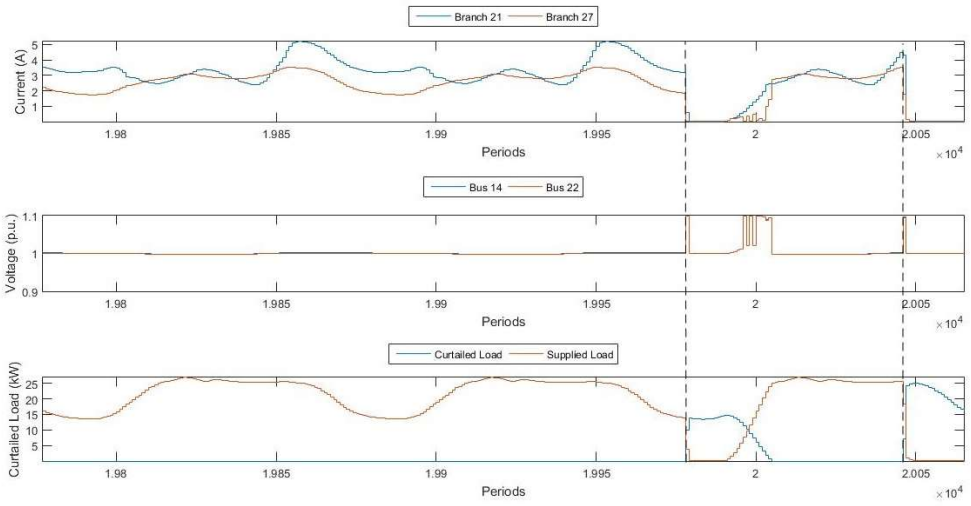

Figure 4.16 - Evolution of the voltage magnitude in bus 14 and 22 (pu), the current in the branch 21 and 27 (A) and the supplied and curtailed load (kW) of the MG - IM+ 20E.

4.2.2 MG Performance with the IM 20P ESS Model

The IM 20P ESS model was the one whose implementation in the MG led to the worst levels of reliability, due to its low SOC. Figure 4.17 shows the battery SOC and power output throughout the event.

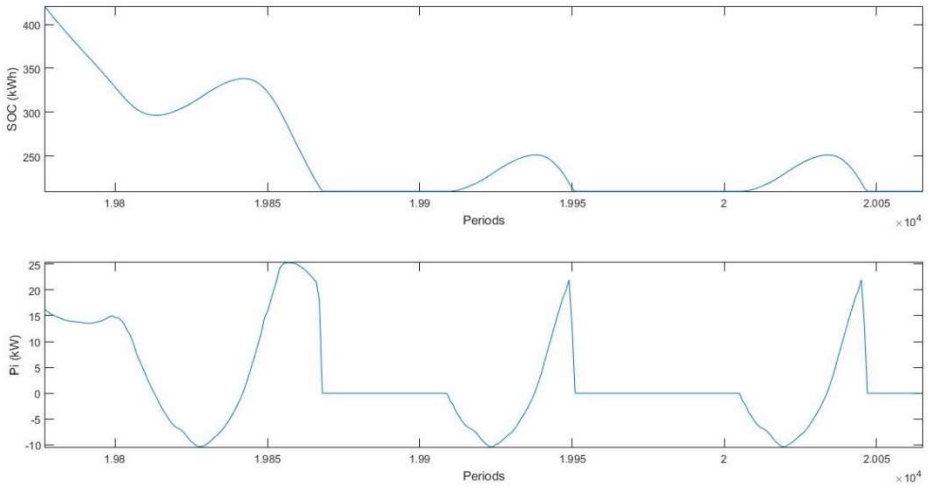

Figure 4.17 - Battery SOC (kWh) and power output (kW) – IM 20P.

This ESS reaches its minimum SOC in the end of the first day. That behavior is explained by the fact that this battery SOC is approximately half of the one guaranteed by IM+ 20E, thus, with the same conditions in both simulations, it was expected that this battery would reach its minimum SOC in half of the time observed with the model tested in the last sub section. The levels of power provided by this ESS are similar to the ones obtained with the IM+ 20E model, although for a briefer number of periods.

Since the battery will provide less power, due to its inherent electric characteristics, the need to curtail load will be felt sooner than with the IM+ 20E model. This phenomenon is represented in figure 4.18.

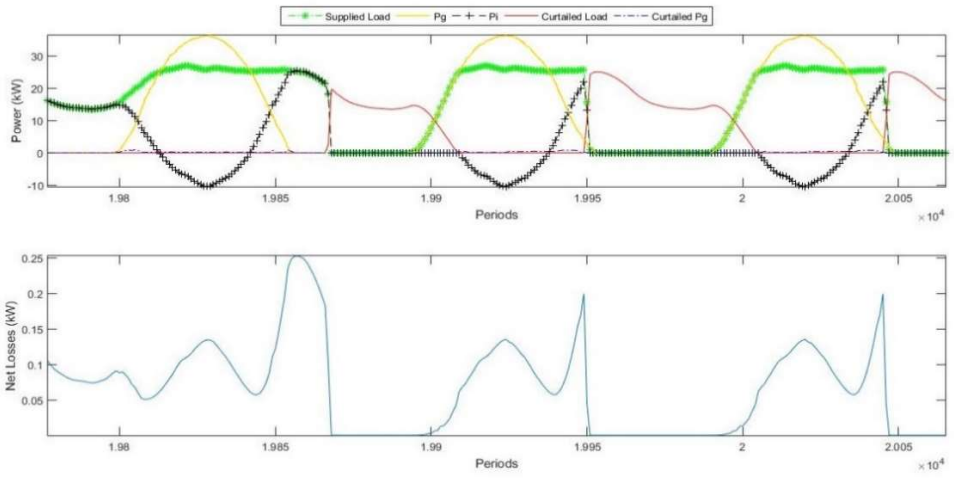

Figure 4.18 - Evolution of the PV generation (Pg), the battery power output (Pi), the supplied and curtailed load and the active net losses (kW) - IM 20P.

With this model, MG load starts to be curtailed in the end of the first day, when the battery can't inject more power into the MG. Despite the fact that the implementation of this model causes only one more load curtailment, the values of EPNS are considerably higher than the ones achieved with the IM+ 2OE, as can be observed in figures 4.19 and 4.20.

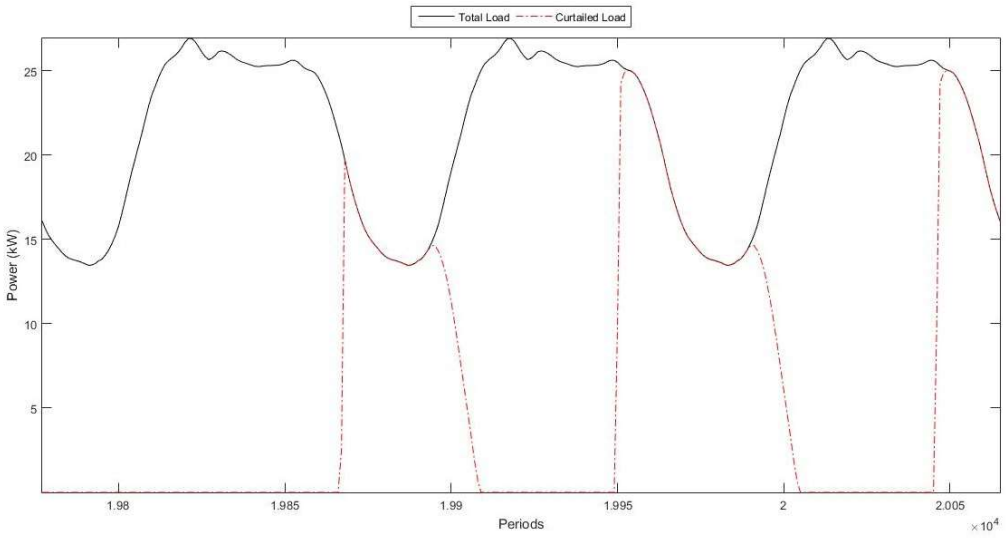

Figure 4.19 - Curtailed and total load (kW) in each period of the simulation - IM 20P.

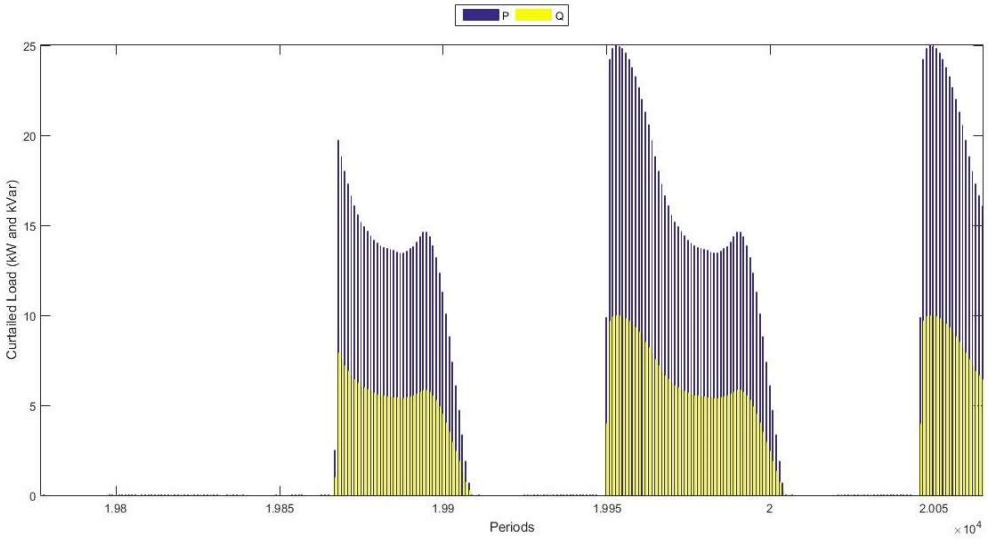

Figure 4.20 - Real (kW) and reactive (kVar) curtailed load in each period of the simulation - IM 20P.

Regarding the value of the current in the chosen branches it was noticed that the values, until the first load curtailment, are equal to the ones attained with the other energy storage model. After the occurrence of one load curtailment, the currents are identical in both simulations, since the conditions are the same. This illation is supported by figure 4.21.

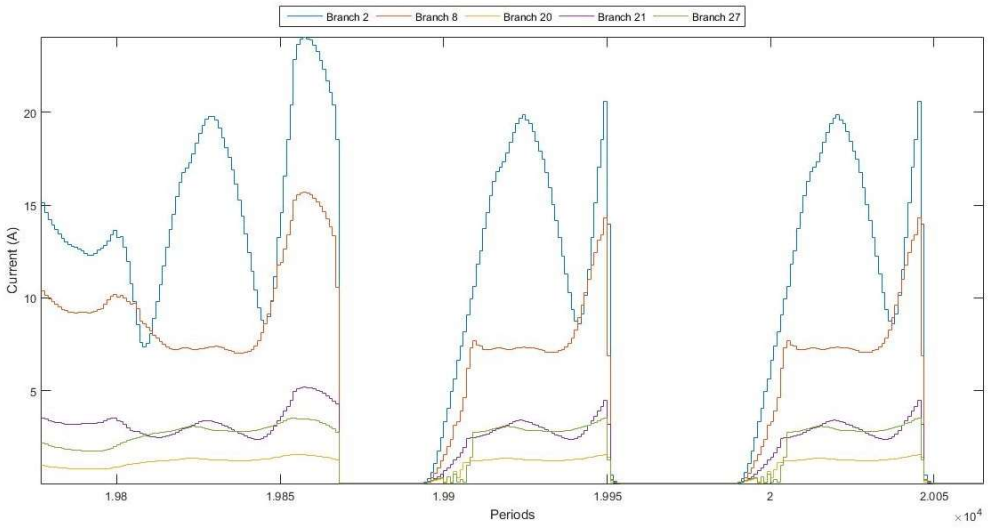

Figure 4.21 - Current (A) in branches 2, 6, 20, 21 and 27 - IM 20P.

The voltage fluctuation is analogous with the one described in the former sub section, as presented in figure 4.22. Nevertheless, the maximum voltage is reached sooner and more often, due to the higher number of load curtailments that come from the employment of the IM 20P model.

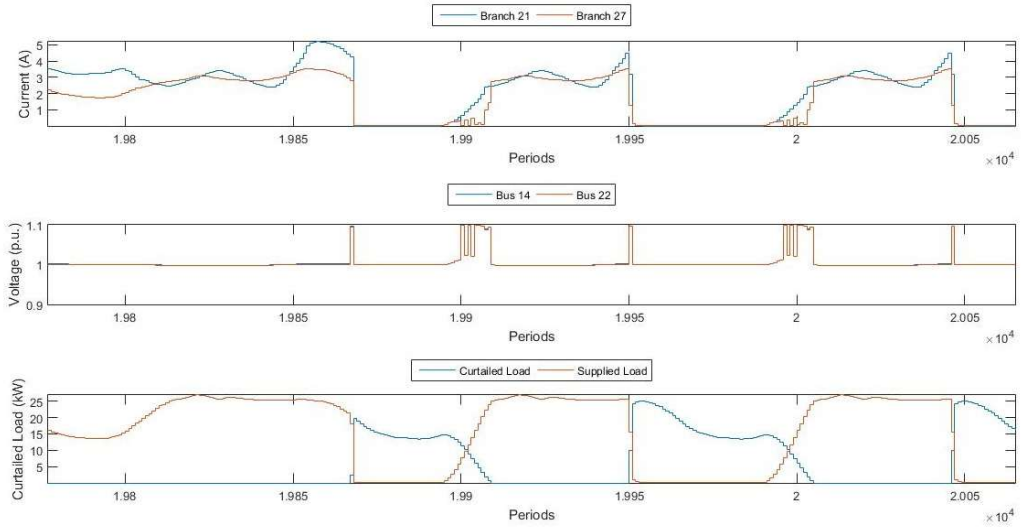

Figure 4.22 - Evolution of the voltage magnitude in bus 14 and 22 (pu), the current in the branch 21 and 27 (A) and the supplied and curtailed load (kW) of the MG - IM 20P.

4.3 Evaluation of the Impact of Different λ on the System Reliability Indexes

In this section, the effect of diverse failure rates (λ) in the system reliability performance, with and without considering the presence of the previously described MG, will be assessed. The chosen ESS model is the IM+ 20E. Table 4.10 presents the multiple values of λ used, as well as the correspondent MTTF, MTBF, cycle frequency and P_0. A constant MTTR of 1 hour was assumed, thus only one simulation was required.

The implementation of the MG will result in better reliability indexes for any value of λ, since, without MG, the LOLP will be equal to 1. Thus, according to (3.46), the LOLP in an annual basis will be identical to the value of the upper system unavailability. So, as the LOLP attained when considering the MG is always inferior to 1, its value, after the conversion to an annual basis, will be inferior to the one obtained without the MG. The quotient between both of them will be constant and equal to the LOLP obtained with MG before the conversion to an annual basis. This logic is mathematically explained in (4.4).

$$\frac{LOLP_{anual\ basis_{With\ MG}}}{LOLP_{anual\ basis_{Without\ MG}}} = \frac{LOLP_{event\ basis_{With\ MG}} \times P_0}{P_0} = \\ = LOLP_{event\ basis_{With\ MG}} \tag{4.4}$$

Table 4.10 - Upper system parameters for the diverse failure rates.

λ (events/year)	MTTF (hours)	MTBF (hours)	f (events/year)	P0
0,5	17520	17521	0.499971463	5.7E-05
1	8760	8761	0.999885858	0.00011
2	4380	4381	1.999543483	0.00023
5	1752	1753	4.997147747	0.00057
10	876	877	9.988597491	0.00114
25	350,4	351,4	24.928856	0.00285
50	175,2	176,2	49.71623156	0.00568

Table 4.11 and table 4.12 present the reliability indexes obtained with and without MG, respectively.

Table 4.11 - Reliability indexes with MG.

λ (events/year)	LOLP	LOLF (load curt./year)	LOLE (hours/year)	LOLD (hours/load curt.)	EPNS (kW)	EENS (kWh)
0.5	2.07744E-06	0.02587	0.01820	0.70343	2.4014	21036.5
1	4.15464E-06	0.05174	0.03639	0.70343	4.8026	42070.7
2	8.30833E-06	0.10347	0.07278	0.70343	9.6041	84131.7
5	2.07637E-05	0.25858	0.18189	0.70343	24.0020	210257.3
10	4.15038E-05	0.51686	0.36357	0.70343	47.9766	420274.8
25	1.03582E-04	1.28994	0.90738	0.70343	119.7366	1048893.0
50	2.06577E-04	2.57257	1.80961	0.70343	238.7937	2091833.1

Table 4.12 - Reliability indexes without MG.

λ (events/year)	LOLP	LOLF (load curt./year)	LOLE (hours/year)	LOLD (hours/load curt.)	EPNS (kW)	EENS (kWh)
0.5	5.70744E-05	0.49997	0.49997	1	81.9342	717743.8
1	1.14142E-04	0.99989	0.99989	1	163.8591	1435405.6
2	2.28258E-04	1.99954	1.99954	1	327.6808	2870483.6
5	5.70451E-04	4.99715	4.99715	1	818.9216	7173752.9
10	1.14025E-03	9.98860	9.98860	1	1636.9093	14339325.9
25	2.84576E-03	24.92886	24.92886	1	4085.2860	35787105.2
50	5.67537E-03	49.71623	49.71623	1	8147.3865	71371105.4

The immutability in the value of the LOLD of the system with MG can be explained by:

$$LOLD_{annual\ basis} = \frac{LOLE_{annual\ basis}}{LOLF_{annual\ basis}} = \frac{LOLP_{annual\ basis} \times 8760}{LOLF_{event\ basis} \times f} =$$

$$= \frac{LOLP_{event\ basis} \times P_0 \times 8760}{LOLF_{event\ basis} \times f} = \frac{LOLP_{event\ basis}}{LOLF_{event\ basis}} \times \frac{MTTR}{MTBF} \times MTBF =$$

$$= \frac{LOLP_{event\ basis}}{LOLF_{event\ basis}} \tag{4.5}$$

One can observe that the value of the LOLE, non-considering the MG, for the different failure rates is identical to the respective frequency cycle. This phenomenon is described in (4.6). The same can be said about the achieved LOLF in the system without the MG, which is explained through (3.42) and (3.47).

$$LOLE_{annual\ basis} = LOLP_{annual\ basis} \times 8760 = P_0 \times 8760 =$$

$$= \frac{MTTR}{MTBF} \times 8760 = MTTR \times f = f \tag{4.6}$$

Like it was expected, the reliability of the system, for both cases, deteriorates with the increasing of λ, since the unavailability of the MV grid is approximately directly proportional to its failure rate, due to the fact that the MTTR is considerably lower than the MTTF. Figure 4.23 depicts the aforementioned correlation, considering the existence of the MG.

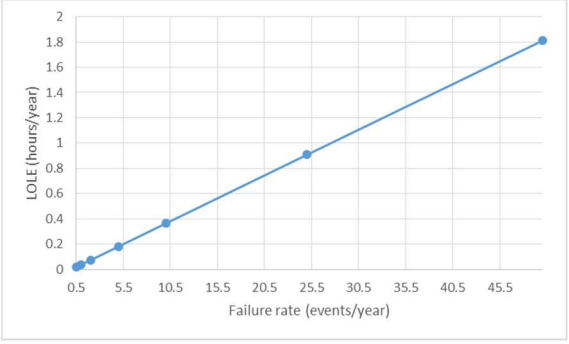

Figure 4.23 - Attained LOLE (hours/year), with MG, for the various failure rates (events/year).

Through (3.43) is possible to conclude that, if the quotient between the LOLP with and without MG is constant, the one that derives from the division of the two values of LOLE also is. Figure 4.24 confirms that assumption.

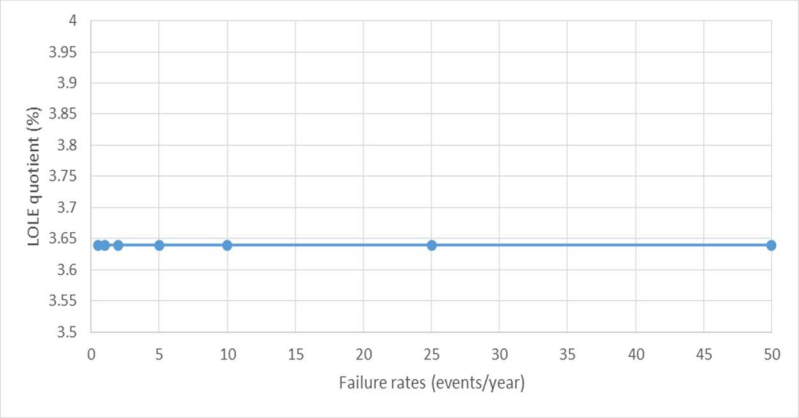

Figure 4.24 - Quotient between LOLE system with and without MG.

From the aforementioned invariability results that the benefits derived from the implementation of a MG in the system will be constants, in terms of reliability, no matter the failure rate associated to the upper system. The achieved LOLE with MG will be approximately 3.64 % of the one attained without it.

The same logic can be applied to the other reliability indexes, as it is demonstrated in (4.7), (4.8) and (4.9). The value of EENS is the product between the EPNS by the number of hours in one year. Therefore, the value of the reduction attained with the implementation of the MG, regarding the EENS, is identical to the one achieved in the EPNS, analogously to the verified with the LOLP and the LOLE. For simplification purposes, the number "1" indicates that the index is in an event basis, while the number "2" suggests that the corresponding basis is the annual one.

$$\frac{LOLF_{2_{With\ MG}}}{LOLF_{2_{Without\ MG}}} = \frac{LOLF_{1_{With\ MG}} \times f}{LOLF_{1_{Without\ MG}} \times f} = LOLF_{1_{With\ MG}} \tag{4.7}$$

$$\frac{LOLD_{2_{With\ MG}}}{LOLD_{2_{Without\ MG}}} = \frac{LOLP_{1_{With\ MG}}}{LOLF_{1_{With\ MG}}} \tag{4.8}$$

$$\frac{EPNS_{2_{With\ MG}}}{EPNS_{2_{Without\ MG}}} = \frac{EPNS_{1_{With\ MG}} \times f}{EPNS_{1_{Without\ MG}} \times f} = \frac{EPNS_{1_{With\ MG}}}{EPNS_{1_{Without\ MG}}} \tag{4.9}$$

In table 4.13 the relative achieved reduction in the reliability performance of the system, regarding the implementation of the MG, is presented.

Table 4.13 - Relative reduction in the reliability indexes with the implementation of the MG.

Reliability Index	Relative Reduction (%)
LOLP	96.36
LOLE	96.36
LOLF	94.83
LOLD	29.66
EPNS	97.07
EENS	97.07

The increasing in the reliability performance of the system with the implementation of the MG is remarkable, although, it is noteworthy that other aspects play an important role, such as the amount of the investment required to install the battery and the PV microgeneration units. This improvement is so marked also because the fact that the worst case scenario, in which all the load is curtailed in the course of an event, is considered to assess the reliability of the system without the MG. Thus, the values presented in table 4.13 can be interpreted as the maximum achievable improvements in the reliability indexes with the introduction of the test MG.

Other relevant comparison regards the levels of EENS in both cases, since that, with a reduction on the levels of curtailed load, the agents that manage and operate the MG can have pecuniary advantages. This source of profit derives from the fact that, if the curtailed load exceeds some specified thresholds defined by the regulatory authorities, monetary penalties are assigned to the responsible entities. Figure 4.25 depicts the system EENS without MG and the difference between the last one and the system EENS with MG.

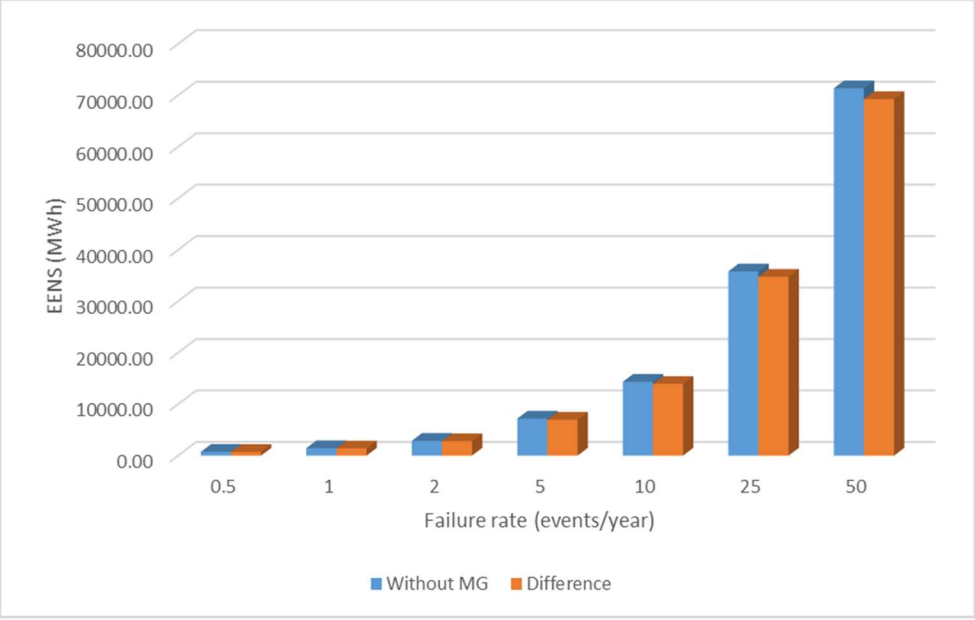

Figure 4.25 - EENS (MWh) without MG and the difference between the EENS values without and with MG.

It can be concluded that almost all the EENS obtained without considering the implementation of the MG is used, in the system with the MG, to supply the demand.

4.4 Evaluation of the Impact of Different MTTRs on the System Reliability Indexes

In this section, the consequences of diverse MTTRs in the system reliability performance, with and without considering the implementation of the MG, will be evaluated. The chosen ESS model is the IM+ 20E. Table 4.14 shows the values of MTTR used for each simulation, as well as the MTTF, MTBF, cycle frequency and P_0. A constant λ of 2 events/year was assumed in all the seven different simulations.

Table 4.14 – Upper system parameters employed in each simulation.

MTTR (hours)	MTTF (hours)	MTBF (hours)	f (events/year)	P0
0.5	4380	4380.5	1.9997717	0.0001141
1	4380	4381	1.9995435	0.0002283
2	4380	4382	1.9990872	0.0004564
4	4380	4384	1.9981752	0.0009124
8	4380	4388	1.9963537	0.0018232
16	4380	4396	1.9927207	0.0036397
32	4380	4412	1.9854941	0.0072529

Similarly to what was observed in the last section, the value of the reliability indexes will increase with the raising of the MTTR, since its MTTF >>> MTTR.

In tables 4.15 and 4.16 the attained system reliability indexes with and without MG are shown, respectively.

Table 4.15 - Reliability indexes with MG.

MTTR (hour)	LOLP	LOLF (load curt./year)	LOLE (hours/year)	LOLD (hours/load curt.)	EPNS (kW)	EENS (kWh)
0.5	2.8984E-06	0.08134	0.02539	0.31215	5.039	44143.67
1	8.3083E-06	0.10347	0.07278	0.70343	9.604	84131.70
2	2.9504E-05	0.16528	0.25845	1.56374	25.948	227303.64
4	1.0769E-04	0.27383	0.94333	3.44490	80.456	704792.29
8	3.7329E-04	0.54481	3.27006	6.00219	248.962	2180906.83
16	1.1981E-03	1.00128	10.49506	10.48159	730.907	6402745.39
32	3.3528E-03	2.04273	29.37087	14.37824	2153.131	18861425.76

Table 4.16 – Reliability indexes without MG.

MTTR (hour)	LOLP	LOLF (load curt./year)	LOLE (hours/year)	LOLD (hours/load curt.)	EPNS (kW)	EENS (kWh)
0.5	0.00011	1.99977	0.99989	0.5	250.213	2191866.23
1	0.00023	1.99954	1.99954	1	327.681	2870483.63
2	0.00046	1.99909	3.99817	2	494.477	4331619.03
4	0.00091	1.99818	7.99270	4	833.229	7299086.22
8	0.00182	1.99635	15.97083	8	1572.337	13773673.25
16	0.00364	1.99272	31.88353	16	2873.616	25172874.67
32	0.00725	1.98549	63.53581	32	5942.816	52059069.23

The majority of the reliability indexes improved with the implementation of the MG, for any assigned MTTR. This amelioration was expected, since, as it was already explained in the last section, the LOLP without MG, in an event basis, is equal to 1. According to (3.40), this index will be identical to the respective unavailability of the upper system, whereas the attained LOLP with MG will always be inferior to 1, for the considered values of MTTR. If one continued to perform simulations for larger values of MTTR, the value of the LOLP, in an event basis, would increase up to values close to the unity.

One exception to this improvement are the attained LOLFs for an MTTR of 32 hours. This is due to the fact that the LOLF without MG is considered equal to 1, since each event is considered as one uninterrupted load curtailment, in an event basis. Regarding the implementation of the MG and a continuous increasing of the upper system MTTR, it's obvious that the mean duration of the simulated events will increase as well. With a longer islanding, the probability of having more than one load curtailment per event increases, with the consequence of a larger LOLF.

Another noteworthy fact is the value of the attained LOLD without MG, which is identical to the value of the MTTR assigned to the upstream network.

The abovementioned phenomenon is described in (4.10).

$$LOLD_{2_{Witho\quad MG}} = \frac{LOLE_{2_{Without\ MG}}}{LOLF_{2_{Without\ MG}}} = \frac{LOLP_{2_{Without\ MG}} \times 8760}{LOLF_{1_{Witho\quad MG}} \times f} =$$

$$= \frac{LOLP_{1_{Witho\quad MG}} \times P_0 \times 8760}{f} = \frac{P_0 \times 8760}{f} =$$

$$= \frac{MTTR}{MTBF} \times MTBF = MTTR \tag{4.10}$$

In figure 4.26 the evolution of the system LOLE with and without MG is presented. It is perceptible that the attained LOLE without MG follows a resembling directly proportional relation with the MTTR, while the evolution of the achieved LOLE with MG is similar to an exponential function. This can be explained through (4.11) and (4.12).

$$LOLE_{2_{Without\ MG}} = LOLP_{1_{Without\ MG}} \times P_o \times 8760 = P_o \times 8760 \tag{4.11}$$

$$LOLE_{2_{With\ MG}} = LOLP_{2_{With\ MG}} \times 8760 \tag{4.12}$$

Equation (4.11) displays a directly proportional relation between the value of the LOLE and the unavailability of the upper grid. Therefore, given that the MTTR is significantly inferior to the MTTF, the curve of the obtained LOLE without MG is explained, since the unavailability is, approximately, directly proportional to the MTTR.

With the method followed in the last section, only one simulation was required, as the value of the upstream grid MTTR was kept constant. Therefore, the attained reliability indexes, in an event basis, were transversal to all the evaluated cases with different failure rates. To evaluate the impact of diverse MTTR on the reliability indexes, several simulations needed to be employed. Thus, the reliability indexes attained, considering an event basis, are not the same to each assessed scenario with a specific MTTR. From (4.12) it can be observed that the diverse LOLPs need to be contemplated, in order to understand the evolution of the LOLP with MG, in an annual basis.

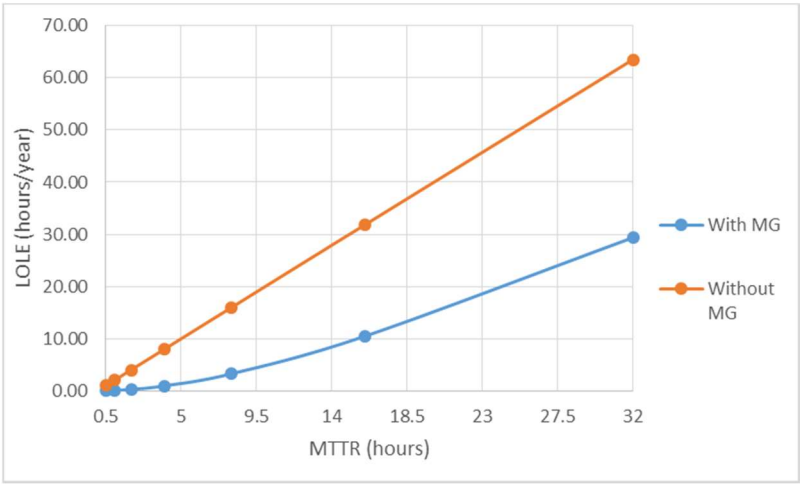

Figure 4.26 – LOLE (hours/year) for the different MTTR (hours) assigned to the upper system.

The attained LOLP in each simulation is presented in figure 4.27, from which it can be seen an identical evolution to the one registered in figure 4.26, regarding the case with MG.

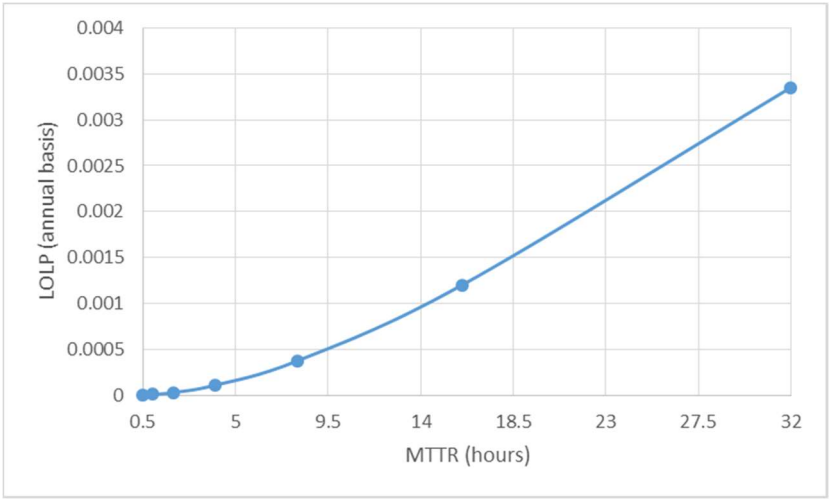

Figure 4.27 – LOLP (annual basis) obtained in each simulation.

Equations (4.4), (4.7), (4.8) and (4.9) are still valid in this section. However, the result provided by them is not constant anymore, since the reliability indexes obtained after each simulation are different, due to the MTTR assigned to the MV grid.

In table 4.17 the relative reductions of the reliability indexes achieved with the implementation of the MG are presented. To enable a broader comprehension over the benefits of implementing a MG, three new simulations, with higher MTTRs, were performed.

The higher the MTTR of the upper system, the less the improvement in the reliability performance of the system. This correlation derives from the fact that with a bigger MTTR, the time frame where the MG will operate in stand-alone mode will increase, expanding the possibility of the occurrence of load curtailments, since the low levels of PV generation can't be enough to charge the battery to its previous capacity. Figures 4.11 and 4.17 are examples of this lack of generation required to enable the ESS to reach its preceding SOC.

Table 4.17 - Relative reduction in the reliability indexes with the implementation of the MG.

	Relative Reduction (%)					
MTTR (hour)	**LOLP**	**LOLF**	**LOLD**	**LOLE**	**EPNS**	**EENS**
0,5	97.461	95.933	37.570	97.461	97.986	97.986
1	96.360	94.825	29.657	96.360	97.069	97.069
2	93.536	91.732	21.813	93.536	94.752	94.752
4	88.198	86.296	13.878	88.198	90.344	90.344
8	79.525	72.710	24.973	79.525	84.166	84.166
16	67.083	49.753	34.490	67.083	74.565	74.565
32	53.773	-2.883	55.068	53.773	63.769	63.769
64	43.286	-96.149	71.086	43.286	56.195	56.195
150	34.070	-325.314	84.498	34.070	49.167	49.167
300	28.013	-715.741	91.175	28.013	44.323	44.323

Figure 4.28 depicts the evolution of the relative reduction of the LOLE with the implementation of the MG.

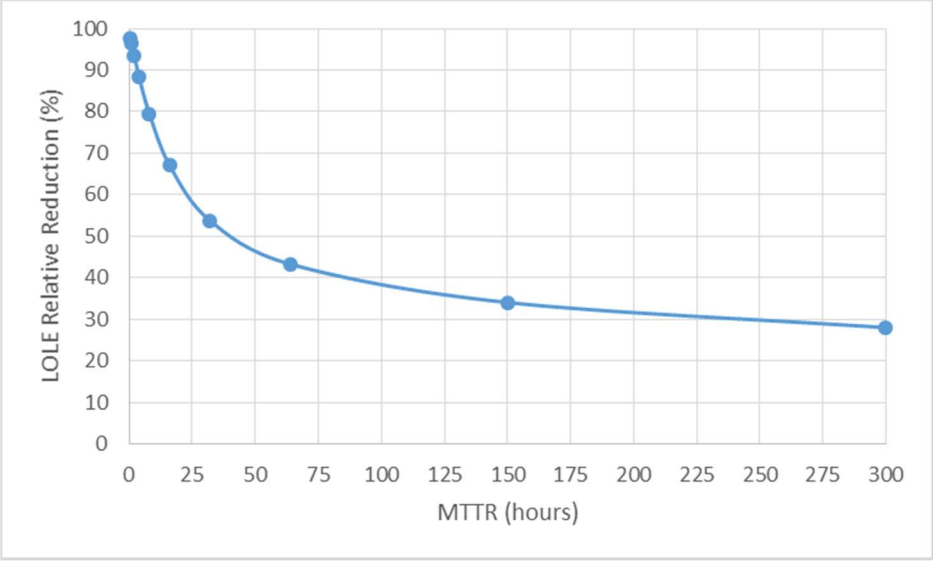

Figure 4.28 - LOLE relative reduction (%) for each MTTR assigned to the upper system.

The imposed reduction on the system LOLE, through the implementation of the MG, suffers higher decreases for low values of MTTR. It can be seen that, as the MTTR keeps increasing, the value of the LOLE relative reduction starts to stagnate between 20 and 30%. Although the last three values of the MTTR introduced are ludicrous when compared to the typical ones, they allow a clear awareness about the evolution of the reliability-related benefits when the MG is considered.

As it was previously stated, the obtained LOLF when higher MTTRs are assigned to the upper system is superior to the one achieved without the MG. This translates into a negative relative reduction, i.e., the LOLF is being increased, which gets worse if one continues to increase the MTTR, as can be observed in figure 4.29, in a linear way.

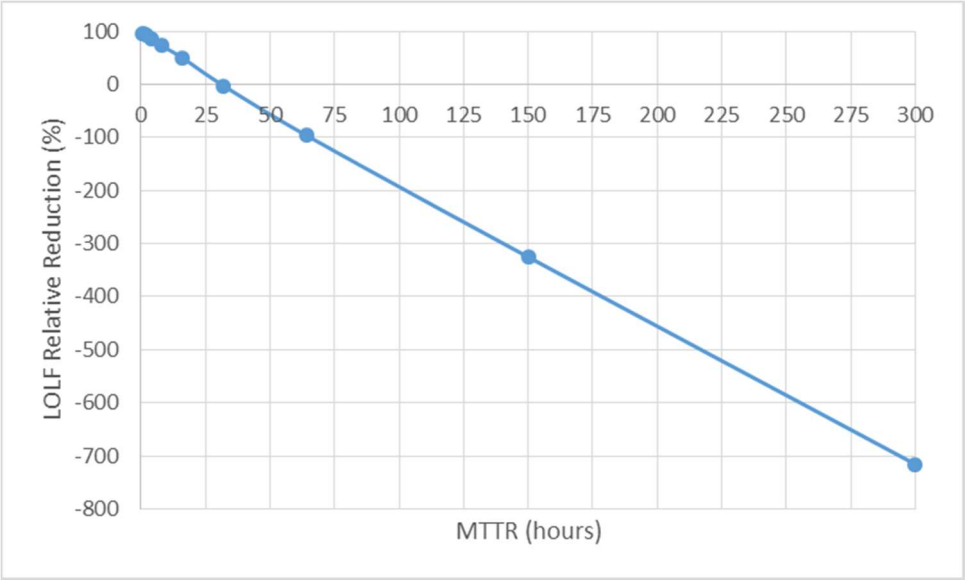

Figure 4.29 - LOLF relative reduction (%) for each MTTR assigned to the upstream network.

A curious behavior is the one depicted in figure 4.30, regarding the LOLD relative reduction obtained for the diverse MTTR.

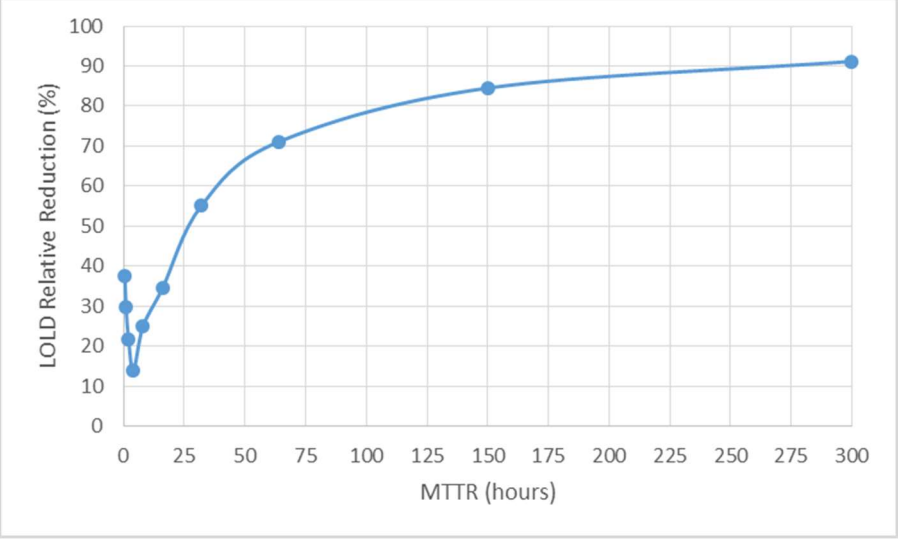

Figure 4.30 - LOLD relative reduction (%) for each MTTR assigned to the upstream grid.

For the first four chosen values of MTTR, the reduction on the LOLD provided by the employment of the MG decreases. Afterwards, the relative reduction increases until it starts to stagnate at around 90%. This can be explained through the high values of LOLF obtained, for the system with MG, when the assigned MTTR starts to increase. Therefore, since the LOLD is equal to the quotient between the LOLE and the LOLF, its value will start to increase at a slow rate when compared to the growing of the LOLD without considering the MG, resulting in a higher LOLD relative reduction.

Figure 4.31 presents the progress of the relative reduction of the EPNS, which is equal to the one showed by the EENS, with the implementation of the MG. The depicted evolution is similar to the one exhibited regarding the LOLE, although, it stagnates in a higher value – around 40%.

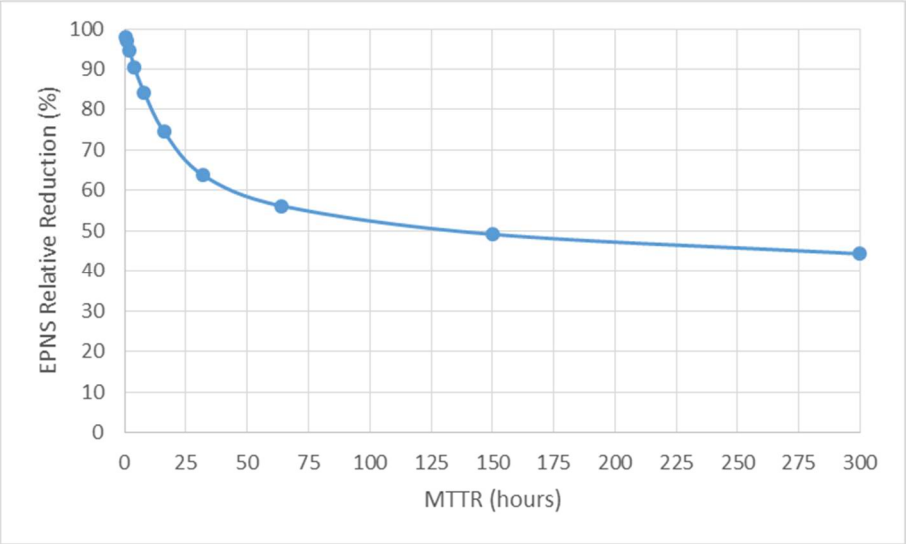

Figure 4.31 - EPNS relative reduction (%) for each MTTR assigned to the upper system.

Figure 4.32 depicts the system EENS without and with MG, as well as the difference between them.

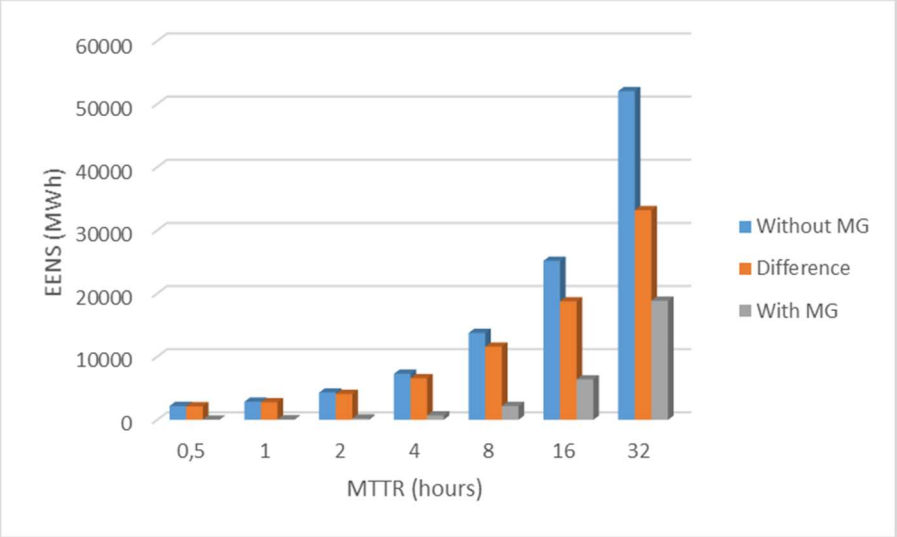

Figure 4.32 - System EENS (MWh) with and without MG, and the difference between both.

The EENS attained with MG is always inferior to the one obtained without it, albeit the advantages are more expressive for lower MTTRs, since the EENS relative reduction is higher for lower MTTRs, as it observed in table 4.17.

4.5 Value of the MG

In this section a method to evaluate the monetary value, subsequent to the improvement in the system reliability, derived from the employment of the MG is proposed. This method is based on the difference between the EENS obtained without and with the MG, i.e., in the energy that is supplied due to the implementation of MG.

To settle the Value of the MG (VMG), the Portuguese Gross Domestic Product (GDP) and total annual demand were investigated [58], [59]. Their values, referred to the year of 2014, are presented in table 4.18.

Table 4.18 - Portuguese GPD (M€) and total annual demand (MWh).

GPD (M€)	Total Annual Demand (MWh)
173446.2	46180709.3

Afterwards, the VMG was attained by dividing the GPD by the total annual demand, resulting in:

$$VMG = \frac{GPD}{Total\ annual\ demand} = 3755.81\ €/MWh \tag{4.13}$$

The VMG achieved through (4.13) is a conservative profit, since this value is an agglomerate of the annual national consumption. Therefore, it disregards the type of clients that would benefit from the implementation of the MG: it would be higher if the clients whose EENS would decrease were from the industrial type, and lower if the clients were residential, since a load curtailment affecting the first ones would result in elevated financial losses, whereas a load curtailment in a residential house wouldn't be that harmful, in normal conditions.

Due to the fact that the value of money is volatile, a proper cash-flow analysis is required. Considering an interest rate of 10% and a 20 years capitalization, the future value of the MG is given by (4.14):

$$VMG_{FV} = VMG \times (1+i)^n = 25267.24\ €/MWh \tag{4.14}$$

where i represents the interest rate and n the number of period, equal to 0.1 and 20, respectively.

It is now possible to evaluate, from an economic perspective, the implementation of a MG in all the cases presented in the previous sections.

4.5.1 Value of the MG for Different Failure Rates

The VMG for different failure rates is computed through the product of VMG_{FV} by the difference between the EENS obtained without and with the MG, like is presented in table 4.19.

Table 4.19 - Attained VMG (M€) for different failure rates.

λ (events/year)	EENS With MG (MWh)	EENS Without MG (MWh)	Diff (MWh)	VMG (M€)
0.5	21.0365271	717.7437804	696.7072533	17.60387295
1	42.07065305	1435.405636	1393.334983	35.20573655
2	84.13170312	2870.483629	2786.351925	70.40343709
5	210.2572683	7173.752867	6963.495599	175.9483502
10	420.2747906	14339.32586	13919.05107	351.6960751
25	1048.892975	35787.10523	34738.21225	877.738924
50	2091.833095	71371.10543	69279.27233	1750.496356

The VMG increases with the rise of the failure rate, since the difference between the EENS achieved without and with MG grows when the failure rate is higher, due to the fact that the upper system probability of being in the failure state is approximately directly proportional to λ. Figure 4.33 depicts the evolution of the VMG for the various failure rates.

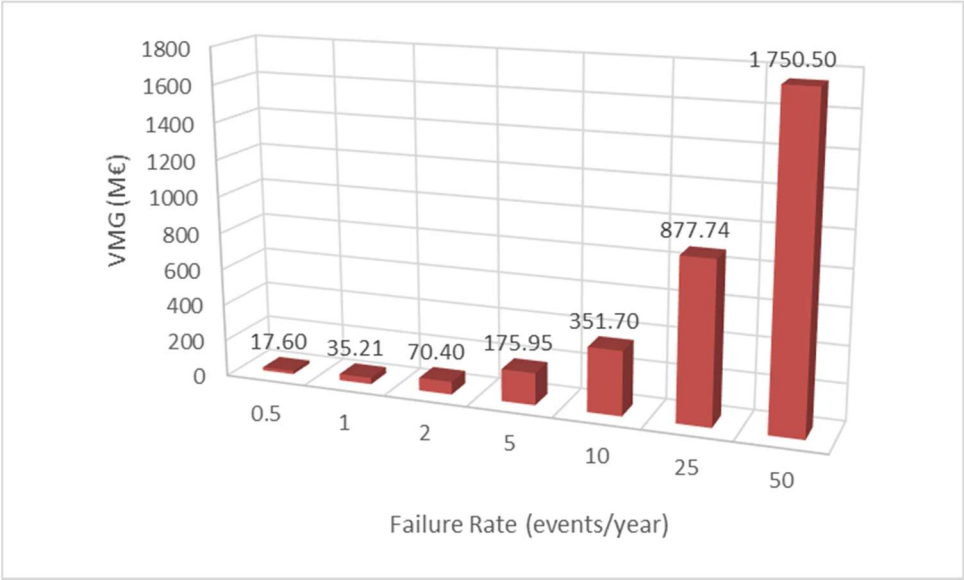

Figure 4.33 - VMG (M€) for different failure rates (events/year).

4.5.2 Value of the MG for Different MTTR

The VMG for the diverse upper system MTTR was attained through an identical process to the one employed for the various failure rates, being the results exhibited in table 4.20 and figure 4.34.

Table 4.20 - Attained VMG (M€) for different MTTR.

MTTR (hour)	EENS with MG (MWh)	EENS without MG (MWh)	Diff (MWh)	VMG (M€)
0.5	44.14367369	2191.866231	2147.722557	54.26703231
1	84.13170312	2870.483629	2786.351925	70.40343709
2	227.3036372	4331.61903	4104.315393	103.7047431
4	704.7922914	7299.086223	6594.293931	166.6196412
8	2180.906831	13773.67325	11592.76642	292.9172708
16	6402.745386	25172.87467	18770.12928	474.2694575
32	18861.42576	52059.06923	33197.64347	838.8129949

Although the VMG presented in table 4.19 and table 4.20 is higher for parameters that induce an unsatisfactory reliability performance, their results are deceptive. For instance, a failure rate of 10 events/year would entail several costs related to the reposition in service of the devices that caused the islanding and would yield an unacceptable service in terms of reliability, according to the nowadays standards.

It can be seen that even for admissible levels of λ or the MTTR the VMG obtained through the proposed technique is significantly high.

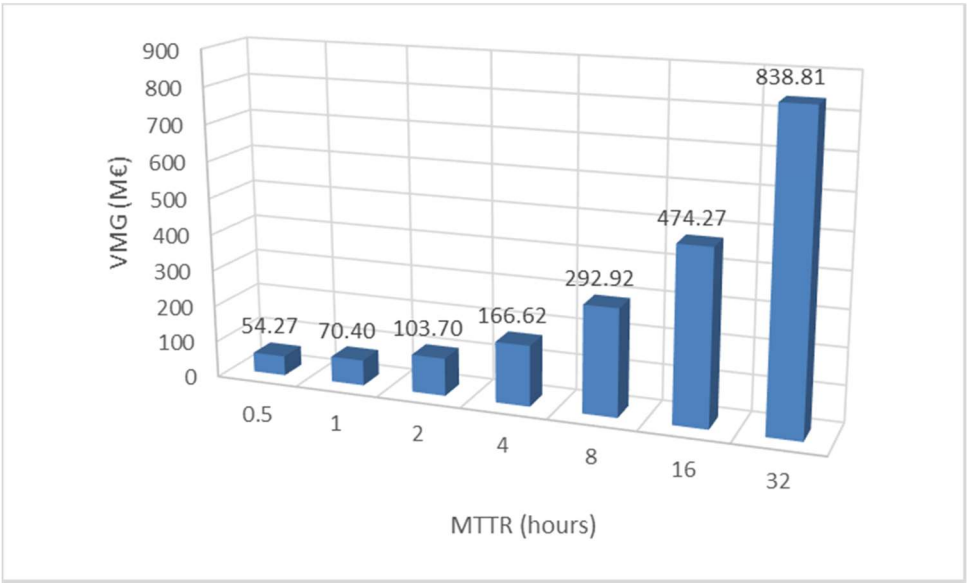

Figure 4.34 - VMG (M€) for different MTTR (hours).

4.6 Conclusions

The main results of the work developed in the dissertation, through the employment of the method proposed in chapter 3, were presented in this chapter.

In order to evaluate the impact of distinct ESS models on the performance of the MG, its operation in stand-alone mode was simulated for five batteries with different SOCs and power constraints. It was demonstrated that the reliability performance of the MG improves with the increasing of the battery SOC. Therefore, the power constraints don't play an important role in this specific case, since the levels of PV generation don't allow the battery to discharge or

charge values near the specified power limits, in one period. It is expected, thus, that with higher levels of PV generation, the choice of the most advantageous ESS model would result from a trade-off between the SOC, the continuous discharge power and the nominal charge power.

From the results showed in the following sections, one can conclude that the reliability performance of the system deteriorates with the increasing of the upper system failure rate and MTTR. Regarding the evaluation of the impact of the diverse failure rates, it was proved that the LOLE increases linearly with the rise of the failure rate, for both the system with and without MG. In relation to the MV network MTTR, the conducted study showed that when the implementation of the MG was considered, the increase in the LOLE is similar to an exponential function, due to the LOLP attained in each simulation.

The implementation of the MG led to a better system reliability performance in all the different scenarios, as it was expected. Contrary to what was observed with the failure rates, with the increase of the upper system MTTR, the improvement in the reliability wasn't constant.

With the introduction of a new concept to evaluate the possible economic benefits in implementing a MG – the VMG -, it was shown that a source of profit, considering solely the difference between the EENS without MG and the EENS with MG, in the order of millions can be achieved, since the load that ceases to be curtailed brings pecuniary advantages to the MG operator.

The subsequent chapter, the last one, regards the final conclusions of the dissertation. Suggestions about how to improve this study are also presented in the following chapter.

Chapter 5 - **Conclusions**

In this chapter, the main conclusions of this dissertation, regarding the reliability assessment of a MG operating in IM and its impact on the upstream network, will be revealed. A deliberation about the achievement of the proposed objectives in the first chapter will be given.

Moreover, an enumeration of recommendations in order to pursue researches based on the presented work will be yielded.

5.1 Conclusions

During the last decade a vivid attention to the employment of the MG concept, in order to increase the distribution system reliability, was verified. To achieve a full implementation of that concept, it is required to understand and quantify the possible improvements envisaged with the presence of a MG.

The main goal of this dissertation arises from the aforementioned fact. Therefore, an evaluation of the MG reliability, while operating in stand-alone mode, and its impact on the distribution system reliability are conducted. A new technique, based on the sequential MC method, is, thus, presented. Since the reliability security assessment is beyond the scope of this study, the dynamic behavior of the MG isn't addressed.

Aiming to contextualize this thesis, a brief description of the employment of the MC method as a tool to assess the reliability of an electric system was provided in chapter 2, where the chronological and the non-chronological simulations were referred, as well as its advantages and drawbacks. Moreover, a Markov's based model of a two state component was formulated in this chapter. Finally, a set of researches that addresses the problem of assessing the reliability of a MG, operating in only one or both modes, is exhibited, being explained the main topics of the developed work in each study. Most of the studies presented in chapter 2 don't focus on the reliability assessment of a MG operating in IM mode and on quantifying the increasing in the reliability performance of the system when considering its implementation, instead of seeing all the MG load as a single load-point. The execution of this thesis was boosted by the realization of the last statement.

The first step to achieve the proposed objectives was the development of a new MC-based algorithm, in order to assess the reliability of a MG composed by PV microgeneration units and a battery. It is relevant to highlight that the life cycle of the device whose failure leads the MG to an abrupt islanding is not drawn as in a classical sequential MC simulation. Instead, the 15

minute period, within a year, in which the failure occurs and the islanding duration are randomly attained, considering that the duration of the failure follows an exponential distribution.

Several results were obtained through the employment of the abovementioned algorithm. Chapter 4, where the final results are presented, starts with the evaluation of the MG reliability for five different ESS models, while operating in stand-alone mode. The goal in doing so was to conclude about the impact of the ESS characteristics on the performance of the MG. It was demonstrated that the MG reliability improves with the increasing of the battery SOC, regardless the value of the continuous discharge power and the nominal charge power. However, it is expected that, for higher levels of PV generation, the power constraints of each battery would play a relevant role in the choice of the more beneficial ESS, due to the fact that the battery would have more available energy to absorb and inject in one period, which could result in fewer and less severe load curtailments.

Afterwards, a study regarding the impact of diverse upper system failure rates and MTTR was conducted. As expected, the reliability of the system, with and without MG, deteriorates for higher values of the aforementioned parameters. This behavior is intuitive, since a higher failure rate implies that the occurrence of more system disconnections and a higher MTTR means that the MG will stay islanded for a longer time period.

It was shown that the attained LOLE with MG increases linearly with the rise of the upper system failure rate, due to the fact that, as the MTTR is significantly lower than the MTTF, the upstream network unavailability is approximately directly proportional to its failure rate. Regarding the evolution of the LOLE with MG, facing the increment in the MTTR, it was observed that its increase is similar to an exponential function, due to the LOLP obtained in each simulation, for the diverse MTTR. Without considering the implementation of the MG, the LOLE increases linearly with the rise of the upper system MTTR.

Since the life cycle of the upper system wasn't obtained, a set of assumptions, regarding the absence of the MG, was stipulated, namely: one events corresponds to one load curtailment, the total number of periods with load curtailments is equal to the total duration of the diverse events and all load is curtailed during the occurrence of an event. With these presumptions, it was possible to calculate upper bounds that define the reliability of the system without MG, enabling the comparison with the case in which the implementation of the MG was considered. It is noteworthy that with the aforementioned assumptions the worst case scenario, in which all the load is curtailed, was assumed. With the employment of load curtailment schemes the reliability of the system without MG could be improved.

The implementation of the MG improved the system reliability in all the diverse simulated scenarios. The improvement induced by the employment of the MG was measured in terms of the relative reduction, in percentage, observed in the reliability indexes. It was concluded that the improvement attained in each index was constant for the diverse failure rates, since this parameter doesn't affect the operation of the MG in IM mode, only defines the number of events per year. Therefore, the number of events can be higher and the system reliability will be, inexorably, inferior, but the attained improvements in the reliability indexes provided by the implementation of the MG will be constant. The same wasn't observed with the increasing of the upper system MTTR, since this value impacts the stand-alone mode of the operation of the MG, affecting the islanding duration. It was concluded that the higher the MTTR of the upper system, the less the benefits in the improvement of the system reliability with the implementation of the MG. Although the achieved improvement decreases for a decrease in the

reliability of the upper system, the relevance of implementing a MG rises with the decrease of the upper system reliability, since it can prevent the occurrence of lengthy blackouts for a specified number of consumers that are covered by the MG.

The achieved relative reduction in most of the reliability indexes doesn't decrease linearly with the rise of the MTTR, it stagnates in a certain value. This allows the representation of a curve that characterizes the improvements obtained for various MTTR. The impact of the natural degradation of the upper system devices, whose outage causes the interruption of the supplying provided by the upstream network, on the reliability of the system can, thus, be predicted, if the increase on the upper system MTTR follows a known chronological pattern. Therefore, this can be of high relevance to the planning of MGs.

A simple method to evaluate the possible economic benefits that derive from the implementation of one MG was also presented. This method, based on the value of the GPD and the total annual demand of one country, estimate the amount of profit through the difference between the attained EENS without MG and the EENS with MG, since that, if less load is curtailed, the system has less expenses related to the violation of the limits imposed by the regulatory entities. It can be seen that even for low levels of λ or the MTTR the VMG obtained through the proposed technique is significantly high. Then, and considering the amount of money required to install one ESS and the RES, an evaluation of the economic feasibility of the project can be employed.

The work developed in this dissertation contributed to the endowment of the framework from which the full implementation of the concept of MG is expected to arise.

5.2 Future Works

This dissertation can serve as a basis for the employment of other researches related to this field of study. Therefore, an enumeration of some aspects passible of improving the developed work is presented:

- Provide the proposed algorithm with mechanisms in order to allow a reliability security assessment, in which the dynamic behavior and the transient perturbations of the MG when the transition from the NIM to the IM occurs are considered;
- Draw the system life cycle, instead of solely drawing the period in which the event occurs and its duration. This would make the assumptions presented in section 3.7 dispensable, since the reliability indexes obtained without the MG would cease to represent an upper bound;
- Build load curtailment schemes, in order to represent loads with different levels of prioritization. This would allow to provide a more complete and real reliability assessment;
- Consider that the equipment that compose the MG can suffer outages, such as the PV generators and the lines. This would also allow the proposed algorithm to be more realistic.
- Instead of contemplating a distribution system with only one MG, or with only one load when the implementation of the MG is not considered, perform the reliability assessment of one system with multiple loads and RES and find the MG topology that would bring more benefits to the system, in terms of reliability.

References

[1] EURELECTRIC, “Power Choices - Pathways to Carbon-Neutral Electricity in Europe by 2050, Full Report,” Union of the Electricity Industry – EURELECTRIC, Brussels, Belgium, 2010.

[2] P. P. Varaiya, F. F. Wu, and J. W. Bialek, “Smart Operation of Smart Grid: Risk-Limiting Dispatch,” *Proc. IEEE*, vol. 99, no. 1, pp. 40–57, Jan. 2011.

[3] H. Liang, A. K. Tamang, W. Zhuang, and X. S. Shen, “Stochastic Information Management in Smart Grid,” *IEEE Commun. Surv. Tutor.*, vol. 16, no. 3, pp. 1746–1770, 2014.

[4] B. Kroposki, R. Lasseter, T. Ise, S. Morozumi, S. Papathanassiou, and N. Hatziargyriou, “Making microgrids work,” *IEEE Power Energy Mag.*, vol. 6, no. 3, pp. 40–53, May 2008.

[5] W. Alharbi and K. Raahemifar, “Probabilistic coordination of microgrid energy resources operation considering uncertainties,” *Electr. Power Syst. Res.*, vol. 128, pp. 1–10, Nov. 2015.

[6] X. Xu, J. Mitra, T. Wang, and L. Mu, “Evaluation of Operational Reliability of a Microgrid Using a Short-Term Outage Model,” *IEEE Trans. Power Syst.*, vol. 29, no. 5, pp. 2238–2247, Sep. 2014.

[7] J. A. P. Lopes, N. Hatziargyriou, J. Mutale, P. Djapic, and N. Jenkins, “Integrating distributed generation into electric power systems: A review of drivers, challenges and opportunities,” *Electr. Power Syst. Res.*, vol. 77, no. 9, pp. 1189–1203, Jul. 2007.

[8] H. Jiayi, J. Chuanwen, and X. Rong, “A review on distributed energy resources and MicroGrid,” *Renew. Sustain. Energy Rev.*, vol. 12, no. 9, pp. 2472–2483, Dec. 2008.

[9] K. Moslehi and R. Kumar, “A Reliability Perspective of the Smart Grid,” *IEEE Trans. Smart Grid*, vol. 1, no. 1, pp. 57–64, Jun. 2010.

[10] A. Ipakchi and F. Albuyeh, “Grid of the future,” *IEEE Power Energy Mag.*, vol. 7, no. 2, pp. 52–62, Mar. 2009.

[11] C. S. T. Gouveia, “Experimental Validation of Microgrids: Exploiting the Role of Plug-In Electric Vehicles, Active Load Control and Micro-Generation Units”, Ph.D. dissertation, FEUP, Porto, Portugal, 2014.

[12] S. A. Arefifar, Yasser A-R. I. Mohamed, and T. H. M. EL-Fouly, “Supply-Adequacy-Based Optimal Construction of Microgrids in Smart Distribution Systems”, *IEEE Trans. Smart Grid*, vol.3, no.3, pp. 1491-1502, Sept. 2012.

[13] J. A. P. Lopes, A. G. Madureira, and C. C. L. M. Moreira, “A view of microgrids: A view of microgrids,” *Wiley Interdiscip. Rev. Energy Environ.*, vol. 2, no. 1, pp. 86–103, Jan. 2013.

[14] R. Yokoyama, T. Niimura, and N. Saito, “Modeling and evaluation of supply reliability of microgrids including pv and wind power,” in *Power and Energy Society General Meeting-Conversion and Delivery of Electrical Energy in the 21st Century, 2008 IEEE*, 2008, pp. 1–5.

[15] D. E. Olivares, A. Mehrizi-Sani, A. H. Etemadi, C. A. Canizares, R. Iravani, M. Kazerani, A. H. Hajimiragha, O. Gomis-Bellmunt, M. Saeedifard, R. Palma-Behnke, G. A. Jimenez-Estevez, and N. D. Hatziargyriou, “Trends in Microgrid Control,” *IEEE Trans. Smart Grid*, vol. 5, no. 4, pp. 1905–1919, Jul. 2014.

[16] Q. Fu, A. Hamidi, A. Nasiri, V. Bhavaraju, S. B. Krstic, and P. Theisen, “The Role of Energy Storage in a Microgrid Concept: Examining the opportunities and promise of microgrids.,” *IEEE Electrification Mag.*, vol. 1, no. 2, pp. 21–29, Dec. 2013.

[17] A. Ahmad Khan, M. Naeem, M. Iqbal, S. Qaisar, and A. Anpalagan, “A compendium of optimization objectives, constraints, tools and algorithms for energy management in microgrids,” *Renew. Sustain. Energy Rev.*, vol. 58, pp. 1664–1683, May 2016.

[18] G. Cardoso, M. Stadler, A. Siddiqui, C. Marnay, N. DeForest, A. Barbosa-Póvoa, and P. Ferrão, "Microgrid reliability modeling and battery scheduling using stochastic linear programming," *Electr. Power Syst. Res.*, vol. 103, pp. 61–69, Oct. 2013.
[19] S. Bahramirad, W. Reder, and A. Khodaei, "Reliability-Constrained Optimal Sizing of Energy Storage System in a Microgrid," *IEEE Trans. Smart Grid*, vol. 3, no. 4, pp. 2056–2062, Dec. 2012.
[20] J. A. P. Lopes, C. L. Moreira, A. G. Madureira, "Defining Control Strategies for MicroGrids Islanded Operation", *IEEE Power & Energy Society*, vol. 21, no. 2, pp. 916-924, May 2006.
[21] C. Gouveia, J. Moreira, C. L. Moreira, and J. A. Pecas Lopes, "Coordinating Storage and Demand Response for Microgrid Emergency Operation," *IEEE Trans. Smart Grid*, vol. 4, no. 4, pp. 1898–1908, Dec. 2013.
[22] C. Marnay, H. Asano, S. Papathanassiou, and G. Strbac, "Policymaking for microgrids," *IEEE Power Energy Mag.*, vol. 6, no. 3, pp. 66–77, May 2008.
[23] F. Farzan, S. Lahiri, M. Kleinberg, K. Gharieh, F. Farzan, and M. Jafari, "Microgrids for Fun and Profit: The Economics of Installation Investments and Operations," *IEEE Power Energy Mag.*, vol. 11, no. 4, pp. 52–58, Jul. 2013.
[24] M. E. Khodayar, M. Barati, and M. Shahidehpour, "Integration of High Reliability Distribution System in Microgrid Operation," *IEEE Trans. Smart Grid*, vol. 3, no. 4, pp. 1997–2006, Dec. 2012.
[25] M. Nemati, K. Bennimar, S. Tenbohlen, L. Tao, H. Mueller, and M. Braun, "Optimization of microgrids short term operation based on an enhanced genetic algorithm," in *PowerTech, 2015 IEEE Eindhoven*, 2015, pp. 1–6.
[26] P. M. Costa and M. A. Matos, "Assessing the contribution of microgrids to the reliability of distribution networks," *Electr. Power Syst. Res.*, vol. 79, no. 2, pp. 382–389, Feb. 2009.
[27] E. Perea, J. M. Oyarzabal, and R. Rodríguez, "Definition, evolution, applications and barriers for deployment of microgrids in the energy sector," *E Elektrotechnik Informationstechnik*, vol. 125, no. 12, pp. 432–437, Dec. 2008.
[28] R. Lasseter, A. Akhil, C. Marnay, J. Stephens, J. Dagle, R. Guttromson, A. Meliopoulous, R. Yinger, and J. Eto, "The CERTS microgrid concept," *White Pap. Transm. Reliab. Program Off. Power Technol. US Dep. Energy*, vol. 2, no. 3, p. 30, 2002.
[29] M. A. Aguado-Monsonet, "Power to the 21st century," *foresight*, vol. 1, no. 6, pp. 537–545, 1999.
[30] Microgrids. Available in http://www.microgrids.eu/default.php. Accessed in 01/June/2016.
[31] EDP InovGrid. Available in http://www.inovgrid.pt/. Accessed in 01/June/2016.
[32] Home | InSmart. Available in http://www.insmartenergy.com/. Accessed in 01/June/2016].
[33] N. W. A. Lidula and A. D. Rajapakse, "Microgrids research: A review of experimental microgrids and test systems," *Renew. Sustain. Energy Rev.*, vol. 15, no. 1, pp. 186–202, Jan. 2011.
[34] K. Hongesombut, T. Piroon, and Y. Weerakamaeng, "Evaluation of battery energy storage system for frequency control in microgrid system," in *Electrical Engineering/Electronics, Computer, Telecommunications and Information Technology (ECTI-CON), 2013 10th International Conference on*, 2013, pp. 1–4.
[35] Y. Ma, P. Yang, Y. Wang, S. Zhou, and P. He, "Frequency control of islanded microgrid based on wind-PV-diesel-battery hybrid energy sources," in *Electrical Machines and Systems (ICEMS), 2014 17th International Conference on*, 2014, pp. 290–294.
[36] V. Miranda, "Fiabilidade em Sistemas de Potência – Uma Introdução", version 3.2, Sept. 2015.
[37] L. M. Carvalho, "Using Evolutionary Swarms (EPSO) in Power System Reliability Indices Calculation", M.S. thesis, FEUP, Porto, Portugal, 2008.
[38] R. Billinton and P. Wang, "Teaching distribution system reliability evaluation using Monte Carlo simulation," *Power Syst. IEEE Trans. On*, vol. 14, no. 2, pp. 397–403, 1999.
[39] Billinton, Roy and Allan, Ronald N., "Reliability Evaluation of Power Systems", Second Edition, New York, Plenum Press, 1996.
[40] M. V. F. Pereira, M. E. P. Maceira, G. C. Oliveira, and L. Pinto, "Combining analytical models and Monte-Carlo techniques in probabilistic power system analysis," *Power Syst. IEEE Trans. On*, vol. 7, no. 1, pp. 265–272, 1992.

[41] V. Miranda, L. de Magalhaes Carvalho, M. A. da Rosa, A. M. L. da Silva, and C. Singh, "Improving Power System Reliability Calculation Efficiency With EPSO Variants," *IEEE Trans. Power Syst.*, vol. 24, no. 4, pp. 1772–1779, Nov. 2009.
[42] L.M. Carvalho, D. Issicaba, M. A. Da Rosa, J. P. V. Ramos, V. Miranda, "Reliability Evaluation of Generation Systems via Sequential Population-Based Monte Carlo Simulation", presented at the 12th International Conference on Probabilistic Methods Applied to Power Systems (PMAPS), Istanbul, Turkey, June 2012.
[43] L. de M. Carvalho, R. A. Gonzalez-Fernandez, A. M. Leite da Silva, M. A. da Rosa, and V. Miranda, "Simplified Cross-Entropy Based Approach for Generating Capacity Reliability Assessment," *IEEE Trans. Power Syst.*, vol. 28, no. 2, pp. 1609–1616, May 2013.
[44] P. S. Georgilakis and Y. A. Katsigiannis, "Effect of customer worth of interrupted supply on the optimal design of small isolated power systems with increased renewable energy penetration," *IET Gener. Transm. Distrib.*, vol. 7, no. 3, pp. 265–275, Mar. 2013.
[45] S. Conti, R. Nicolosi, and S. A. Rizzo, "Generalized Systematic Approach to Assess Distribution System Reliability With Renewable Distributed Generators and Microgrids," *IEEE Trans. Power Deliv.*, vol. 27, no. 1, pp. 261–270, Jan. 2012.
[46] Z. Bie, P. Zhang, G. Li, B. Hua, M. Meehan, and X. Wang, "Reliability Evaluation of Active Distribution Systems Including Microgrids," *IEEE Trans. Power Syst.*, vol. 27, no. 4, pp. 2342–2350, Nov. 2012.
[47] S. Kennedy and M. M. Marden, "Reliability of islanded microgrids with stochastic generation and prioritized load," 2009, pp. 1–7.
[48] S. Wang, Z. Li, L. Wu, M. Shahidehpour, and Z. Li, "New metrics for assessing the reliability and economics of microgrids in distribution system," *Power Syst. IEEE Trans. On*, vol. 28, no. 3, pp. 2852–2861, 2013.
[49] L. H. Koh, P. Wang, F. H. Choo, K.-J. Tseng, Z. Gao, and H. B. Puttgen, "Operational Adequacy Studies of a PV-Based and Energy Storage Stand-Alone Microgrid," *IEEE Trans. Power Syst.*, vol. 30, no. 2, pp. 892–900, Mar. 2015.
[50] Y. M. Atwa and E. F. El-Saadany, "Reliability Evaluation for Distribution System With Renewable Distributed Generation During Islanded Mode of Operation," *IEEE Trans. Power Syst.*, vol. 24, no. 2, pp. 572–581, May 2009.
[51] Z. Li, Y. Yuan, and F. Li, "Evaluating the reliability of islanded microgrid in an emergency mode," in *Universities Power Engineering Conference (UPEC), 2010 45th International*, 2010, pp. 1–5.
[52] S. Kennedy, "Reliability evaluation of islanded microgrids with stochastic distributed generation," in *Power & Energy Society General Meeting, 2009. PES'09. IEEE*, 2009, pp. 1–8.
[53] In-Su Bae and Jin-O Kim, "Reliability Evaluation of Customers in a Microgrid," *IEEE Trans. Power Syst.*, vol. 23, no. 3, pp. 1416–1422, Aug. 2008.
[54] Portal ERSE - Documentos complementares. Available in: http://www.erse.pt/pt/electricidade/regulamentos/acessoasredesaasinterligacoes/Paginas/SubregulamentacaoRARI.aspx. Accessed in 06/June/2016.
[55] PV potential estimation utility. Available in http://re.jrc.ec.europa.eu/pvgis/apps4/pvest.php#. Accessed in 07/June/2016.
[56] R. D. Zimmerman and C. E. Murillo-Sanchez, "Matpower 5.1-User's Manual," *Power Syst. Eng. Res. Cent. PSERC*, 2015.
[57] R. D. Zimmerman, C. E. Murillo-Sanchez, and R. J. Thomas, "MATPOWER: Steady-State Operations, Planning, and Analysis Tools for Power Systems Research and Education," *IEEE Trans. Power Syst.*, vol. 26, no. 1, pp. 12–19, Feb. 2011.
[58] PORDATA - Ambiente de Consulta. Available in http://www.pordata.pt/DB/Europa/Ambiente+de+Consulta/Tabela. Accessed in 21/June/2016.
[59] PORDATA - Consumo de energia eléctrica: total e por tipo de consumo - Portugal. Available in http://www.pordata.pt/Portugal/Consumo+de+energia+el%C3%A9ctrica+total+e+por+tipo+de+consumo-1124. Accessed in 21/June/2016.

Annex A – Test MG

In this annex it is presented the data referring to the test MG used for the application of the proposed method for assessing the reliability.

Table A.1 presents the load contracted in each bus, as well as the annual consumed energy and the correspondent profile class of the client.

Table A.1 – Bus data of the test MG.

Bus	Contr. Power (kVA)	Annual Consumed Energy (kWh)	Profile Class
2	6.9	4621.49	C
5	3.45	2791.41	C
6	3.45	2600.67	C
7	10.35	7661.14	B
8	6.9	4623.25	C
9	13.8	10575.47	B
10	13.8	11344.34	B
11	10.35	5833.11	C
12	6.9	4652.62	C
13	13.8	9212.68	B
16	6.9	4798.83	C
17	10.35	5819.90	C
18	6.9	5786.68	C
19	6.9	4561.36	C
20	6.9	5131.51	C
21	6.9	4123.20	C
22	17.25	15852.28	A
23	3.45	2758.67	C
24	17.25	15180.95	A
25	13.8	11209.79	B
26	10.35	7302.60	B
27	13.8	10254.76	B
28	6.9	3909.70	C
29	17.25	16613.07	A
30	10.35	5715.63	C
31	6.9	4723.04	C
32	6.9	5427.85	C
33	3.45	2442.50	C

In table A.2 the parameters of each branch of the MG are displayed.

Table A.2 – Branch data of the test MG.

Branch	From	To	R (pu)	X (pu)
1	1	2	0.088594	0.013281
2	1	3	0.029688	0.00625
3	1	4	0.057344	0.008594
4	2	5	0.048438	0.010156
5	3	6	0.120156	0.028125
6	3	7	0.109375	0.016406
7	4	8	0.104219	0.015625
8	5	9	0.072969	0.010938
9	5	10	0.1625	0.008281
10	5	11	0.341719	0.016406
11	6	12	0.455781	0.021875
12	7	13	0.036406	0.005469
13	8	14	0.310781	0.015313
14	8	15	0.194063	0.015313
15	9	16	0.036406	0.005469
16	11	17	0.39	0.008281
17	11	18	0.149219	0.011719
18	12	19	0.059531	0.0125
19	13	20	0.23875	0.01875
20	13	21	0.756406	0.024688
21	14	22	0.189375	0.039844
22	15	23	0.417813	0.032813
23	16	24	0.072969	0.005469
24	18	25	0.252188	0.008281
25	19	26	0.037188	0.007813
26	20	27	0.292969	0.014063
27	23	28	0.146094	0.032813
28	24	29	0.288125	0.009375
29	26	30	0.083281	0.00625
30	27	31	0.334688	0.016406
31	28	32	0.504219	0.016406
32	31	33	0.252188	0.008281

Finally, in table A.3, the installed power in each bus with a PV generation unity is exhibited.

Table A.3 – Generator data of the test MG.

Bus	Installed Power (kW)
7	3.68
9	1.7
10	3.68
11	3.45
13	5.15
16	3.45
17	3.68
22	5.35
24	3.68
25	3.68
26	3.68
27	5.15
29	3.68
30	3.68
31	3.45